Progress in Energy and Combustion Science 37 (2011) 125–171

Contents lists available at ScienceDirect

Progress in Energy and Combustion Science

journal homepage: www.elsevier.com/locate/pecs

Review

On-line spectroscopic and spectrometric methods for the determination of metal species in industrial processes☆

Penelope Monkhouse*

Physikalisch-Chemisches Institut der Universität Heidelberg, Im Neuenheimer Feld 253. 69120 Heidelberg, Germany

ARTICLE INFO

Article history:
Received 26 November 2009
Accepted 10 May 2010
Available online 23 June 2010

Keywords:
On-line flue gas analysis
Alkali metals
Heavy metals
Solid fuel combustion
Incineration
Glass furnaces

ABSTRACT

The status of on-line methods for determining metal species, particularly alkali and heavy metals, is reviewed. The background and motivation is discussed first, including current environmental and economic issues associated with release of metal species in industrial processes as well as control measures. Then general diagnostic problems such as optical access and sampling design are considered, followed by an overview of selected diagnostic methods, including recent contributions to technique development and to the understanding of fundamental combustion processes. The main focus is on absorption (tunable diode laser and differential absorption spectroscopies) and emission (spontaneous atomic emission, laser induced fluorescence, photofragment fluorescence as well as several varieties of plasma spectroscopy), but on-line ionisation methods (molecular beam and single particle mass spectrometry and surface ionisation) are also reviewed briefly. In the final section, the capabilities of the selected methods are illustrated by examples of field measurements in the conversion of solid fuels as well as waste incineration, glass production and other processes.

Contents

☆ In memory of Rolf Hernberg, who contributed much to this field of research.

* Tel.: +44 6221 545044; fax: +44 6221 544255.
E-mail address: d63@ix.urz.uni-heidelberg.de

0360-1285/$ – see front matter © 2010 Elsevier Ltd. All rights reserved.
doi:10.1016/j.pecs.2010.05.002

1. Scope of article

This article reviews *on-line* methods for the measurement of metal species, particularly alkali and heavy metals, in solid fuel conversion (heat, electricity, waste disposal) and in several other industrial systems, including glass and blast furnaces. The main emphasis is on those methods that have actually found application in realistic industrial environments, though some attention is given to techniques with potential for such applications. Important spectroscopic and optical issues are considered, as well as steps needed for obtaining quantitative data, including determination of optical transmission and of collisional transfer of excited states for conditions typical of industrial processes. Not covered here are off-line ash and fuel analysis, although these provide essential supporting/complementary data for interpretation of on-line data. Also not considered are off-line analysis methods, such as XAFS, XRF, EDX, SEMS, NMR, XRD, ESR, classical IR- and UV-emission and -absorption, nor are off-line mass spectrometric and plasma methods and their applications. Information on these techniques is to be found in the literature [1,2]. Acronyms used are listed in Table 1.

2. Introduction

Feedstocks and additives used for heat and power production and other industrial processes may contain a wide range of metal species in differing quantities. Biofuels (e.g. straw, salix, agricultural or forest products) are increasingly being used for energy production, either on their own or in blends with coal, although their heating values are much lower than for coal [3–5]. Heating values for biomass are in the range 14–16 MJ/kg, whereas hard coals are defined as coals with heating values above 23.8 MJ/kg. However, the heating values are strongly dependent on the moisture content, which, for example, can be up to 50–60% in wood and forest residue chips. The heating value is then $<$10 MJ/kg. On the other hand, the effective heating value of dry wood varies little, since the ash content is typically low.

Table 1
Acronyms.

a) Measurement methods	
AAS	Atomic absorption spectroscopy
AES	Atomic emission spectroscopy
AMS	Aerosol mass spectrometry
ATOFMS	Atmospheric time-of-flight mass spectrometry
CEM	Continuous emission monitor
CRDS	Cavity ring down spectroscopy
CVAAS	Cold vapour atomic absorption spectroscopy
CVAF	Cold vapour atomic fluorescence
DOAS	Differential optical absorption spectroscopy
ELIF	Excimer laser induced fragmentation fluorescence
ETA	Electrothermal analysis
HEAMON	Heavy metals monitor
HPMS	High Pressure mass spectroscopy
IACM	In-situ alkali chloride monitoring
ICP	Inductively coupled plasma
LIB(P)S	Laser induced breakdown (plasma) spectroscopy
LIF	Laser induced fluorescence
MBMS	Molecular beam mass spectrometry
OES	Optical emission spectroscopy
PEARLS	Plasma enhanced atomic resonance line spectroscopy
PFF	Photofragment spectroscopy
SHG	Second harmonic generation
SI	Surface Ionisation
SIBS	Spark induced breakdown spectroscopy
SPMS	Single particle mass spectrometry
TDLAS	Tunable diode laser absorption spectroscopy
TOF	Time of flight
b) Light sources, detectors and other equipment	
ATOF	Acousto-optic filter
DFB-DL	Distributed feedback diode laser
ECDL	External cavity diode laser
FPDL	Fabry-Pérot diode laser
ICCP	Intensified coupled channel plate
MCP	Multichannel plate
MCA	Multichannel analyser
VCSEL	Vertical cavity surface emitting laser diode
c) Technical	
AASB	Analytical alkali sorber bed
BFB	Bubbling fluidised bed
CC	Combined cycle
IGCC	Integrated gasification combined cycle
MCFC	Molten carbonate fuel cell
PFBC	Pressurised fluidised bed combustion
PCC	Pulverised coal combustion
SOFC	Solid oxide fuel cell
TSCA	Toxic substances control act

Depending on the process and the properties of the species of interest, metals can be released partially or fully in gaseous and/or particulate form. Heavy metals such as Cd, Hg, Pb, As, especially in atomic, oxide or chloride form, tend to remain in the gas phase or as submicron aerosols in the hot flue gas, whereas other metals (such as Ni and Co) are found predominantly in particulate form [6–10]. In addition, re-condensation on cooling the flue gas may lead to enrichment of metal compounds.

Most heavy metal species are of environmental and health concern, whereas sodium, potassium, vanadium and zinc species cause damage to materials in heat and power plants, leading to reduced efficiencies and high maintenance costs. Particulate matter itself causes both health and maintenance problems. Furthermore, the situation is exacerbated by ever increasing energy needs as well as amounts of waste to be incinerated. Emissions limits for both greenhouse gases (CO_2, CH_4, N_2O etc.) and toxic emissions (NO_x, SO_2, CO, Hg, Pb, Cd etc.) will continue to be lowered, therefore control devices (filters etc.) and emissions management as well as overall efficiency must be steadily improved. This means that the demands on in process fuel screening, emissions control and gas cleaning will increase and hence also demands on sensitive, on-line diagnostics for a wide range of chemical species. To support the development and implementation of monitoring methods, the relevant institutions and agencies have produced guidelines that set out standards and good practice for emissions monitoring. Guidelines (such as [11–13]) should include information on current legislation (national, EU or other), certification schemes, monitoring and sampling strategies and a hierarchy and index of specific monitoring methods. Current limits for heavy metal emissions are given in Table 2a [14,15]. The EU limits are presently those for incineration/co-incineration plants, but from 2016, these will also be valid for normal energy production plants.

The improvement of efficiencies of conversion processes as a whole and the development of cost-effective technologies for controlling and removing metal species from process flue and stack gases are thus paramount to the future environmental and economic success of all industries, whether heat and power, production or waste management. However, it is also clear that the successful design of abatement measures depends on a detailed knowledge of the processes involved in the release, transformation and partitioning of metal species into different physical forms.

2.1. Environmental aspects

Contributors to the release of heavy metals include combustion or gasification of coal, heavy oils, biomass and waste as well as production of iron and steel, non-ferrous metals and cement [16–24]. These emissions add to pressures on the environment already made by pollutants such as NO_x and SO_2. Present limits are given in Table 2b [25]. In addition, environmental policies as well as the situation in the energy and waste economies have changed markedly in recent years. For example, it is hoped to reduce the use of fossil fuels by co-combustion with waste materials and residues from agriculture and industry. In the near future, waste materials will have to be processed by thermal or mechanical methods, since landfilling or using waste as animal fodder will no longer be permitted.

Past and current trends of emissions of mercury, lead and cadmium in the environment were recently reviewed by Pacyna et al. [16]. These authors also consider possible future scenarios as well as impacts of emission changes and control strategies. Trace metals can be inhaled as fine particles and deposited in the lungs. Small mode (<2.5 μm) particles are considered particularly dangerous since they are inhaled far more deeply than the coarser particles. Furthermore, total amounts of specific metals say little about the biologically effective dose. Uptake in the blood stream will depend on deposition patterns and on solubility and these are, in turn, influenced by chemical form and particle size. In addition, airborne toxic metals can reach humans via deposition on soil and vegetation, and through food chains. A recent brochure has set out the health risks of transboundary heavy metal pollution in detail [26].

Table 2a
Toxic metal limits for industrial plants.

EU [14]	
Total particles	10 mg/m^3 < 100 MW
Total particles	20 mg/m^3 > 100 MW
Cd + Tl	50 $\mu g/m^3$
Hg	50 $\mu g/m^3$
Sb + As + Pb + Cr + Co + Cu + Mn + Ni + V	500 $\mu g/m^3$
USA (Hazardous waste combustor rule) [15]	
Total particles	34 mg/m^3
Semi-volatiles (Cd, Pb)	240 $\mu g/m^3$
Hg	130 $\mu g/m^3$
Low volatiles (Be, Cr etc.)	97 $\mu g/m^3$

Table 2b
Limits for NO_x and SO_2 (mg/Nm^3), referred to O_2 content of 3% for new and existing plants [25] (solid fuels for NO_x 6% O_2).

Type of fuel	NO_x
Solid: 50–500 MWth	600
Solid: >500 MWth	500 (from 2016: 200)
Liquid: 50–500 MWth	450
Liquid: >500 MWth	400
Gaseous: 50–500 MWth	300
Gaseous: >500 MWth	200
	SO_2
Solid, general: 50–100 MWth	850
Solid, biomass: 50–100 MWth	200
Solid: > 100 MWth	200
Liquid: 50–100 MWth	850
Liquid: 100–300 MWth	400–200 (linear decrease)
Liquid: >300	200
Gaseous:	35

A major problem of coal combustion is that a large proportion of the ash leaves the combustor as fly ash, entrained in the flue gas, whereby the proportion of fly ash is greater in pulverised and fluidised bed combustion than in grate combustion. Major constituents are silica, alumina and oxides of iron and calcium. Oxides of magnesium, potassium and sodium occur in percent amounts. In addition to these components, fly ash contains trace metals, including toxic heavy metals. Although efficient particulate control systems (Filters, ESP etc.) are now available and the quantities of particles in the atmosphere is much reduced, some fine particulate (PM_{10} and below) will still reach the atmosphere. Fine particulate is itself a serious health hazard, but the presence of heavy metals on the particles adds to the risks. Inhalation of particles containing transition metals, for example, has been shown to cause cardiopulmonary damage [27]. If metal species are water-soluble, this may increase their bioavailability [28]; such species include copper, iron, nickel, vanadium and zinc as well as lead and cadmium. About 6% of lead emission to the atmosphere has been estimated to originate from coal combustion [29]. Of particular concern are Hg, Cd, Pb and As, which have relatively high vapour pressures (Section 2.4.3) and high bioavailability [14,26]. Therefore these species will underlie increasingly stringent limits (Table 2a).

For example, mercury is emitted during the thermal conversion or treatment of solid, liquid and gaseous fuels and from industrial operations such as chlorine-alkali plants [21] and finds its way into the environment. Mercury can also be emitted in mining, transport and materials processing. Although the amounts emitted are well below those emitted by the natural cycle (water, volcano eruptions, leaching from landfill sites), heavy local or regional pollution does occur, as corresponding studies have shown [16,21].

2.2. Plant operation problems

Problems associated with compounds of metals such as the alkalis, vanadium and zinc include abrasion, corrosion, and erosion of system parts; slag flow in wet-bottom systems, fouling and slagging of heat transfer surfaces leading to poor heat transfer, plugging of gas-filtering systems as well as disposal problems and restricted utilisation of ash residuals [30–34]. Thus alkali species also influence the energy and mass flows in boilers and furnaces and hence affect their energy consumption.

The damage caused to plant materials by alkali species is largely a result of their low-melting points and high reactivity; vapour pressures for several alkali compounds are given in Table 3. The highest risk fuels are those with high chlorine concentrations and the alkali acts as a carrier of Cl to the superheaters where elemental Cl is released. Hot combustion gas is generally contaminated with alkali compounds. If the gas is to be sent directly to a gas turbine (as in combined cycles), limits specified by manufacturers for alkali concentrations and particle sizes have to be observed in order to minimize corrosion and fouling problems [35–38]. For an economically acceptable turbine lifetime, particulate limits of 4.7 mg/m^3 and alkali concentrations below 24 ppbw have been stated [38].

Table 3
Vapour pressures (mbar) for the chlorides and hydroxides of sodium and potassium.

Temperature, K	NaCl	NaOH	KCl	KOH
800	0.004	0.02	0.0013	0.021
1000	0.09	1.0	0.23	1.5
1200	4	21	7.5	30
1400	50	172	89	232
1600	350	740	557	1009

Corrosion and deposition due to molten alkali species has been studied intensively for different conditions and fuel types [33–40] and a range of materials has been tested for resistance to corrosion [33,34,41–43]. These include corrosion tests on turbine blades [44,45], which are especially relevant to combined-cycle technology development. More recently, with the increasing utilisation of biomass fuels, especially agricultural biomass residues, the severe effects of chlorine-induced corrosion have come to the fore. In comparison, wood fuels with low alkali and chlorine contents pose a lesser risk. In this context, recycled fuels (from household and industrial waste) should be mentioned, since these may contain considerable amounts of chlorine. Corrosion mechanisms are discussed by Nielsen et al. [45], referring to boilers firing straw and by Tillman et al. [46] referring to pulverised fuel boilers firing coal and/or biomass.

Glass furnaces represent another area where alkali corrosion is of high concern, especially since the advent of oxy-fuel fired furnaces. Accelerated silica crown corrosion is caused by large increases in gaseous alkali species, especially the hydroxides. In the past decade however, the "tall crown furnace (TCF) design has helped to mitigate the problem [47]. By increasing the burner height above the glass melt, "hot spots" on the glass melt surface and hence the rate of alkali volatilisation could be reduced by about 50%. In this way, the lifetime of the glass furnace is expected to be lengthened to ten years or more.

In FB systems, a high degree of alkali vaporisation leads to sintering and agglomeration of bed material and consequently defluidisation [37,48,49]. Alkali chlorides vaporise in the furnace and alkali is then carried to the sand surface. Natural sand is rich in SiO_2, so low-melting compounds can be formed and this process initiates agglomeration. In addition, deposition of alkali species such as NaCl, Na_2SO_4 or Na_2CO_3 can poison and deactivate catalysts (e.g. DeNO_x-catalysts [50–56]). Catalyst poisoning by alkali species is also relevant to fuel cells, particularly SOFCs [57] and MCFCs [58,59].

Vanadium and zinc are also implicated in corrosion processes, particularly for low-grade liquid fuels. Accelerated corrosion is likely to occur when deposits containing vanadium are found on high-temperature components [60]. In steam tube deposits, zinc chlorides have also been implicated in corrosion mechanisms [61]. Thus detailed knowledge about the behaviour of all these metal species in the plant processes of interest is needed, both for design and operation.

2.3. Occurrence and abundance of metals in fuels and additives

The composition of solid fuels, including the forms, associations and abundances of metals varies widely and depends on

geographical location and chemical origin. The main mineral constituents of coal are silica, alumina and iron oxides, usually together with some calcium and magnesium as well as chlorine and/or sulphur. Biomass, on the other hand, shows major differences; for example, wood ash is dominated by calcium and potassium and amounts of Fe, Al, S and Si are low. The relative proportions of the different constituents depend on fuel type. Detailed information on the different fuels can be obtained using range of methods including selective leaching, XAFS, Mössbauer spectroscopy, ICP-AES and (off-line) LIBS [1,2,62,63].

The chief alkali species are Na and K; typical ranges for several types of feedstock are given in Table 4. Quantities of Li are generally below ca. 15 ppm and those of Cs and Rb below about 1 ppm [63] (both per weight). The main halogens present are chlorine, with average contents of 90–1100 ppm for coals and 100–6000 for biomass [46] and fluorine with 20–500 ppm [64]. Coal analyses show that the water- and mild acid-soluble fractions contain alkali metals inorganic structures and simple inorganic salts, while the strong acid-soluble fraction holds the mineral-bound alkali metals. Biofuels on the other hand contain sodium and potassium, largely in accessible, mobile forms that can readily be released during combustion [65,66], such as organic moieties or simple inorganic salts. Potassium, as an essential plant nutrient, is particularly abundant in annual crops, although the actual content varies strongly with type of biomass and also with agricultural practices [67].

The heavy metal species Hg, Pb, Cd, Zn, Ni, As, Cr, Cu and Mn occur in at least trace amounts (0.1–100 ppm) (Table 4). In coal, Hg, As and Se are frequently associated with pyrite or organic constituents. Chromium is found mainly in the amorphous CrOOH phase and/or clay minerals in bituminous coals, but organically associated in sub-bituminous coals.

Depending on their origin, heavy oils often contain considerable quantities of Ni and V, which can be enriched on distillation in the high-boiling fractions by a factor of 10^3–10^4, compared to a factor of 5–20 for coal [68]. Feedstocks containing waste materials usually contain high amounts of heavy metals, such as materials from scrapped cars (Zn, Cr), slags, other residues from combustion and incineration as well as sludges from wastewater treatment (Pb, Zn, Cu) [17,69].

As well as the fuels themselves, additives such as calcite ($CaCO_3$) or dolomite ($CaCO_3 \cdot MgCO_3$) used as desulphurisation agents in fluidised bed (FB) combustion usually contain traces of heavy and alkali metals.

Table 4
Modes of occurrence and quantities of metals in fuels.

Metals	Fuel	Form	Typical quantities (ppmw)
Na, K	Bituminous coal	Mineral matrix e.g. feldspat, Muskovit Inclusions (NaCl, KCl)	Na: 300–1250 K: 600–4600
Na, K	Lignite/sub-bit. coal	Organic structure (phenolic OH/ carbonate); pore structure	Na 30–480 K: 60–1400
Na, K	Biomass	Water solutions in vacuoles; organic structures	Straw/grass Na: 70–15,000 K: 5000–30,000 Wood: Na: 30–2000 K: 450–7000
Heavy metals	Coal	Pyrite + associated sulphides, carbonates, clays, organic matter	Mn: 10–200 Cd: 0,05–3 Cu: 5-154 Hg: 0,05-2 Ni: 4–55 Pb: 4–250 Zn: 6–180
Heavy metals	Biomass	Enzymes; organic/ organic acid groups; counter ions (carbonate, oxalate, phosphates) in aq. soln.	Mn: 20–240 Cd: 0.1–0.3 Cu: 1–90 Hg: 0.01–0.05 Ni: 0.2–10 Pb: 1–5 Zn: 20–150

2.4. Chemical and physical transformations in processes

2.4.1. General aspects

A large body of literature has accumulated in recent years that considers different aspects of this topic, including vaporisation, transformation, partitioning into different chemical and physical phases, enrichment and gettering, In general, the transformation of metal species during conversion and post-conversion processes depends on the following factors:

1. Firing technology (pulverised fuel, fluidised bed, grate-fired, stoker-fired), and specific operating conditions. A key factor is the temporal temperature profile of the burning fuel particles since this influences the rate and extent of vaporisation, chemical reactions and later condensation. In pulverised coal combustion (PCC), temperatures may reach around 1700 °C, high enough for ash fusion. In contrast, FBC firing temperatures are not more than 1000 °C, i.e. well below ash fusion temperatures, and this limits the potential for chemical reaction and slag formation. On the other hand, the relatively long residence times of ash particles in fluidised beds result in greater inter-particle contact and hence a greater potential for reaction between surfaces and for in-bed agglomeration. Another important factor is the particle temperature: in FB furnaces, this is not more than 400 °C above that of the sand. Thus if the sand temperature is 900 °C, some particles can be at around 1300 °C but the proportion of these particles is low [70]. Under PF conditions, in contrast, the particle temperatures can be up to 2000 °C [71]
2. Fuel specific factors: metal concentrations, form of occurrence (chemical species) and mineralogy. The latter two affect volatility. For example, high proportions of clay (aluminosilicate) minerals in the coal can act as natural getters, thus hindering the release of trace element vapours. Indeed, natural gettering is often desirable to suppress the release of problematic chemical species, however, their amount and effectiveness is not always sufficient and the addition of sorbents may be required. To determine whether this is the case, reaction rates of trace elements with clay minerals and fly ash particles need to be measured under both conversion and post-conversion conditions. A number of studies have observed gettering by clay minerals [Section 2.5], but these need to be extended to a wider range of species and conditions.
3. Physical and chemical properties of the metal species of interest, affecting volatility and chemistry. This includes chemical kinetic and thermodynamic information on the species of interest.
4. Other factors, including humidity and additives used for desulphurisation (mentioned at the end of Section 2.3) and as sorbents of metal species (Section 2.5)

2.4.1.1. Reaction kinetic data, reaction mechanisms. Reliable kinetic models are needed to understand the complex transformations of metal species in combustion and gasification as well as in the

synthesis of nanoscale solids, corrosion processes and catalytic formation of molecules e.g. halogenated aromatics. In turn, the construction of reaction mechanisms requires reliable data of all important *elementary reactions* involved in the system. Unfortunately, most mechanisms rely, at least to some extent, on assigning guessed or estimated values to reactions that are difficult or impossible to measure directly and thus usually contain some degree of speculation. Kinetic studies are also undertaken with a view to improving knowledge on chemical reactivity and electronic structure. Thus the need for new data opens a further field of application for on-line measuring methods.

Early kinetic work on alkali species was reviewed by Davidovits [72]. The reactions of sodium atoms with oxygen and nitrous oxide have been the most frequently studied [73–83], but reactions with SO_2 have also been investigated [84,85]. Kinetic studies of alkali species in flames are reported in Refs. [86–88] and Steinberg and Schofield [89,90] have described the flame chemistry of sodium with sulphur.

Elementary reactions of other metal atoms have been reviewed by Fontijn [91], but since this, a considerable amount of work has been performed [92–103], mainly using fast flow or shock wave systems, photolytic methods to form atomic species and detection by AAS, AES or LIF to follow the reactive depletion of metal atoms.

A kinetic modelling study was recently performed by Qiao et al. [104] using *ab initio* molecular orbital (MO) methods to investigate reactions of Sn with different oxidants. This work showed that the reactions with O_2 and CO_2 are the two main oxidants for Sn oxidation.

Considerable efforts have also been made to advance understanding of mercury chemistry [105–112] though it is fair to say that this has been highly controversial. A comprehensive review of 2008 [105] concludes that Hg oxidation chemistry is a solely heterogeneous on the grounds that the homogenous oxidation mechanism is far too slow. The review cites kinetic investigations of Taylor et al. [106], Ariya et al. [107] and Donohue et al.[108] on the kinetics of elementary reactions of this element. However, it should be noted that these kinetic studies were performed at room temperature and below and refer to atmospheric rather than combustion chemistry. Some elementary reaction rates and their temperature dependences have not been determined directly but estimated from concentration measurements or calculated from kinetic-thermodynamic theory.

2.4.2. Alkali chemistry

The chemistry of alkali species in combustion processes has been considered in detail by Glarborg [113] and Glarborg and Marshall [114] Earlier investigations relating to combustion and gasification processes include Mojtahedi et al.[115]; Niksa et al. [116]; Thambimuthu [117]; Wall [118]; Wibberley and Wall [119]. Model simulations linked to thermodynamic databases predict the proportions of metal species formed during combustion or gasification as a function of temperature. Condensed-phase alkali species usually consist mainly of silicates and sulphates. The main gas phase species are chlorides and hydroxides, whereby the ratio between these two depends strongly on the amount of chlorine in the fuel. Indeed, the chlorine content of the fuel can affect alkali release, as discussed in Section 5.5.1. Up to about 1450 °C and for Cl contents of around 0.5 wt%, the chlorides are the dominant species, thereafter the hydroxides. If the Cl content is only about 0.05 wt%, the proportion of the hydroxides exceeds that of the chlorides from ca. 1200 °C. Kinetic modelling for the Na–Cl system [86] shows that the gas phase species NaOH and NaCl generally reach their equilibrium values on the millisecond timescale. In contrast, equilibrium between gas and condensed phase components is not normally reached.

The formation of gaseous *alkali sulphates* is another subject of controversy. Older studies [89,90] indicated that sulphation of NaCl is kinetically limited. A key factor in the process is the formation rate and availability of SO_3 [120]. The more recent model of Glarborg and Marshall [114] shows that SO_3 subsequently recombines with alkali hydroxide or alkali chloride to form an alkali hydrogen sulphate or an alkali oxysulphur chloride. These compounds are expected to be stable enough in the gas phase to work as precursors for formation of alkali sulphates. However, in the presence of chlorine or water, alkali sulphates do react away rapidly. Also, the corresponding vapour pressures of the chlorides and hydroxides are much higher and equilibrium does not lie on the sulphate side, so that mainly chlorides and hydroxides are observed in the gas phase. Nevertheless, quantities of sulphates corresponding to the equilibrium should exist, though at lower temperatures these may lie below the limit of detection for available measurement techniques (see also discussion in Section 5.7.2). Slow kinetics can delay reaching equilibrium but do not disturb an equilibrium once reached.

In the flue gas, alkali species occur as gaseous chemical compounds, metal-containing particles and ash particles. The fraction found on ash particles can be present either as condensed metal species or as inclusions in chemical compounds with the ash particles. The chief parameters affecting the alkali species in the process gas are the contents of sulphur, silicon and chlorine and the air ratio, pressure and temperature. In FB coal combustion, alkali attached to organic moieties and inorganic alkali (such as NaCl) is released that can later condense on bed materials and metal surfaces [121]. Mineral-bound alkali remains on ash particles and melt, and can later, together with the ash, become fixed to the bed material and the surfaces of components. Gas phase alkali compounds can undergo homogenous condensation, heterogeneous (particle) condensation, reactions with the ash or filter material, or condense on cool surfaces.

In the conversion of biofuels, a much higher proportion of the alkali is released to the gas phase, since it is present in the fuel mainly in mobile, easily volatilised forms, as noted in Section 2.2. In biomass types such as straw, the content of both potassium and chlorine is often at the percent level, posing a severe danger for both boiler and downstream plant parts, since nearly all the alkali will be in the form of chloride. In wheat straw combustion, where up to 70% of available potassium and 15% of sodium is predicted to be released, giving about 2000 ppm KCl and 440 ppm NaCl, respectively [65]. However, the actual amount of alkali in the gas phase, measured at some point downstream of the combustion chamber, can be an order of magnitude less than this, depending on the temperature and other conditions in the flue gas. For example, alkali may condense on fly ash particles or on furnace or pipe walls, form aerosols in the flue gas or be transformed to other chemical forms.

The level of oxygen in biomass is also relatively high (typically $40 \pm 5\%$), as a result of the carbohydrate structure, and Wornat et al. [122] have suggested that K and Na are associated with oxygen-containing functionalities within the organic matrix, which means that the vaporisation of alkali under combustion conditions would be similar to that of low-rank coals.

In all, vapour alkali concentrations from sub-ppb to ppm ranges have been observed in coal combustion processes, but in gasification and particularly in conversion of biomass the concentrations can reach the 1000–10,000 ppm range [66]. Alkali emissions as a function of specific parameters e.g. chlorine content, clay mineral content and process temperature have been investigated experimentally for some fuels and processes [123–127]. Further such studies for a wide range of feedstocks and conditions are needed, particularly since equilibrium calculations give only limited

information about metal emissions behaviour. Only then can one build up a full picture of alkali release processes, so that suitable measures can be taken to protect plant parts.

2.4.3. Heavy metal chemistry

Recent reviews on heavy metal measurements in combustion processes were published by Lundholm et al. [128] and Nelson [7]. An earlier, though comprehensive review by Linak and Wendt [129] considered particularly incineration processes. Models for predicting alkali and heavy metal emissions include those of Helble et al. [130], Yan et al. [131], Verhulst et al. [132]. However, simulations require on-line data for validations and so far, experimental investigations mostly concern fuel analyses and off-line measurements on residues [2,133–140]. On-line, continuous process data have only been gradually appearing, with the recent developments in monitoring methods.

In general, the greater part of heavy metal emissions is associated with the fly ash, but species such as Hg and Cd are emitted mainly or completely in gaseous form; indeed, vaporisation of Hg species begins from about 100 °C, that of Cd (as $CdCl_2$) from 300 °C [132]. Coal fly ash usually has bimodal size distributions with sub- and supermicron modes [7,9,10,141]. Significant amounts of trace elements can be emitted with the submicron fly ash particles and these preferentially penetrate commercial gas cleaning devices. Furthermore, the smaller particles tend to be enriched in semi-volatile trace elements. It is these fine particles, bearing heavy metal elements that are likely to be inhaled and therefore pose a high risk for human health.

A particularly important case is mercury. On-line measurements would help in controlling the effectiveness of mitigating measures, being the only way to determine Hg species in ppb concentrations with sufficiently high temporal resolution. In particular the exact relation between molecular and elementary forms of Hg in the temperature range 300–700 °C is of paramount importance, since this critically affects the control and removal of mercury. In spite of the many investigations and development of models [105–112] for oxidation of elementary Hg, important details are still unclear or are disputed.

2.5. Control of metal emissions

As discussed above, metal emissions have to be curtailed for both environmental and economic reasons. A large proportion of these emissions are part of particulate matter in the flue or stack gas and can be removed by devices such as cyclones, scrubbers, electrostatic precipitators and barrier filters. However, such devices control only the solid material in the gas flow and unless there is a further removal device in the clean-up system, metals in vapour form will still be emitted to atmosphere. The amount so emitted will depend on the equilibrium vapour pressure at filtration.

For operators of combustion plants, mercury is a particular problem since it a) is almost entirely released from the fuel and is predominantly present in the flue gas in gaseous form and b) is only partly removed by cleaning devices such as desulphurisation units and particle filters or captured by the fly ash. Just after combustion, at temperatures above 700 °C, Hg is present almost entirely in elementary form. Below this temperature gaseous molecular species exist and below 300 °C also liquid or solid compounds. Molecular species (mainly $HgCl_2$) dissolve well in aqueous solution whereas elementary Hg does not dissolve and passes through wet scrubbers unhindered. The present EU-directive for Hg, which gives an upper limit of 50 $\mu g/m^3$ (daily average) [14] for power plants, would require a removal rate of 90%. With a vapour pressure of about 2 bar at 400 °C, Hg will not be sufficiently controlled by a high-temperature barrier filter. Thus additional devices containing catalysts or sorbents such as zeolite or active coal are needed. Similar problems exist for arsenic and antimony, which are mostly present as the trioxides As_2O_3 and Sb_2O_3, also with relatively high vapour pressures.

Other investigations concerned with controlling heavy metal release in combustion [142–146] include Yao et al. [142,143], who screened sorbents for capturing Pb and Cd during sewage sludge combustion. Wendt and Lee [144] studied the sequestration of a series of volatile and semi-volatile metals including Hg, Cd, Pb and Na in a 20 kW downflow combustor and then in a quartz reactor. For the latter three metals, work was concentrated on kaolinite and lime powders, whereas for Hg, mixtures of kaolinite, lime and calcite were used. At high-temperatures, the sorbents undergo chemical and morphological changes which markedly affect the mechanisms of capture. Quantitative rate models were developed to describe reactions of kaolinite with Pb, Cd, and Na vapours. Another laboratory-scale investigation [145] in a furnace at 700 or 1000 °C considered the capture reactions of Cd and Pb in flue gases by in-situ generated nano-sized sorbents (an intercalated clay and two silica and titania). These large surface areas of these sorbents allowed nucleation of Cd and Pb vapours to be suppressed effectively.

In the case of alkali species, (ceramic) hot gas filters operated in the 700–900 °C region need to be installed before the entrance to a turbine [147,148], where the hot combustion gas has to be used directly. Alkali concentrations have to be reduced to ppb levels to avoid corrosion and related problesm and in the case of biomass fuels, such as straw, this poses enormous challenges. To sequester alkali species and ensure they are removed from the vapour phase, additives such as clay minerals, e.g. kaolinite [149–157] may be added to the process. Alternatively, fuels giving high alkali release may be co-combusted with a fuel (such as coal) containing clay minerals [123]. A further method involves adding salts such as ammonium sulphate [158], which leads to formation of alkali sulphates which are less harmful than the chlorides with respect to corrosion effects. It is also possible to reduce agglomeration in fluidised beds by co-combustion. For example, Lundholm et al. [159] found significant effects on combusting peat fuels (as little as 5%) with forest fuels in the temperature range 760°–1020 °C.

2.6. Need for on-line monitoring

As this short overview shows, many situations arise where continuous (time resolution 1 min or less) on-line monitoring will be essential or at least advantageous for economic and/or environmental reasons. In particular, abatement devices for all metals to be controlled will need to be operated in conjunction with on-line measuring devices in order to verify their effectiveness, especially during plant start-up or on changing the fuel or operating conditions. For example, gas quality between hot-gas filters and turbine entrance in combined-cycle plants has to be continuously assured. Gas quality is also important for NO_x catalysts with respect to deactivation by alkali or other metals combined (potential) combustion/gasification –fuel cell systems of MCFC- and SOFC-type. Even ppm quantities of alkali can cause catalyst deactivation. A real-time measuring system that collects and integrates signals over 1 min or less will record short-term concentration peaks. In addition, a non-intrusive and in-situ (and therefore optical) system also dispenses with the need for physical sampling. In contrast, conventional wet-sampling methods, which may require up to several hours of material collection, only provide average values for the time sampled and so peak values will be averaged out.

In addition, continued research using on-line monitoring is needed to understand kinetics and mechanisms of metals capture and release under a wide range of conditions and fuels as well as for

different sequestering materials (including minerals). Deposition and gas/particle partitioning represent further topics that need study in the real-time mode.

As noted in Section 2.1, emission limits are now in force in the EU, US and other countries, with the consequence that extensive measurements will become increasingly necessary and for the reason cited above, long-term averages will not be sufficient to prove full compliance.

3. Requirements for quantitative on-line measurements

3.1. General aspects

When designing an optical access or a sampling system for on-line measurements of metal species, careful consideration of the process conditions has to be made. Many power plants are pressurised in the range 10–50 bar, though some operate at atmospheric pressure. In power generation systems, hot (flue) gas produced in the combustion or gasification process will normally be used to drive a turbine. Depending on the firing concept, the requirements for hot gas cleaning and desired monitoring location, temperatures at the intended measurement point can be anything from 600 to 1800 °C. On the other hand, in blast or glass furnaces, incinerators etc. the flue gas will generally be cooled and monitoring is then performed in the *stack gas* between 100 and 350 °C. High pressures and/or temperatures lead to major challenges for optical measurements, especially as a result of strong absorption of excitation light beams in the UV by gases such as CO_2, and O_2 in the measurement volume. In addition, interference is caused by scattering of light by particles and undesired background emissions e.g. from glowing hot pipes and walls.

In combustion environments, the flue or stack gas will consist largely of N_2, CO_2, O_2 and H_2O with minor amounts of CO, NO_x and SO_2. In gasification environments, the main components of the process gas are N_2, CO, H_2 and CH_4 with traces of H_2S, NH_3 and several other species. In addition, the particle load can vary enormously, again depending on the conditions at the chosen position of monitoring, such as directly after the combustor, after a cyclone, hot gas or particle filter or other cleaning or cooling sections of the plant. For pyrolysis, the main products are CO, CO_2, H_2 CH_4, C_2H_4 and C_2H_6 with small amounts of larger hydrocarbons. The proportions of the components depend on the severity of the cracking process. In general, the main chlorine species are usually HCl and the alkali chlorides, but their respective amounts in the flue gas depend strongly on the combustor/gasifier temperature and the (relative) amounts of alkali and chlorine in the fuel.

3.1.1. Detection of metal species – spectroscopic data

For the development of quantitative optical detection schemes, a thorough study of the relevant spectroscopic data is required. Here, just the principle sources of basic data are mentioned. Details of specific excitation and detection strategies are discussed in the appropriate sections of Section 4, including the changes in spectra at the temperatures and pressures relevant to industrial conditions.

a) *Atomic species*: Spectroscopic data for many atomic species can be found, for example, in the NIST database [160].
b) *Molecular metal species*: The main gas phase species of interest in combustive systems are chlorides, oxides, sulphides and hydroxides. Spectroscopic data for many metal compounds are available; a good review of work up to 2000 is presented in Ref. [161] and a review of diatomic 3d transition metal oxides in Ref. [162]. For NaO and LiO fluorescence spectra in the visible have been recorded and assigned to the $C(orB)^2\Pi$-$X^2\Pi$ transitions of these molecules [163,164] and for NaO, infrared spectra corresponding to the $A^2\Sigma^+$–$X^2\Pi$ transition have been observed [165]. In contrast, the alkali chlorides and hydroxides are dissociative and so cannot be detected by molecular spectroscopy. Spectra of a number of heavy metal molecules of interest in combustion have been recorded in the IR, visible and UV including AuO [166], CuO [167], CuS [168], PbCl [169], PbO [170], FeO [171], FeCl [172], VO [173], VCl [174], NiCl [175,176]; $NiCl_2$ [177], PtO [178]. However, even though metal species are in the form of small molecules, many of them show a large proliferation of energy levels, leading to highly complex spectra. This will make it difficult to develop an interference-free, quantitative detection scheme. Therefore detection of atomic species via photofragmentation (Section 4.2.3) as described below may be a simpler solution.
c) *Non-metal species*: For development of detection schemes, in particular to determine possible spectral interferences, detailed information on important combustion species such as O_2, H_2O, HCl, NO, N_2O, SO_2 etc. should be obtained. The best source for these is the HITRAN database [179].

3.1.2. Temporal resolution

Industrial processes will increasingly require fast-responding, continuously monitoring instruments that facilitate rapid control of offending species. If the time resolution needed is on the order of minutes or less, the measurement technique has to be on-line, i.e. the process has to be probed directly and continuously – whether using sampling or direct optical access. Data can often be collected with frequencies down to 1 Hz, but for many purposes, resolutions of minutes may be sufficient and furthermore, signal-to-noise and hence sensitivity is improved by appropriate signal averaging. Obviously, if gas composition, pressure and/or temperature vary significantly in the course of the measurement, data on these parameters will also be needed at the same resolution as the metal species of interest, for evaluation and interpretation.

3.1.3. Detection limits, speciation, discrimination of physical phase

There are many challenges in obtaining quantitative data under realistic industrial conditions, whether they concern energy production, waste disposal or other services or production processes. On one hand, environmental regulations for a range of heavy metals are becoming ever more stringent and are being extended to further types of installations. For species that cause materials damage, such as alkali compounds at the entrance to turbines, even ppb limits may be set [38]. Measurement of such low concentrations with high time resolution (1 min or less) necessitates ultrahigh sensitivity. On the other hand, a sufficient dynamic range is also required. For combustion or gasification of fuels with high metal and chlorine content and for reactor temperatures >1000 °C, quantities of some species in the flue gas may reach levels in excess of 1000 ppm. In some cases, determination of the total species concentration present in the flue gas is sufficient. In others, the dynamics of metal condensation on particles may be of interest, so discrimination of physical phase (i.e. particle vs. gas phase) will be needed. Such discrimination may be realised using two complimentary methods, as discussed in Sections 4.2.3.1 and 5.5.1.

3.1.4. Calibration

In general, this topic can refer to all or part of the quantification of raw measurement data to obtain absolute concentrations. Depending on the specific features of the method in question as well as measurement and evaluation practice, calibration can be defined in different ways. For emission measurements, where the light to be detected is scattered isotropically in all directions,

calibration can be defined initially as the characterisation of the optical geometry at the measurement point i.e. how much of the light emitted can be collected and imaged on to a detector or optical cable. The calibration in this sense should also include other optical factors such as lenses, filters, optical cables etc as well as electrical settings (sensitivities etc.) in the detection system. So defined, the calibration is obviously independent of the conditions of temperature and pressure in the measurement volume and is performed by measuring the species of interest at a *known* temperature, pressure and species concentration. It does not have to be performed under any *specific* set of temperature or pressure conditions. On the other hand, in some applications, calibration may be defined to include other factors such as fluorescence quenching by gases in the measurement volume, which are temperature and pressure dependent. Precision and accuracy depends on the specific technique and methodology of interest as well as on the time or number of scans over which data are averaged. Examples of specific figures of merit are therefore given in the individual chapters of chapters 4 and 5.

An in-situ calibration of an optical method in an industrial plant during actual operation is seldom feasible, but can sometimes be performed in small bench-scale reactors. For example, in work described in Ref. [180], a quantity of the substance was suspended in the measurement volume in the reactor and heated. The signal was then measured as a function of temperature (and hence of vapour pressure). However, during the calibration measurements, the reactor itself was not actually running and the substance of interest was a stable compound. On the other hand, in a continuously operating, reactive system, if the form of the substance monitored changes upstream of the probe (measurement) region, this can lead to significant interpretative errors. In addition, concentrations of accompanying species (e.g. O_2) in the flue or stack gas frequently change, introducing variable effects such as optical transmission (Section 4.2.4.1) or collisional quenching of emission (Section 4.2.4.2). Thus important gas components need to be monitored separately at a sufficient time resolution to allow for appropriate corrections to measured signals.

Nevertheless, an external calibration in a flowing or static cell under standardised conditions can be satisfactory, provided that the optical geometry is close to that of the combustion system and any chemical or physical side effects (e.g. dimerisation, diffusion) can be accounted for. Alternatively, raw data may also be quantified using another method, such as calibration of fluorescence using optical absorption measurements [181] ,refs.therein]

Emission measurements. Operators of emission methods usually quantify their raw data by measuring signals from known quantities of the species of interest in a standardised system at known temperature and pressure. Such a system can be a simple flame on a well-characterised burner [182] or a heatable static [183] or flow [183] cell. In each case, the same optical set-up and electronic settings as for the actual measurements are used. In the case of a flame, standardised solutions of the metal species are nebulised into it. If using a cell, a quantity of the metal salt is vaporised from a salt reservoir into a known atmosphere of gas (such as N_2) in the cell [183,184]. For this purpose, the vaporisation behaviour of the species of interest with temperature has to be known. This entails obtaining the appropriate Clausius-Clapeyron or Antoine parameters, which can normally be calculated from thermochemical data (such as Ref. [185]). If the species of interest is not a stable commercial product, it may be produced, for example, by thermal dissociation or a collisional process, from a suitable precursor. However, the certainty with which calibration factors can be determined by such methods depends on how well the vaporisation curve is known and also on the accuracy with which the temperature can be determined.

Absorption measurements, in contrast to measurements performed by emission methods, are essentially self-calibrating, since there is no geometrical dispersion of light. However, both the absorption coefficient of the species of interest and the path length must be known (Section 4.1).

Finally, it should be mentioned that ultimate acceptance of a measuring technology in commercial plants normally requires an (additional) calibration by an independent reference method [186].

3.2. Equipment requirements

3.2.1. Optical access, optical geometries

Applicability: Optical measurements are described as being both on-line and *in-situ* if the species of interest is observed directly by purely optical means without extracting material from the process. This requires that ports holding windows be installed at the measurement point. In industrial-scale systems, the large dimensions and often high pressures and temperatures involved make high demands on optical access design, including materials for flue gas piping, flanges and windows. The large dimensions also mean that light sources with high spectral densities (such as excimer lasers) will be needed to overcome strong beam absorption in pressurised, dust-laden flue gas, especially if short UV-wavelengths are involved.

The (in-situ) optical access design is applicable if the metal species of interest is directly detectable in molecular form (e.g. by DOAS or LIF), already atomised (AAS, TDLAS, CRDS) or can be atomised and/or excited by a light source (laser or lamp)(atomic LIF, PFF). On the other hand, if a spark, furnace or flame or plasma is needed to atomise the metal compound, the gas has to be sampled first (except for LIBS). Mass spectrometric methods (MBMS, SPMS) require special types of sampling interface. A sampling facility will also be needed if the conditions at the measurement point (dimensions, pressure, temperature etc.) are such that construction of a direct optical access is technically not feasible. Sampling methods are considered in Section 3.2.5.

Optical arrangements. Fig. 1a–e shows several different geometries for in-situ measurements. Their applicability depends on the dimensions, design and materials of the flue gas pipe as well as the excitation and detection scheme to be used. In geometries 1a, 1c, 1d and 1e, the recorded signal is a measure of absorption or emission across the path of the light source, so line-of-sight information is obtained. In geometry 1b, in contrast, a point measurement is made. Although not shown here, a facility for flushing the windows will most likely be needed in all geometries, to keep the optical surfaces clear of particles in the flue gas flow. As flushing gas, nitrogen or other non-UV-absorbing gas should be used.

Fig. 1a is the usual arrangement for absorption and has occasionally been used for *forward scattering* emission measurements. However, the forward scattering arrangement can only be used for emission measurements if the exciting light can be effectively separated from the emission signal using dichroic mirrors, as was done in the work of Ref. [187]. This may reduce the sensitivity for some wavelength regions due to changes in transmittance.

Fig. 1b is the more common geometry for fluorescence and is also applicable when the exciting and detection wavelength are similar or the same, since scattered light from the exciting source can be better separated from the fluorescence. Other advantages are that the measurement volume is well defined and the optical transmission can be measured directly, as long as the laser beam is measureable on the opposite side of the pipe. The main disadvantage is that several access ports are required and in an industrial application, this leads to higher effort and expenditure in construction and in fulfilling safety requirements. In addition, where UV-wavelengths and high pressures and temperatures are

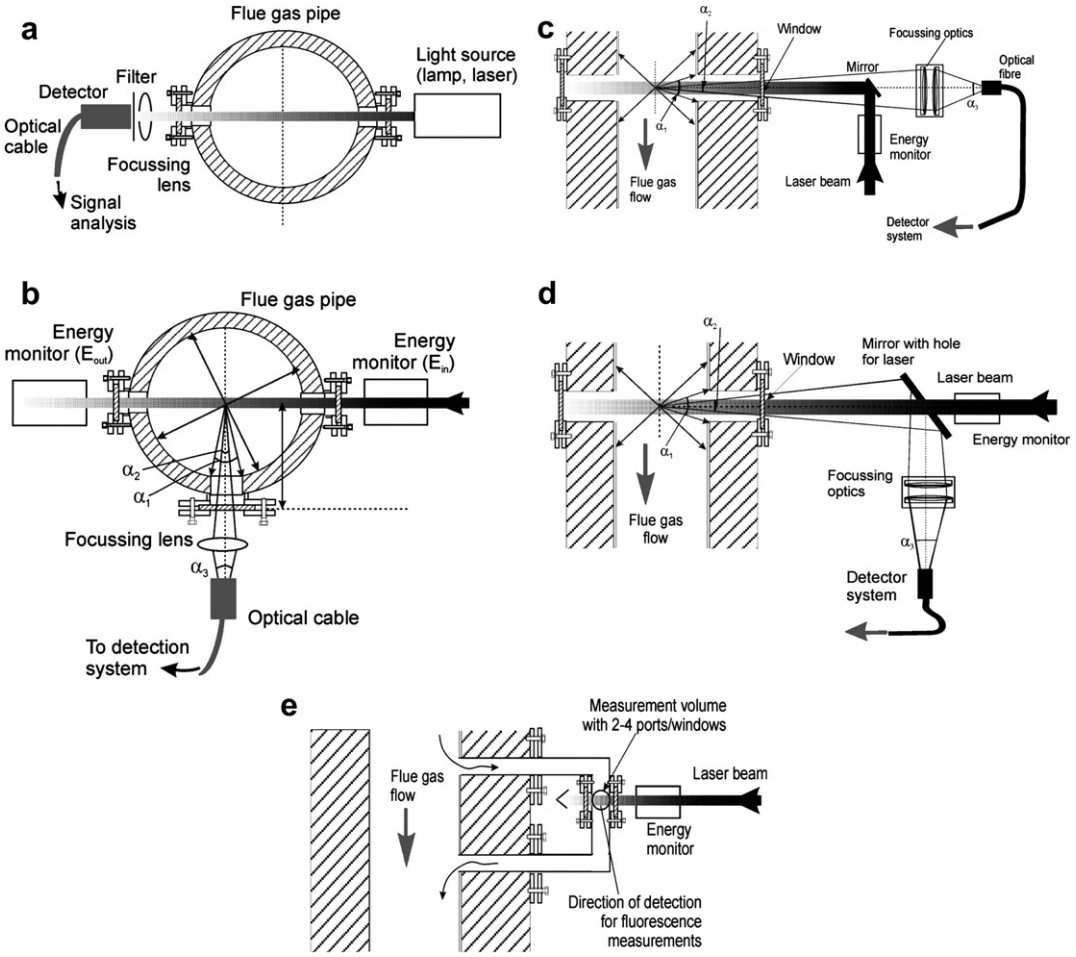

Fig. 1. a. Geometry for absorption measurements (occasionally also used for fluorescence in the forward scattering mode, though with dichroic mirrors to block the excitation beam). b. 90°-geometry for fluorescence measurements.c. Optical geometry for fluorescence (backscatter mode I). d. Optical geometry for fluorescence (backscatter mode II). e. By-pass arrangement for large flue gas pipes.

involved, geometry 1b will not be adequate for measurement distances of more than 10–20 cm, since the exciting light will not reach far enough across the intended measurement region. This problem may be solved by choosing the arrangement of Fig. 1c or d or the bypass arrangement of Fig. 1e.

The *backscatter* geometry for fluorescence measurements shown in Fig. 1c and d requires only one access port and thus a single pressure interface. This means that the construction effort is much less than for geometry 1b and that the light beam does not have to reach across the pipe. A few centimetres may be sufficient to generate a signal. The design shown in Fig. 1c was selected for the work of Ref. [188] whereas the arrangement of Fig. 1d was chosen by Farnsworth et al. [189]. Both these geometries require that the detection and excitation wavelengths are quite different. For example, in the case of Ref. [188], excitation was performed at 193 nm and detection at 589 or 769 nm. The two arrangements are functionally equivalent, though 1c has the advantage of direct focussing on the optical fibre. In deciding for one option or another, as well as optical considerations, the feasibility of construction, mechanical stability, ease of installation, adjustment and exchange of components should be considered.

Disadvantages of the single-port access are:

i) The optical transmission, needed for evaluating the measured signals, cannot be measured simultaneously with the fluorescence signal. If there are no particles present, the transmission may be calculated using literature data and the composition of the absorbing gases (Section 4.2.4.1). Otherwise separate transmission measurements have to be performed under the conditions of interest and the data included in the evaluation. However, if a second optical port is available on the opposite side of the pipe, then direct transmission measurements may be feasible. Then the raw fluorescence signals can be corrected (post-measurement) with the appropriate routine in the evaluation programme.
ii) The measurement volume is less well defined than with the 90°-arrangement. If there is a strong and rapid variation in temperature, leading to strong changes in refractive index, some way to determine the transmission directly must be found.

Geometrical considerations. In this respect, the access is characterised by the *angle of acceptance.* This term can refer to two different angles (Fig. 1b–d):

i) The angle, with which a point X in the measurement volume contributes to the measured signal (α_1, α_2). This angle depends on the distance *d* of this point X to the opening of the measurement probe (usually the window) and the distance from the line of symmetry. Also of interest is the *relative* acceptance angle (α_1/α_2), i.e. the angle from the first point, where a signal could (in theory) be collected, to that at the actually feasible measurement point.

ii) The maximum angle, with which light can be imaged onto a detector or optical fibre (α_3). In the case of the detector, the size of the angle depends on the size of the receiving surface. In the case of an optical fibre, the angle is set by the acceptance angle of the fibre itself.

Thus optical parts (lenses etc.) have to be chosen and arranged to optimise the collection of light by the collecting surface.

For illustration, two examples are given below for the case of emission measurements. i) a small-scale 90°-arrangement (Fig. 1b) (shown for example in [190]; ii) a single-port arrangement (Fig. 1c) [188].

i) For a distance of 100 mm through the flue gas pipe, such that the earliest detection point is 120 mm from the centre of the measurement cell. The window diameter is 30 mm, giving a full angle of 14°. The distance from the centre of the tube to the cell window is 18 mm and gives a full angle of 40° and a relative acceptance angle of 0.35.
ii) In the actual design corresponding to that of Ref. [188], the access window was mounted on a ball (safety) valve, then on a transition flange and finally on the flange of the flue gas pipe. The total distance from the valve to the beginning of the flue gas area was 460 mm. Since the opening of the probe to the flue gas was 10 mm, one obtains an acceptance angle of 1.6°.

Dimensional considerations: Whatever geometry is preferred, the size of the measurement area is still a critical factor and as mentioned above, difficulties resulting from strong beam absorption in the UV at elevated temperature and pressure may limit the range of conditions that can be investigated (Section 4.2.4.1) or may force an alternative arrangement, such as allowing for a bypass flow in a narrow pipe, which would hold the optical access.

Window materials: For the types of applications under consideration here, the most usual materials are sapphire and quartz. A variety of optical data, mechanical properties and chemical resistances can be found on the web sites of various optical companies as well as Refs. [191,192]. However, for extreme conditions, for example, temperatures above 1600 °C, great caution is needed. For example, the melting point of sapphire is 2000 °C, but Ref. [189] gives a maximum usage temperature of 1600 °C (cf. quartz 1100 °C), because above this temperature it looses it structural integrity. In addition, following laser irradiation, considerable transmission losses can be expected, especially below ca. 250 nm.

Roeloffs et al. [192] report experience with optical accesses in a combustion facility operated at 31 bar and up to 2052 °C. These authors tested several different optical designs with sapphire or quartz as window materials. They found that for these conditions, a cooling system in the window area would be essential. However, not all reactor systems are amenable to the inclusion of cooling systems and in such cases the operating temperature has to be restricted accordingly.

3.2.2. Atomisation and excitation of species – light sources

Depending on the temperature and chemistry at the measurement point, the metals to be detected can be present in atomic or molecular form. For example, for alkali species below ca. 1000 °C, most species will be present in molecular form. Very commonly, detection is by atomic emission or atomic absorption spectroscopy, so that the species must first be atomised, either in a plasma or thermally (in an electrothermal atomiser, discharge or flame or on a heated surface) or optically with a UV-light beam. If detection is by *induced fluorescence*, especially using excitation wavelengths below ca. 250 nm, only laser light sources will provide sufficient spectral intensity to allow penetration of the measurement volume *and* specific excitation of molecules. As will be shown in Section 4.2.4.1, if a UV-light source below 250 nm is to be used, it is advisable to estimate the probable degree of beam absorption by gases (such as O_2 or CO_2) in the measurement volume before planning experimental details.

Much development work has been done on excitation schemes for a wide range of metal species using atomic fluorescence; examples are described in Section 4.2.2.1. Up to now, most of this work was performed with dye laser systems, since previously these were the only widely tunable light sources. Since the mid-1990s, however, solid-state systems (Ti-sapphire or Nd:YAG-OPO) with tuning ranges from 440 nm to 2 μm and pulse energies up to hundreds of mJ have become available, which would be more rugged and reliable for use in industrial applications than dye lasers. These lasers can also be frequency-doubled or -tripled to the UV as required.

An interesting possibility for both absorption and fluorescence measurements is now offered by tunable diode-pumped solid-state lasers (DPSS); these offer wavelengths that are not accessible with standard diode lasers. These very compact diode-pumped crystal lasers, which include Nd:YAG, Nd:YVO_4, Nd:YLF and Yb:YAG lasers, are available in CW- or Q-switched versions and feature single longitudinal mode (SLM) and TEM00 operation with low amplitude noise.

For *absorption* measurements, lamp sources (such as xenon or hollow cathode lamps) may offer adequate intensity for some applications, but are normally not tunable. For species-specific detection down to the red region of the spectrum and, using frequency doubling or mixing from the red or special GaN-diodes, to the near UV, tunable diode lasers (TDLs) have often been the light source of choice. This topic is considered further in Section 4.1.

3.2.3. Detection systems

Effective spectral (and/or temporal) discrimination of the light from the species to be detected against background light and other interferences is an essential aspect of detection. This section considers general aspects while spectroscopic aspects of detection strategies including specific background suppression/correction methods are discussed in the relevant parts of Section 4.

Depending on the overall requirements of the system, spectral and temporal discrimination can be effected in two basic ways:

a) Set of interference filters + photomultiplier (PMT) + Signal integrating system (boxcar integrator). This type of system is suitable for 1–3 simultaneous detection channels (as, for example, in Fig. 2). Modern dielectric interference filters allow greater compactness and higher light collection efficiency. In the wavelength range 214–404, filters are usually available down to FWHM (=full width at half maximum) of 10 nm with transmissions of 10–30%, but for some wavelengths 3–5 nm widths are obtainable. Filters in the range 430–750 nm can also be made with FWHM between 0.8 and 0.15 nm, according to customer requirements. Instead of a multichannel system with spectral filters, a Rowland polychromator can be used with several PMTs and boxcar integrators for multi-element detection.
b) A multichannel plate (MCP)-system may be employed to obtain time resolution instead of the PMT/Boxcar integrator combination. In this case, a spectrometer such as the Czerny-Turner type combined with a multichannel analyser (MCA) or an échelle or Czerny-Turner spectrometer + ICCD- or CCD-camera will be needed. These types of system are also suitable for multi-element detection. Broad experience with different

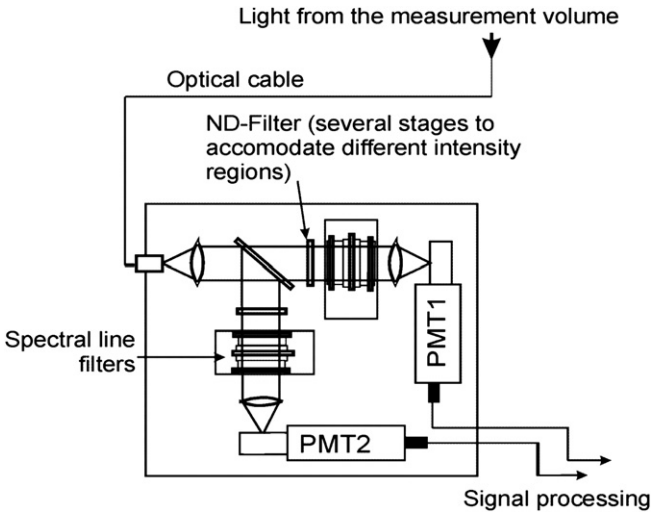

Fig. 2. Two-channel detection system.

spectrometer/camera combinations has been obtained. The ICCD-camera with its gating facility has often been favoured, especially in LIBS measurements for discriminating against broadband emission in the early stages of the plasma [193,194]. The ICCDs can be advantageous when detecting weak signals on a strong background. However, care should be taken when making comparisons, since different spectrometer/combinations and light collection geometries are not equivalent in light collection efficiency and throughput. More recently, it has been shown that a CCD-camera with a mechanical chopper can produce signal-to-noise ratios and detection limits as good as or even better than the ICCD-camera [195]. This results from the higher quantum efficiency and lower noise of the CCDs. In addition, the CCDs are generally less costly than the ICCDs.

For absorption spectroscopies such as TDLAS, a Si photodiode is normally used as a detector, together with a suitable interference filter. The photocurrents measured by the photodiode are then preamplified, digitised by an A/D-converter and stored. Background noise has conventionally been suppressed by mechanical modulation (choppers) together with phase-sensitive detection but frequency modulation devices are now more common.

In all cases, the use of fibre optics will simplify the transport of light from the optical access to the detection system, though there are some limitations for UV-wavelengths (Section. 3.2.4).

3.2.4. Transport and collection of light

Light delivery to the measurement volume. Light from the chosen light source (laser, lamp) can be delivered to the measurement volume in three different ways.

i) Direct coupling with mirror- and/or lens arrangements (Fig. 1a–d). This type of solution allows for conservation of beam coherence and polarisation (as long as no polarising optical components are used) as well as beam quality. Disadvantages are (in some spatial situations) that positioning can be inconvenient and that if the measurement object is subject to vibrations, the optics will also be. In some cases, the latter problem may be solved by mounting the receiving and collecting optics onto a small platform and affixing this to the exterior of the measurement object.
ii) Articulated arm (as used, for example in medicine or material processing). Here again, beam quality, coherence and polarisation are conserved. However, commercial arms are relatively expensive and may have limitations in positioning and flexibility.
iii) Fibre optics. This option offers the highest flexibility and can be easily removed and replaced e.g. to move the measuring point to different positions on the reactor or flue/stack gas pipe. Cost is moderate. However, light coherence and refocusability are affected. With multimode fibres, any pre-existing polarisation is destroyed. For polarised light, however, "Polarisation Maintaining"(PM)-fibres are available, which are also single-mode. However, it is doubtful at present, whether such fibres will work well in the far-UV, for example, at 193 nm, particularly if laser energies of millijoules or more have to be coupled into the measurement volume.

In cases i) and ii), depending on the distances from the light source to the optical access involved, the light energy density and the size of light beam, focussing or shaping optics may be required. Special windows, such as Brewster windows, will be required for laser absorption measurements. In case iii) corrective optics may be required if the incoming light has to possess specific properties (coherence, polarisation etc.).

Light collection and detection. Having considered the geometrical situation and light transport to the optical access, as discussed above, the optical set-up can be designed: this will generally consist of a suitable focussing system (lenses, mirrors etc.) and mountings, according to specific requirements.

Beam alignment problems. Difficulties in aligning light beams for measurements at high-temperatures and pressures are common, especially when conditions are fluctuating. One reason is the resulting fluctuations in density and hence in refractive index. In any case, adjustment needs to be done when the reactor is operating and may need to be repeated periodically. Alignment problems can also arise as a result of mechanical vibrations. Important here is the choice of optical components (including detectors) of sufficient diameter.

3.2.5. Sampling lines and sampling trains

Metal-containing samples can be collected by direct sampling, by adsorption onto specific materials or by condensation. If gas is to be extracted from the flue or stack pipe for analysis, a sampling line should be constructed that is made of an inert material and kept at or as near as possible to pressure and temperature conditions within the pipe or reactor. In any case, the temperature of the sampled gas has to be maintained above the dew point of the metal species. Even then, sampling is not always straightforward, since metallic vapours (such as Na, K, V, Fe, Zn) can interact chemically and/or physically with reactor or pipe materials, leading to various sampling artifacts [41,196]. High purity alumina has often been favoured for probe lines at the flue gas [197,198]. Information on high-temperature materials, including their corrosion behaviour, can be found in Ref. [199]. Errors caused by interactions with the sampling line materials can be minimised by using a short ($<$1 m), simple tube, avoiding valves etc. as far as possible and by ensuring that at least some gas flows through the tube even when data are not being recorded.

Direct sampling from process gas. Sampling with on-line analysis. The flow of gas to be analysed, typically 2–5 l/min, is lead to the measuring system through short sampling lines, which usually consist of a sampling tube (ca. 0.5 m) with feedthroughs for thermocouples and heating currents. Condensation in the sampling tube is minimised by maintaining the process pressure during measurements, restricting the length of the sampling tube and by heating the entire tube to above the dew point of the species of interest (e.g. for alkali ca. 900 °C). In addition, contamination of the

sampling line and feedthroughs can be minimised by allowing for a small nitrogen flow when the line is not in use. Such sampling lines are used in (non-plasma) optical methods as well as surface ionisation (Section 4.4.1) [127,148]

For mass spectrometric studies, two main types of interface to the technical process are available. For molecular beam mass spectrometry (MBMS), a three-stage pumping system to successively lower pressures is normally used. Flue gas to be analysed is drawn through a small orifice, expanded into a free jet and then collimated into a molecular beam before arriving at the ion source of the mass spectrometer. This type of system is well established for combustion studies [65,66,154] and minimises chemical reactions and condensation of the gaseous molecules in the sampling process. For single-particle mass spectrometry (SPMS), the inlet system consists of an orifice of about 100 μm diameter and an aerodynamic lens system with several orifice lenses along the inlet tube. As a result of successive compressions and expansions of the particles on their way through the lens system the particles form a narrow collimated beam. Basic principles and several SPMS systems are described in Ref. [200].

In plasma methods, with the exception of LIBS and SIBS (Section 4.3) gas samples are first drawn from the process gas to fill a sampling loop, valves are then switched and the sampled gases forced into the plasma. In this way, gas is sampled isokinetically, usually at flow rates of several tens of 1/min. However, the duty cycle limits exposure times for the optical measurements and time is lost during plasma equilibration. In addition, particles can be lost at the slower velocities used for sample injection.

Sampling with off-line analysis. Up to now, most trace element sampling in industrial applications has employed manual sampling methods, most of which are based on wet chemical sampling from the flue gas. The samples are collected by impingement into a series of washing bottles (impingers), which contain water or dichloromethane for alkali species [115,201] and nitric acid in the case of trace metals [202]. The impinger solutions are then analysed off-line by AAS, AES, ICP-MS, XRD (X-ray diffraction) or NAA (Neutron activation analysis). Normally at least one cubic metre of gas has to be extracted, in order to have a sufficient amount of the species of interest for an accurate analysis. This is time-consuming, typically requiring extraction periods of 1–2 h and obviously provides only one average value for the period in question. The sampling system must also be able to remove dust particles in the flue gas. However, care is needed to ensure samples are not changed on their way through the impinger system. For example, mercury has been found to be oxidised to the dichloride by SO_2 and chlorine in the first impinger, leading to an overestimate of the degree of mercury oxidation [203].

Manual sampling with off-line analysis includes standard (batch) methods of determining metal concentrations from the flue gas such as the EPA Methods 101A and 30A (mercury) and 29 (multimetals) [204] or the Ontario Hydro-Method, ASTM standard for distinguishing elemental, oxidised and particulate mercury [205]. In addition, the European Standard EN 13211:2001, has been validated for the determination of total mercury in waste incinerator flue gas, but cannot discriminate between the three forms of mercury [206]. A multimetal method EN 14385, for the determination trace elements in waste incinerator flue gas is also available [207].

Sampling by adsorption. Extensive studies of adsorption of metal species onto different materials have been carried out; materials investigated for adsorption of alkali species include activated bauxite (SiO_2 7–10%, Al_2O_3 81.5–88.0%) and diatomaceous earth (SiO_2 92%, Al_2O_3 5%) [150,208–211]. Efficiencies obtained for removing alkali from simulated dry flue gas were 93–98% for activated bauxite and 96–98% (NaCl/KCl) and 72% (K_2SO_4) respectively, for diatomaceous earth [209]. Bed material from PCFB has also been used as an adsorption material [212]. After the adsorption process, the material is washed with water, dissolved in concentrated HF + $HClO_4$ and then analysed by atomic absorption spectroscopy (AAS) for the metal species.

Based on the knowledge from these adsorption studies, Lee and co-workers [198,209,210] developed sampling systems for alkali species. In the analytical alkali sorber bed (AASB), the flue gas passes through a ceramic filter before entering the bed. Each section of the sorbent is then dissolved in water by NH_4HF_2-fusion, transferred to a flame photometer and analysed by atomic emission spectroscopy (AES). Alternatively ICP/AES may be used.

Sampling by condensation. In this category, the only system that allows *on-line* sampling and real-time measurements of metal-containing species is the *Condensation Interface*, which works by rapidly quenching the process gas using a cold water aerosol vapour mixed in a counter current. In this way, a constant fraction of the metals in the cooled carrier gas can be transferred to the analyser. Such a system, using analysis by ICP-AES, has been reported ([213] and Section 5.6.1).

Other condensation methods operate by conventional batch sampling, requiring sampling times of up to several hours, depending on the concentrations to be determined, flow rates etc. Analysis is then performed *off-line.* Concentrations so determined are average values for the period of the sampling time and sudden concentration peaks due to process instabilities etc. will be averaged out. Batch condensation sampling involves a) extracting process gas from an off-gas stream into a heated probe line (where quartz or zirconia fibre filters may be used to remove particles [115,210,214,215]; b) subsequent cooling of the sampled gas to the required temperature. In the case of alkali species, these can be cooled below their dew point by water or air [115,214,216]. For other trace metals, steam-cooled condensers have been used to maintain the sample at 200 °C (above the dew point) and so avoid corrosion [202]. Sampling by condensation has been employed for collection of process gas e.g. from PFBC/G effluents [115,215], from the air blown gasification cycle (ABGC) [136,137,202], and at the PFBG facility of the UK Coal Research Establishment [197]. A variant method in this category is cryogenic sampling [217], where volatile metal species are collected in a trap at −175 °C and then analysed using low-temperature packed-column GC with ICP-MS detection.

3.2.6. General features of equipment

As stated in Section 2.6, industrial monitoring devices need to be capable of fast response and continuous on-line measurements. Other key factors are robustness, compactness and straightforward operation. In addition, thermal isolation and/or cooling of the measuring equipment may be needed to facilitate operation thereof in hot environments. Optical and electrical parts will need shielding from dust and leakages of water or other materials.

In recent years, several direct on-line methods have been developed, based on surface ionisation (SI), plasma excitation (PEARLS, LIBS, SIBS, ICP-AES), photofragmentation fluorescence (PFF), differential optical absorption spectroscopy (DOAS), tunable diode laser spectroscopy (TDLAS). Of these, LIBS, PFF, DOAS and TDLAS can analyse process gas for metal species by non-intrusive *in-situ* spectroscopic detection. The other methods are in some way intrusive and/or not truly *in-situ*. The fundamentals and development of these techniques are presented in Section 4 while their capabilities and potential, demonstrated in actual field measurements, are described in Section 5.

If a UV-light source is required, excimer lasers offer reliability, transportability and simplicity of operation. As well as the high-

power models (100 mJ and upwards), there are also small-scale models on the market which are suitable for some types of field measurements, though these do not offer sufficient intensity for applications at high pressures and temperatures. Tunable solid-state lasers (diode lasers, Nd:YAG-Pumped-OPO(optical parametric oscillator) or Ti-sapphire systems), which can be tuned to specific transitions of metal species, will find increasing use, being very compact, transportable and robust.

4. Overview of on-line continuous measuring methods

This section reviews the general status of several on-line techniques, the applications of which are described in chapter 5.

4.1. Absorption

Absorption spectroscopy, in its various forms, is well-established for the detection of metal species in fundamental spectroscopic studies as well as in reaction kinetics [73,75,91,92,96]. However, only a few of the many variants have found application under realistic industrial conditions. These are conventional atomic absorption spectroscopy (AAS), TDLAS, DOAS and plasma-assisted spectroscopy using absorption detection (PEARLS/HEAMON). In addition, cavity ring down spectroscopy (CRDS) may have some potential for application and so is summarised in this section. Microwave absorption, indirect optogalvanic and "pump-probe" methods were discussed previously [218] but have not really progressed beyond fundamental studies at research level, so are not considered again here.

4.1.1. Fundamentals

Fundamentals of absorption spectroscopy were given in the previous review [218] as well as other reviews and books [219,220]. Nevertheless, a short summary is given here and the section is supplemented with some discussion on background suppression and line broadening effects. In general, measurement of concentrations by absorption methods is based on the Beer–Lambert Law.

$$I = I_0 e^{-\alpha n l} \tag{1}$$

where I_0 is the incident beam intensity, n the concentration of absorbing species, α is the absorption coefficient (constant of proportionality, usually given in units of atm^{-1} cm^{-1}) and l the path length through the sample in cm. The factor A is known as the *absorbance* ($=\alpha nl/2.303$) but normally it is the *transmittance* ($=I/I_0$) that is actually measured.

Absorption measurements are self-calibrating provided that the parameters l and α are known and that the detector behaves in a linear manner. If α is not available, it may be determined in a separate experiment under known temperature und concentration conditions. If, on the other hand, α cannot be determined with sufficient accuracy, then a calibration is needed. In addition, if the path length l varies significantly, such as on using purge gas, this will lead to increased uncertainty in measurements of concentration, regardless of whether a calibration is performed or not.

If the transmittance is measured using a finite-bandwidth spectrometer, the Lambert–Beer law has to be integrated over the spectrometer bandwidth:

$$I/I_0 = e^{-\sigma_b l} \cdot e^{-\sigma_{\mathrm{eff}} n l} \tag{2}$$

where σ_b is the background absorption coefficient and σ_{eff} is an effective absorption cross section defined as:

$$\sigma_{\mathrm{eff}} = \int_{\Delta\lambda} \phi_s \alpha_{\mathrm{tot}} \phi_g d\lambda \tag{3}$$

Here, φ_s is the normalised line profile of the light source, α_{tot} the total absorption cross section of the transition of interest, φ_g the normalised absorption line profile of the atoms to be analysed and $\Delta\lambda$ is the spectrometer bandwidth.

Optimising sensitivity. The minimum fractional absorption that can be measured with a conventional absorption instrument with low-noise sources is about 10^{-3}. To improve sensitivity, background noise has to be reduced: conventional methods employ mechanical modulation (choppers) together with phase-sensitive detection but frequency modulation devices are now more common. The use of *multipass* (White or Herriott) cells (Fig. 3) can also improve sensitivity [221,222] and background interference can be suppressed using the Zeeman effect [223], whereby a transverse magnetic field is applied to the absorbing sample. The measured transmittance then depends on the polarisation state of the incoming light. Today, absorptions of $\sim 10^{-5}$ or better and detection limits down to ppt levels can be achieved, although in industrial applications, minimum detectable concentrations are usually in the ppb or sub-ppb range.

Line broadening and shifting. At the high pressures and temperatures of many industrial processes, absorption lines of the species to be detected are usually severely broadened and shifted as a result of collisions with molecules in the measurement volume [219,220,224,225]. Typical spectral linewidths (FWHM) at 1 bar are 3–6 GHz and at 10 bar 30–60 GHz, compared to only about 1–2 GHz at 1 mbar. In the low-pressure regime, absorption lines can be fitted well to Doppler profiles, whereas at 10 bar, the Lorentz profile is the dominant component and the net result can be approximated by a line shape of Lorentz form. In the intermediate range, from 50 to 1000 mbar, Doppler and Lorentz profiles make comparable contributions and then the measured profile has to be fitted to a Voigt profile. This profile is mathematically more complex, but for the intermediate pressure range this is the only profile that gives a really accurate result.

Broadening and shifting of absorption lines has been investigated for atomic spectral lines of several metals such as K [226,227], Rb [228], Cs [229,230] Na [231]; Li [232], Pb [233,234], Hg [235], Sr [236], but only for a limited number of collision partners and pressure/temperature conditions. Thus in most cases, insufficient data on broadening of specific absorption lines are available for a reliable prediction of the total broadening and shift effects under combustion conditions. If the broadened/shifted absorption line can be measured in-situ in the combustion environment, as for K atoms [226], this is clearly the best way to determine the total (net) broadening and shifting effects. At 1 bar, the FHWM of the D1-line in a combustion gas mixture (ca. 1400 K) was measured to be

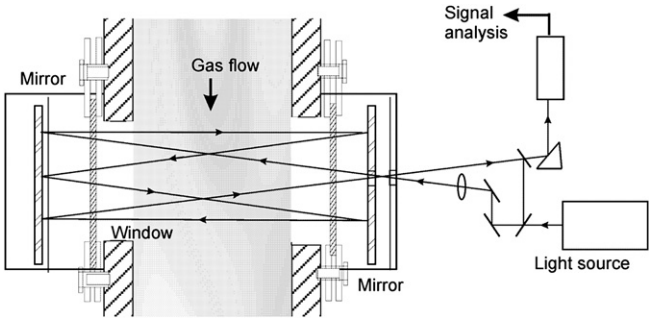

Fig. 3. Multipass arrangement (Herriott type) for absorption measurements.

(5.2 ± 0.5) GHz (0.17 cm^{-1}), compared to (0.9 ± 0.05) GHz measured in a low-pressure K vapour cell. The red shift of the line centre was (−1.2 ± 0.1) GHz (0.04 cm^{-1}). At 11.2 bar and 1540 K, the observed pressure broadening was (60 ± 4) GHz (FWHM), while the red shift of the line centre was (−20 ± 1) GHz, giving a broadening coefficient of (0.18 ± 0.01) cm^{-1}/atm and a line shift coefficient of (−0.060 ± 0.003) cm^{-1}/atm respectively. These values are much greater than those calculated for the O_2 lines using the HITRAN database; the P33Q32 line at the same temperature and pressure, the air broadening is 0.287 cm^{-1} or 8.61 GHz (FWHM)

In addition to Doppler and Lorentz (pressure) broadening, *hyperfine broadening* is a significant effect for many metals, but is usually buried beneath the envelope of the Doppler–Lorentz broadened line. Hyperfine splitting of atomic energy levels is caused either by the presence of isotopes with different masses or by the interaction of nuclear spin with its magnetic moment. This type of broadening is considered for Li, K, Rb [227], Rb [228], Cs [229,230] and in many of the references in Section 4.1.3. For example, the fine-structure splitting (Δλ) of Li is only 0.015 nm or 10 GHz, whereas in K, it is 3.4 nm and in Rb, 14.7 nm [227]. The hyperfine splitting broadens the Doppler absorption profile of K from a halfwidth at full maximum (HWFM) of 0.39 GHz–0.45 GHz at 298 K. However for Rb, the splitting distorts even the pressure-broadened absorption lines at 1 bar, as shown by comparing measured Rb(D2) absorption profiles in a combustor at 1273 K and in a low-pressure (<1 mbar), room-temperature cell; in the latter case, the four hyperfine lines of ^{87}Rb and ^{85}Rb were clearly resolved.

4.1.2. Conventional atomic absorption spectroscopy (AAS)

Atomic absorption with conventional light sources (lamps) is commonly applied for direct detection of various metals. Over the last decade, a fair number of commercial extractive on-line monitors have been developed, especially for mercury [237–239]. They usually include pretreatment procedures to remove fine particles and acid gases. Those methods that work with a dual measurement system can discriminate total and elemental mercury. Atomic Hg is measured directly by AAS (or AES) but molecular Hg must first be converted in to elemental form, either by a wet chemical step or in a dry system by a thermal catalytic converter. However, the relatively short lifetime of catalysts used in the presence of acid flue gas components such as SO_2, SO_3 and HCl is a limitation for the latter method. For their part, wet-chemical monitors require chemicals for operation and generate considerable quantities of waste. Nevertheless the development of these measuring systems is relatively advanced and some are already approved by national authorities (such as TÜV in Germany) for flue gas measurements at full-scale power plants.

The following examples show two ways that atomic and molecular Hg may be discriminated. The first system [240], samples stack gas continuously, which is analysed sequentially for elemental and total mercury. For analysis of total Hg, oxidised Hg species are converted (elemental Hg in a pyrolysis tube heated to 1100 °C. The elemental Hg concentration in the gas stream is then determined by bypassing the pyrolysis tube. In the work of Ref. [240], a measuring cycle (elemental + total Hg) took 5.5 min and included a delay time of 30 s for switching lines to ensure equilibrium gas flow conditions. The detection system includes an échelle spectrometer for simultaneous detection of all of emission lines (253–579 nm) from the light source (Hg lamp) for the optical absorption measurement. Mercury was detected at 253.7 nm, but other lines could be used to correct for interfering gases in the stack gas (e.g. SO_2, NO_2) that also absorb at the Hg detection wavelength. Fluctuations in light source intensity and light scattering by particles can also be corrected in this way. The instrument was used in field tests at a rotary kiln (Section 5.1).

In contrast, Tao and Miller [241] used, for the same task, a $SnCl_2$-loaded reduction column to convert molecular mercury to the atomic form, which was then detected by AAS. Calibration against CVAAS showed that chemical conversion was complete. Absorption measurements were made in a small quartz cell, using a simple Hg pen lamp as light source and for detection an échelle spectrometer coupled to a CCD-camera. The molecular species selected for the tests were $HgCl_2$ and $Hg(NO_3)_2$. The latter was used as a substitute for HgO, since the nitrate decomposes thermally to HgO before analysis. From standard solutions of these compounds, gas streams were obtained with an ultrasonic nebuliser and delivered through the reduction column into the absorption cell. Detection limits were not given, but typical concentrations (molecular + atomic) were about 0.8 μg/L. Potential interference effects by NO_x and SO_2 were estimated by introducing quantities of these gases into the gas mixture.

Very recently, an *in-situ* AAS monitor for atomic Hg has been reported [242]. This instrument is based on Hg lamp absorption at 253.7 nm combined with a light-emitting diode (LED) to correct for background absorption by SO_2, the main interferant in flue gases at this wavelength. Laboratory tests gave a detection limit of 2 $\mu g/m^3$ for a path length of 49 cm and averaging over 1 min. As shown in Section 5.1, first field tests in a commercial coal-fired power plant have also been performed.

4.1.3. Tunable diode laser spectroscopy (TDLAS)

This method allows the determination of metals that are present in atomic form in the measurement volume, by direct absorption of a diode laser beam. The laser is scanned continuously and repeatedly over the spectral line of the metal and the light leaving the measurement volume is detected by a silicon photodiode. Data are evaluated by determining the absorber density N/V of the species of interest according to an extended form of the Lambert–Beer Law using a fitted integrated absorption profile $g(\nu - \nu_0)$:

$$\ln\left(\frac{I_0 \cdot \mathrm{Tr(t)}}{I - \mathrm{Em(t)}}\right) = S_\nu(T) \cdot g_{(\nu-\nu_0)} \cdot \frac{N}{V} \cdot l \qquad (4)$$

$S_\nu(T)$ represents the line strength of the atomic transition (which corresponds to the absorption coefficient integrated overall wavelengths), l is the length of the measurement path. The time-dependent factor Tr(t) accounts for the broadband absorption and scattering by ash, soot, droplets etc., which leads to temporally varying light losses of the laser beam. The factor Em(t) corrects for the thermal radiation of glowing particles and walls as well as light of the environment. These effects are also broadband and can, as Tr (t), be considered constant, since the laser is tuned in the kHz-region.

The main advantages of the method are a) Modulating capability of diode lasers, which allows for effective suppression of background emissions, especially using frequency and wavelength modulation (s. below); b) self-calibrating working method; c) compact, robust apparatus. Reviews of atom detection by TDLAS in graphite furnaces, plasmas and flames etc. are to be found in Refs. [243,244].

For diagnostics in combustive and similar environments, several types of diode laser are commonly used:

a) Fabry-Perot diode lasers (FPDL, AlGaAs, with ca. 1 cm^{-1} tuning range in the kHz modulation range) have been found adequate for scanning, for example, the D-lines of potassium at 1 bar total pressure [226]. These lasers are inexpensive and have a good output power of 3–20 mW, but suffer from the "mode-hopping"-effect, so the lasers have to be selected for single-mode behaviour with a wavemeter before use. The FPDLs used

in [226] had a threshold current of 43.5 mA and an amplitude modulation coefficient of 0.26 ± 0.01 mW per mA at 312.5 K.

b) Vertical cavity surface emitting lasers (VCSEL) have single-mode tuning ranges of up to 30 cm^{-1}, but a lower power of max. 1 mW. This type allows spectrally broadened lines to be scanned fully and thus permits detection up to 10–16 bar total pressure, depending on the species and gas composition. These DLs were used for part of the work reported in [226,227].

c) Distributed feedback (DFB) diode lasers offer a similar output power to the FPDLs but show no mode hops and so do not require selection. They use a Bragg-mirror that consists of a periodically repeating change in refractive index whose period length determines which wavelengths are reflected. Their tuning range (via temperature) is about 27 cm^{-1}. However they are much more expensive than the FPDLs.

d) External cavity diode lasers (ECDL) employ an external resonator to tune to the exact wavelength required, so the selection process mentioned above is dispensed with. The ECDL was tested as an alternative to the FPDL for detection of Rb and Li [227]. However the rather slow (100 Hz) mechanical wavelength tuning makes ECDLs unsuitable for environments where large, rapid transmission changes occur.

Typical experimental set-up: For on-line TDLAS measurements, two opposing ports (cf. Fig. 1a) are needed; these should be equipped with Brewster windows (Fig. 4), which are made with a specific angle, to allow the best possible transmission of the (polarised) laser beam. Note that Fig. 4 actually shows an extended form of TDLAS using wavelength-domain multiplexing, which is described below.

The diode laser unit is driven by a low-noise source connected to a temperature controller. The laser current is modulated by a function generator and the laser scanned with a repetition rate in the kHz range. After passing through the measurement volume, the beam is directed via concave mirrors and filters on to a detector (Si-Photodiode). As long as the atomic transitions concerned are in the visible or near UV region, fibre optics can be used advantageously, both for beam transport into the measurement volume and for the detection side, so that measurements in "remote" fashion (km distances) are feasible.

To keep the laser in the range of the required absorption line, a low-pressure cell containing only the metal vapour is probed by a small diverted part of the laser beam. This gives a reference signal, which is detected by a separate photodiode. The measured photocurrents are preamplified, digitalised by a multichannel A/D-converter and stored on the computer. To obtain sufficient signal-to-noise ratio, scans are averaged; for example, averaging 100 scans provides a time resolution of 1–2 s.

As noted above, modulating the diode laser current allows removal of fluctuations and 1/f noise from the spectrum and, combined with harmonic detection (e.g. 2f), leads to improved detection limits. In the case of wavelength modulation (WM), the modulation depth is very large, generating a large number of sidebands, but the modulation frequency is low (<1 MHz). In contrast, with frequency modulation (FM), the modulation depth is small but the frequency is very high (>100 MHz). Modulation also provides a way to correct for nonspecific absorption and improves the selectivity of TDLAS [245,246].

Multiplexing of diode lasers. In many applications, the need to monitor several species simultaneously arises. The availability of suitable fibre-optic technology has lead to the development of multiplex DL systems, which have been demonstrated under both laboratory and industrial conditions [245–249]. These are of three types:

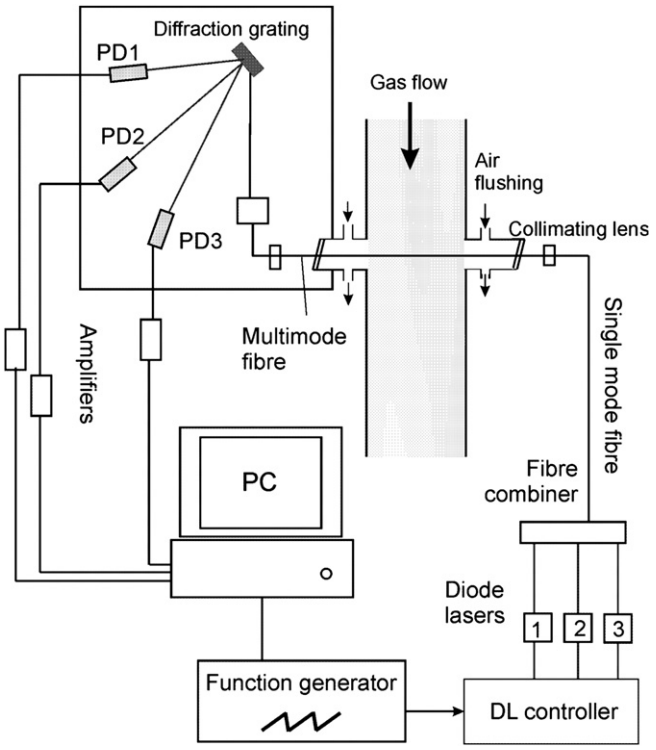

Fig. 4. On-line TDLAS measurements using wavelength-domain multiplexing. PD1-3 = Photodiodes.

a) wavelength-domain multiplexing (WDM) [245,248] (Fig. 4.). Two or more laser beams of different wavelengths are overlapped to form a composite beam using a single-mode fibre coupler before the entrance to the measurement volume and afterwards re-separated using a grating or a dichroic beam splitter/interference filter combination. If, however, the wavelengths are close together (as in the case of the K(D1/D2), Rb (D2) and O2 lines), an alternative strategy must be devised, since the interference filter curve is not sufficiently steep and the grating would have to be too wide to spatially separate the beams. Then multiplexing in the time or frequency domain may be the solution.

b) Time-multiplexing [245,249] means that the different (absorbed) laser beams are tuned at different phases of a common ramp function and then detected sequentially. The result is a quasi-simultaneous measurement, which benefits from the fast (kHz) tuning (amplitude, wavelength) capability of the lasers.

c) Multiplexing in the frequency domain, where each laser beam is modulated at a different frequency; the frequencies are selected to give the minimum interference between different harmonic signals. The output signal from the detector is fed into different lock-in amplifiers set to detect the respective 2f signals [246,247].

Data evaluation: Measurement curves are fitted to an appropriate absorption line shape and a polynomial. At high pressures, the Lorentz-type broadening is dominant and is normally selected for this task. In the course of fitting, corrections for transmission disturbances and emissions from dust and background radiation are performed. The concentration of the species of interest is evaluated from the fitted integrated absorption profile, accounting for the transition probability, tuning coefficient of the DL and the absorption path length and assuming the ideal gas law. Relevant

parameters of the measurement object, such as temperature and pressure are also included in the evaluation. Standard deviations for the measurements and minimum detectable absorption (MDA) are derived from the residuals of the fitting procedure. The level of MDA is determined by disturbances along the measurement path (such as broadband transmission, emissions and interferences by optical elements).

Detection of alkali metals. Using commercial diode lasers (FPDL, VSCEL, ECDL), TDLAS can be applied directly for detection of all alkali metals except sodium. Potassium has been detected at 769 nm down to the ppt-range with 1–2 s time resolution in a pressurised combustion plant up to 11 bar [226]. In addition, TDLAS was employed to detect Li (670 nm), K (770 nm) and. Rb (780 nm) for the determination of residence times in incineration plants at atmospheric pressure and up to 16 bar [227], Section 5.2. The measurement of Li, Rb and other elements by TDLAS using isotope dilution in graphite furnaces is described in Ref. [244], whereas Ref. [250] reports determination of Li, K, Rb, Cs and Sr in both graphite furnaces and analytical flames. For the detection of Na, diode lasers at 589 nm are not so far available so that an arrangement using frequency doubling or mixing would have to be realised. Sodium would be detectable at 330 nm using second harmonic generation (SHG) from 660 nm or at 589 nm using one of the new diode-pumped solid-state (DPSS) lasers.

In addition to the DLs providing D-lines at 767 and 770 nm, a GaN-diode laser exists that can be tuned over the potassium line at 404.8. Gustafsson et al. [251] detected both Pb and K at 405.8 and 404.8 nm with a DL of nominal wavelength 404 nm. Total optical powers with this type of DL range from 0.5 to 30 mW in the main mode, with typical bandwidths of ca. 0.02 GHz. In comparison, electrodeless discharge lamps give about 1 W with bandwidths of 1 GHz.

Other metals. A number of metals have been detected by direct TDLAS in the visible. These include the lanthanides Sm, Eu and Er at 673, 687 and 658/841 nm [252] as well as Y at 668 nm [253], Sr at 689 nm [254] and Ti at 842 nm [255]

On the other hand, many metal species show strong transitions in the UV and these have been accessed using either GaN–UV diode lasers in the region 375–470 nm [251,255–257] or by non-linear optical conversion (frequency doubling/second harmonic generation, SHG/sum-frequency generation, SFG) in crystals of BBO, $LiNbO_3$, $LiTaO_3$ etc. [258–266]. For example, by doubling from the red, 0.1 to 100 μW of laser light in the region 440–320 nm can be generated, depending on the starting power and optical arrangement. In this way, metals such as Cr (425.4) and Mn (403.1 nm) have been detected by AAS in flames [258,259].

Detection of Hg by TDLAS can be realised in several ways. Alnis et al. [261] obtained DL light at 254 nm by sum-frequency mixing (SFM) a blue DL at 404 nm with a DL at 688 nm. The power obtained was 0.9 nW with a tuning range 35 GHz. This range is somewhat short of that needed to scan the entire Hg line at 254 nm. Later experiments [262] using microlensed DLs to increase the efficiency of SFM (413, 662 nm) achieved 50 nW power and 70 GHz tuning range. This allowed the full (broadened) Hg line to be scanned at atmospheric pressure. A further system frequency mixed DLs at 679 and 789 nm to produce 365 nm [263]; here mercury was detected in an RF-discharge in argon at 100–300 Pa with a detection limit of 100 $\mu g/m^3$. Yet another possibility would be the frequency quadrupling of 1014 nm light, but this has so far not been demonstrated.

In recent years, a sum-frequency mixing (SFM) system has been developed and demonstrated for the detection of mercury and applied in coal combustion [264,265]. Light at 254 nm was generated by sum-frequency mixing a 375 nm laser and a 784 nm distributed feedback (DFB) laser in a non-linear β-barium borate crystal. Initially [264], an ECDL was used, but this was then replaced by a single-mode DL at 375 nm [265]. About 4 nW of UV radiation could be generated in the mixing process. By tuning the DFB-laser frequency, one could scan over the Hg line at 253.7 nm. The mode-hop-free tuning range of the DFB-laser was 86 GHz, so that an off-resonant baseline could readily be measured on both sides of the Hg transition. This is important for data evaluation and permits one to correct for interfering absorptions by flue gases such as SO_2 and particulate. As shown in Section 5.2, the system was applied both in extractive and in-situ modes, whereby detection limits of 0.3 and 0.1 ppb, respectively, were obtained for a 1 m path length.

Ultraviolet light can also be generated using the ECDL and subsequent SHG [266]. In this case, frequency doubling to give 320–327 nm was performed using a lithium iodate crystal. The cw UV power obtained was 60 nW (single pass) with a mode-hop-free tuning range of 40 GHz. This diode laser was tested on the 324.75 transition of copper ($4^2S_{1/2}$–$4^2P_{3/2}$) at atmospheric pressure with a single continuous scan. The system has also been used to detect In, Cu and Cd in a flame, a plasma and a discharge.

4.1.4. Cavity ring down spectroscopy (CRDS)

In this method, the *rate* of absorption of the species of interest is measured in an optical cavity formed from two highly reflecting mirrors, rather than the actual absorption. Thus the sample under study is enclosed within the cavity (Fig. 5). On entering the cavity, the light pulse is trapped between the two mirrors and then decays exponentially at a rate determined by the round trip loss experienced by the laser pulse. The corresponding time (ring down time τ) is given by.

$$\tau = d/(c[(1-R) + a_\lambda l_s + \beta_\lambda d]) \quad (5)$$

where d is the cavity length, R is the effective reflectivity of the cavity mirrors, a_λ the absorption coefficient of the sample ($=\alpha_\lambda n$), l_s the optical path length through the sample, β_λ the Rayleigh scattering attenuation coefficient and c the speed of light. When the laser is tuned to a particular absorption transition of the analyte species, the magnitude of a_λ depends on the species concentration in the sample and this in turn is reflected in the measured value of τ. Thus an increase in species concentration and value of a_λ leads to a decrease in τ. Note that β_λ does not normally have to be calculated [267]. If the cavity is setup in air (no sample) and reflectivity of the mirrors measured, one can obtain a measure of the "effective" reflectivity R_{eff} of the mirror and this includes any losses due to Rayleigh scattering or background absorption etc. Equation (5) can then be written

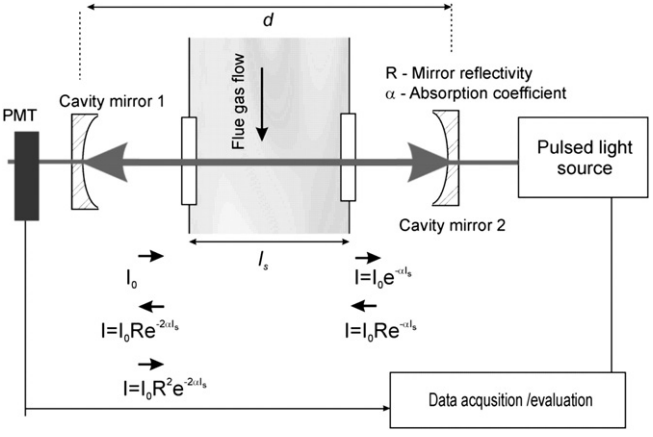

Fig. 5. CRDS: principle and basic set-up.

$$\tau = d/\left[c\left(1 - R_{\text{eff}} + a_\lambda * n * d_s\right)\right] \quad (6)$$

Since all other parameters are known, the change in ring down time following the introduction of sample yields a measurement of the absolute concentration of the analyte.

To optimise sensitivity, the number of passes has to be maximised and here the cavity mirror quality is a highly critical factor. Mirrors with reflectivities of 0.999, which are now commercially available for wavelengths down to ca. 200 nm, allow many thousands of passes to be achieved. For a baseline stability of 1% in the ring-down time measurement, minimum detectable absorptions of 3.6×10^{-5} (3σ definition) are obtainable [268] and by using high-finesse optical cavities as absorption cells [269], absorption sensitivities up to 1.5×10^{-9} cm^{-1} Hz$^{-1/2}$ are feasible. This latter method introduces a single-mode cw laser into the cavity by employing an off-axis cavity alignment geometry to eliminate undesired resonances but to retain properties that amplify the absorption signal. A recent review of CRDS is given in Ref. [270].

Metals detected by CDRS include Pb at 283.3 nm and Hg at 253 nm [268,271–275]. Results using an argon-ICP, a graphite furnace and a cold vapour Hg cell as atomisation sources show that better sensitivity can be obtained for detection by CRDS than for conventional AAS. For example, Hg in the vapour cell gave a detection limit of 25 ng/m^3 for CRDS as against 8.3 μg/m^3 for AAS, while the CRDS detection limit for Pb was 0.9 μg/m^3. This research group also made isotope-resolved measurements of uranium, again using ICP-CRDS [273]. Uranium was detected at three different atomic/ionic transition lines, 286.6, 358.5, and 409.0 nm, of which the largest isotope shift (ca. 9 pm) was measured at the 286.57 ionic line. Detection limits under optimized ICP operating conditions were in the range 70–150 mg/m^3, except for the ^{238}U component of the 286.6 nm line, which gave 300 mg/m^3. The latter, high limit was found to be a result of a strong absorption interference from the argon plasma. The potential of development of a field deployable, on-line uranium isotope monitor using plasma-CRDS is discussed.

Two other groups have detected mercury by CRDS using YAG-pumped dye laser systems and frequency doubling to 253 nm. Jongma et al. [274] detected Hg in air with a detection limit below 1 ppt. Spuler et al. [275] obtained similar sensitivities. Nevertheless, in a realistic combustion system, the sensitivity and dynamic range will probably be limited by broadband absorption by gases such as SO_2 and NO_2. In this respect, diode lasers would be preferable as light sources, since background interferences can more readily be accounted for (Section 4.1.3).

In recent years, solid-state light sources have steadily been replacing dye-laser systems and quite a number of CRDS experiments are now carried out using diode lasers as light source, though not so far on metal species. Such a scheme was realised by Mazurenka et al. [276], where NO_2 was detected. An ECDL with a 410 nm laser diode with associated grating was employed, giving a maximum power of 4 mW. A detection limit for NO_2 was 400 pptv in argon. In addition, a YAG-pumped OPO system has been used to detect by CRDS the refractory metals Fe, Ti, and Al, sputtered from a metal source [277]. Finally a diode-seeded, frequency-converted alexandrite laser was employed to detect Hg in various gases and in a simulated flue gas stream at 200 °C containing 1000 ppm SO_2, as well as NO, NO_2, CO, CO_2, and H_2O [278]. Typically, ppb amounts of Hg were detected and detection limits down to about 100 ppt could be achieved.

4.1.5. Differential absorption spectroscopy (DOAS)

In the DOAS method, concentrations of gaseous metal compounds are determined by another variant of the Lambert–Beer Law [279]. Basis of the method is:

$$N_{\text{alk}} = -\ln[I(\lambda_1)/I(\lambda_2)]/[\sigma(\lambda_1) - \sigma(\lambda_2)]\cdot L \quad (7)$$

Here, $I(\lambda_{1,2})$ represents the measured intensities at the selected maxima and minima, $\sigma(\lambda_1)$ and $\sigma(\lambda_2)$ are the absorption coefficients of the metal compound at the wavelengths λ_1 bzw. λ_2 and L is the path length in the experiment. By forming the ratio of the signals, similarly to TDLAS, interfering emissions (e.g. from dust or gases) disappear, since these vary only slowly during the scanning process. Since the spectra have a known form, overlying spectra can be separated from other components (such as SO_2) by (computational) spectral analysis. Residuals from the fitting procedure are used to derive standard deviations, which are normally of the order of a few percent and include noise and statistical errors.

A variant on the DOAS method, known as IACM (In-situ Alkali Chloride Monitoring), has been developed [280] to monitor total concentrations of gaseous chlorides (Na + K) in industrial flue gases. The experimental details of this system are presented in Ref. [281]; so far, the system has been used for KCl und NaCl only, between 650 and 1300 °C and in the concentration range 1–50 ppm. Several measurement series have been made in commercial PBFB- und PFBC-plants [282–285], but not yet in gasification systems. For a path length of 5 m and a measuring time of 5–10 s, a detection limit of 1 ppm was obtained, with a total uncertainty of roughly 1 ppm. Applications are discussed in Section 5.3.

Experimental set-up. Two current arrangements are shown in Fig. 6. In the case of 6a [279–285] two ports are needed, although normal (straight) windows are useable here. In 6b [286], a measuring tube with a gap of about 0.9 m length leads into the measurement volume. The gas to be analysed flows through the gap. For this second variant only one port/access is required.

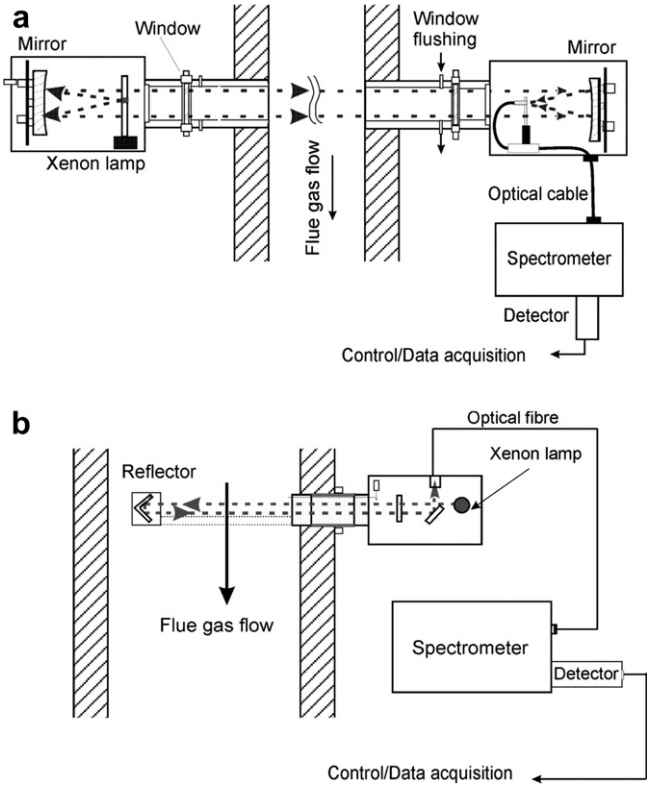

Fig. 6. Set-up for DOAS a) two-window; b) single window.

In both versions of DOAS, a commercial Xe-lamp is used as light source. The lamp window should be of fused silica with transmission in the range 185–2000 nm. After passing the reaction volume, the absorbed beam is analysed in a spectrometer. Also here a multipass arrangement (Section 4.1.1) could be used to increase absorption.

Several informative papers on the measurement technique and experimental set-up are available in the literature [279, refs.therein], from which the most important components can be seen as well as theoretical considerations and information about non-linearity (i.e. at high concentrations) and temperature effects, which are needed for quantifying the data.

4.2. Emission

Several forms of emission spectroscopy on metal species are considered in the following sections. Then details of quantification such as collisional effects and beam attenuation are considered in Section 4.2.4, since many aspects of quantification are common to several emission techniques. Calibration issues were already considered in Section 3.1.4.

4.2.1. Spontaneous emission in flames and other non-plasma environments

Spontaneous emission, such as in a flame, is frequently used to analyse sampled gases, in either the off-line or the on-line mode. For on-line sampling, gas from the plant process is lead through a heated line, nebulised into a burner and determined in the flame using AES (or AAS), as shown in Ref. [218] (pp. 360-1 and 344). Examples of such systems were given there.

In addition, a number of commercial monitors for mercury have been developed that employ emission detection rather than absorption [237,238]. Elemental and total Hg can be measured in two separate channels, whereby Hg in oxidised form has to be reduced to the elemental form before analysis, either by chemical reaction or by a thermal conditioner. Some monitoring systems work by capturing elemental mercury using gold amalgamation and then determining Hg by cold vapour atomic fluorescence (CVAF). The light source is usually a low-pressure Hg lamp at 253.7 nm. Other systems determine Hg directly (without gold-trap preconcentration) either by CVAF or by X-ray fluorescence.

Recently, Cheng et al. [287] tested six commercial continuous emission monitoring systems (CEMS) for mercury at coal combustion facilities. Of interest were linearity, response time, stability and efficiency of the speciation modules. All six systems possessed fast-loop, inertial type sampling probes enabling ash-free flue gas to be extracted from the process as well as heated transport lines and a gas conditioner to convert molecular mercury to the atomic form. All detectors operated by atomic fluorescence. Half the systems used gold amalgamation, in which case the loaded gold trap was afterwards heated and flushed to the detector with argon. Since an absorption–desorption cycle took about 150 s, the measurement time was much longer than for the second half of the detectors, which worked without passage through gold traps. The overall system time response, determined on changing calibration gas levels from a low to high levels, was 4–5 min. On-line measurements with the different analysers were compared with the standard Ontario-Hydro method [205] and a sorbent trap method [287]. In a further study [288], the same group investigated the effects of in-stack and out-of-stack sampling methods as well as sampling times.

A multimetal, quasi-CEM system based on X-ray fluorescence (XRF) has been developed [289] and also evaluated [290]. This automated instrument extracts stack gas samples and concentrates metals on a chemically treated filter tape. The tape then advances, bringing the sample to the analysis area where a dispersive XRF-analyzer determines the metal mass. Concentration data are generated every 10–20 min. The XRF-method is non-destructive, so the filtrate on the tape can be reanalysed later if required. Elements of atomic number 13 and above can be quantified.

4.2.2. Laser induced fluorescence

The LIF technique involves exciting specific electronic, vibrational or rotational transitions in the species of interest but detecting spontaneous fluorescence instead of absorbed light. Some strategies for excitation and detection were considered in the previous review [218, p. 346-7]. Two forms of the method are considered here: direct atomic or molecular fluorescence (LIF) and photofragment fluorescence (PFF), which are both applied in combustive environments. In addition, LIF is often employed for metal detection in reaction kinetic studies (Section 2.4) relating to combustion processes. In addition, the *planar LIF* method is a well-established technique where a 2D-section in the measurement volume is excited using a cylindrical lens arrangement and the species of interest imaged onto an ICCD camera. The use of (single-shot) PLIF allows also (momentary) spatial variations in the measurement volume to be observed, however average images can also provide useful structural information.

4.2.2.1. Laser induced (excited) atomic fluorescence (atomic LIF, LIAF, LEAF). Atoms present in the measurement volume may be detected by atomic LIF/LIAF/LEAF. Atoms may also be produced in a flame, plasma or furnace or by photolysis, but strictly this is only atomic LIF when the atom of interest had initially been in the ground electronic state and the observed fluorescence was excited by the laser light source. Detection schemes have been demonstrated for single- and two-photon excitation. Two-photon excitation schemes permit the use of longer wavelengths to alternative energy levels (the example of Hg is shown in Fig. 7a) and may be more selective than a single-photon scheme, since different emitting states can often be accessed. So far most of the development work has been performed with dye laser systems, since up to the mid-1990s, there was little alternative for atomic LIF. Since then Ti-sapphire lasers (which can be frequency-doubled or –tripled to the UV as required) and Nd:YAG-pumped-OPO systems have become readily available as fully solid-state tunable light sources. These would be more rugged and reliable for use in industrial environments. The following section describes several laboratory-scale investigations which contribute to the development of LIF diagnostics of metal species and/or the understanding of their release in combustive environments.

Conventional, single-photon atomic LIF has been used to measure the temporal release of atomic sodium from single brown coal particles suspended in a flat, natural gas flame [291]. Laser induced fluorescence of atomic Na using the D1 line at 589.6 nm was excited using an Nd:YAG-pumped dye laser and detected with a gated ICCD camera. Planar LIF measurements of Na atoms in the plume of a single particle suspended within the flat flame were made and calibrated by laser absorption. The temporal concentration profile of atomic sodium reached a peak of 64.1 ppb at the end of char combustion, before decaying. A simple kinetic model was used to estimate the rate of sodium decay in the post-flame gases; this estimated rate was in reasonable agreement with the measured decay rates. A related investigation using LIF in the same type of environment measured Na concentrations and particle temperature and size simultaneously [292]. Two-colour pyrometry, with two additional CCD-cameras, was used to determine both the temperature and the diameter of the particles.

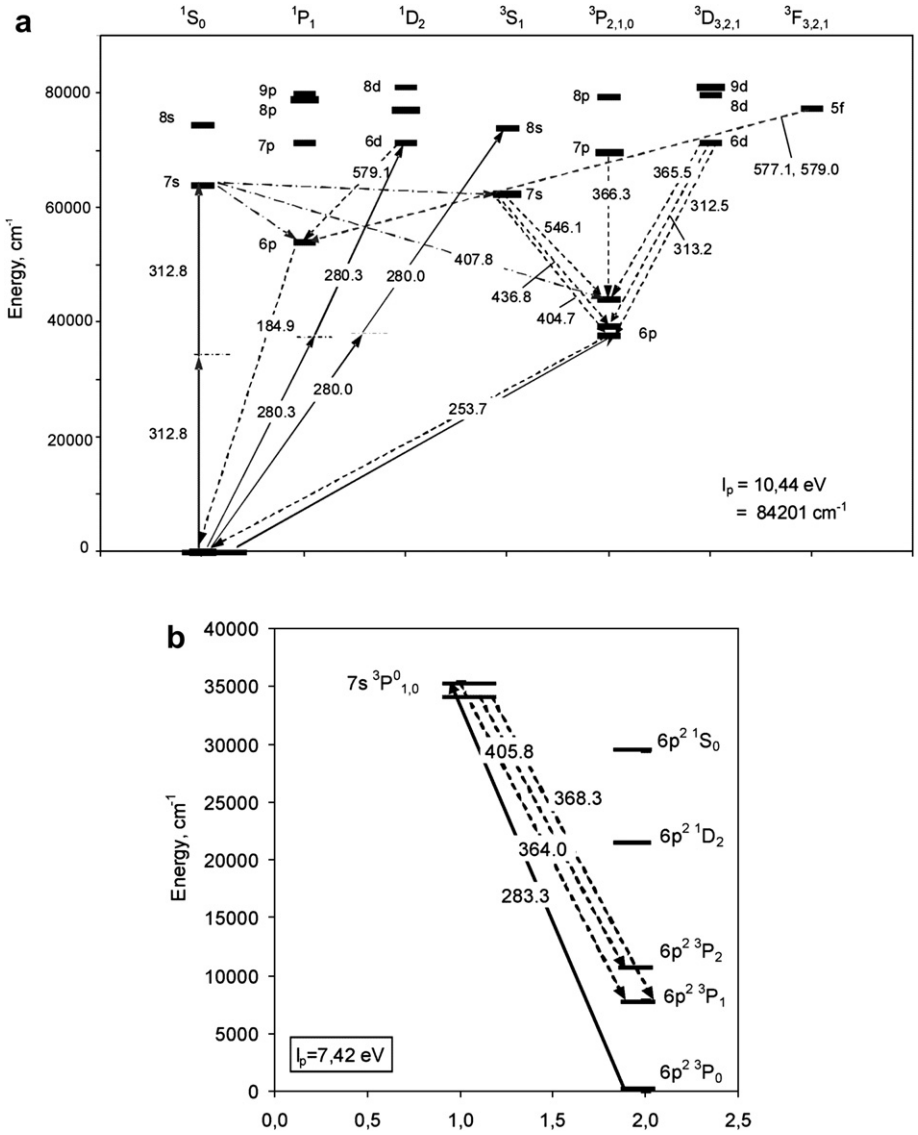

Fig. 7. Partial energy level diagrams a) for Hg, b) for Pb, showing excitation transitions and fluorescence transitions mentioned in the text.

Another study used planar LIF [293] to measure the temporal release of atomic Na release from a burning black liquor droplet above a flat flame burner. Here, the planar LIF images obtained were averaged to obtain concentration data at particular positions in the flame. The measured Na concentrations were then compared with those in the remaining smelt. Quantities of Na atoms released were up to 2 ppm, so measured signals had to be corrected for fluorescence trapping (Section 4.2.4.3). A simple plug-flow reactor model based on the independently measured concentration of residual Na in the smelt as a function of time was used. For this, the dilution ratio of the combustion products in the flat flame entrained into the plume gas from the black liquor particle had to be estimated. The results showed that very little atomic Na is present during the drying, devolatilization or char combustion stages. The highest amounts of atomic Na were seen during the smelt phase and these dominate over those from the other combustion stages.

The combination of 2D, two-colour pyrometry with 2D-LIF imaging of atomic Na allows the relation between particle surface temperature and release of Na from black liquor droplets in a flat flame to be investigated [294]. The pyrometric method was based on that demonstrated and applied in combustive environments by Joutsenoja et al. [70,71].

In some cases, solid-state systems have been used in place of dye lasers. For example, Nd:YAG pumped-OPO system was employed to excite Cu, Co, Pb, Mn and Tl atoms after aspirating metal-containing solutions into atmospheric pressure acetylene-air flames [295]. In this case, the metal atoms were excited in the single-photon mode at 324.8, 304.4, 283.3, 278.5 and 276.8 nm, respectively, and fluorescence was detected off-resonance at 510.5, 340.5, 405.8, 403.3, 352.9 nm respectively. Detection limits were comparable to those achieved previously using flame LEAF with dye-laser excitation, except for that for Co, which was 100 times lower.

Some atomic species have resonance transitions in the far UV (190–220 nm); these include As, Sb and Se. Here, absorption by oxygen in air or by other molecules may hamper detection. Nevertheless, detection of these elements by atomic LIF in atmospheric pressure acetylene/air flames has been demonstrated [296] using tunable (dye) laser radiation in the range 193–213 and detecting the elements off-resonance.

Two-photon atomic fluorescence has been demonstrated for mercury using a number of schemes (see Fig. 7a). Niefer et al. [297] excited Hg to the 6d $^1D_2$ state or 6d $^3D_2$ state using two 280.3 or 280.0 photons, respectively. Fluorescence was detected in the regions 312.5–313.2, 577–580 and 365–366 nm, respectively. Bras

et al. [298] excited Hg to the $7s^1S_0$ state using two 312.8 nm photons and detected direct fluorescence at 407.8 nm or collisionally induced fluorescence at 404.7. However, these studies actually focussed on collisional effects and LODs were not evaluated.

Several other workers have demonstrated *sequential two-photon excitation*. Resto et al. selected the combination 253.7 nm and 435.8 nm using two excimer-pumped dye lasers to excite the $7s^3S_1$ state of Hg, which had been atomised electrothermally (LIF-ETA) [299]. Detecting direct fluorescence at 546.1 nm, a detection limit of 90 fg (9 pptr with 10 μl injection) was obtained. The linear dynamic range was five orders of magnitude and was limited by amplified spontaneous emission (ASE), which occurred at higher concentrations. However, the linear range could be extended to 1 ppm and more by collecting collisionally induced fluorescence with the less sensitive line at 407.8 nm.

A similar dual-laser experiment excited first the 6^3P_1-6^1S_0 transition of Hg at 253.7 nm followed by the 407.8 nm transition to the 7^1S_0 level [300]. Fluorescence was monitored at 184.9 nm and at 546.1 nm, but the shorter wavelength was found to give the lower detection limit of 0.1 ng/m^3 at 10 s integration time and 10 Hz. The dynamic range was again five orders of magnitude. Relative quenching effects for N_2, air, He and Ar were measured and as expected, air showed the strongest effect (predominantly due to oxygen).

4.2.2.2. Laser induced (molecular) fluorescence (LIF). As mentioned in Section 3.1, many heavy metal species show highly complex spectra, which may hamper the design of a truly quantitative detection scheme. Therefore detection of species via photofragmentation (Section 4.2.3), as described below, may be a simpler solution. Photofragmentation fluorescence has to be employed for species such as NaCl and NaOH, whose upper electronic states are dissociative [301], i.e. after excitation the excited molecules fall spontaneously into an alkali atom and a chlorine or hydroxyl radical, respectively. On the other hand, the oxides NaO and KO have a bound excited electronic state, which would, in principle, allow direct LIF detection in the 668–725 nm region [163].

Direct molecular LIF was observed in the $A^3\Pi(0^+)$–$X^1\Sigma^+(0^+)$ system of PbO in a flame and in a furnace [302], excited by an excimer laser-pumped dye laser in the range 566–572 nm. The actual purpose of the work was to study the immobilisation of lead species in combustion environments by a gas phase silica sorbent precursor (here *hexamethyldisiloxane*). The lead precursor, tetraethyl lead, was entrained in an argon stream by bubbling and mixing with the fuel/oxidant mixture before introduction to the flame or furnace. The Q(30) rotational line of the (0,3)-vibrational band was selected for monitoring. The temperature in the flame varied from 1800 to 2400 K over the region of measurements. In this range, the net population of the line detected varied by 10%. In the furnace experiments, the temperature variation was 1000–1200 K and the net population varied 35%. These data were then used in the evaluation of LIF data. Part of the work was done as planar LIF, with the laser beam formed into a sheet using cylindrical optics and detecting LIF by an intensified CCD. The 2D images of PbO distributions obtained were corrected for laser induced particle incandescence and scattering by subtracting images taken off-resonance.

Molecular LIF spectra of halides of Hg, In and Ga and Ni have also been recorded, but these were observed in the course of photofragment experiments; these are considered below in Section 4.2.3.

4.2.3. Photofragment fluorescence (PFF)

The PFF method involves fragmenting molecular species by a UV-light source (usually a UV-laser such as a tripled or quadrupled Nd:YAG or an excimer laser) that is directed through the measurement volume. In the simplest case, a one-step process occurs:

$$MX + h\nu_{UV} \rightarrow M^* + X$$

Here M represents the metal atom and X a radical such as Cl or OH. Thus the measured signal may include contributions from more than one species, depending a) on what is present in the measurement volume and b) whether the exciting UV-light is short enough to generate a PFF-signal from the molecule in question. The resulting excited atoms then emit a spontaneous fluorescence, which can be detected directly. However the exact mechanism for forming M^* in a specific state depends on the nature of the precursor molecule, the chosen excitation wavelength, laser energy and the number of photons participating and may involve two or more steps.

In many cases production of excited atoms proceeds via two-photon processes and this can be generalised as.

$$MX_n + 2h\nu_{UV} \rightarrow M^* + nX$$

in which case the energy dependence of the PFF signal will be quadratic, as opposed to linear in the single-photon case. The exact mechanisms of M^* production depends on the bond energies of the molecule, excitation wavelength and ionisation potential (IP) of the atom M. If the IP is smaller than the equivalent excitation energy, the atom should be ionised first and subsequently recombine with an electron:

$$MX_n + 2h\nu_{UV} \rightarrow M^+ + e^- + nX$$

$$M^+ + e^- \rightarrow M^*$$

On the other hand, if the IP is larger, M^* could be formed via an intermediate MX_{n-y}. If such an intermediate can be detected, this may help to clarify the mechanism. However, the main requirement is to obtain a clear relation between PFF-signal and the concentration of the species to be measured.

The raw measured signals are quantified using optical transmission data for the wavelength of interest, collisional quenching data (Section 4.2.4) and a calibration to account for the optical geometry (Section 3.1.4 as well as [183,218]) of the experiment and the electronic settings.

4.2.3.1. Alkali species. In the case of alkali species, M can be Li, Na, K, Cs, Rb and X is usually Cl or OH but could also be O. So far, mostly the well-known D-lines of K and Na at 769/770 and 589 nm, respectively, were used for detection of alkali species, but other lines may be used for single-photon excitation [180,218]. The notation K^* or Na^* represents the first electronically excited state K ($4p^2P_{1/2}$) or Na($3p^2P_{1/2}$). As noted above, the alkali chlorides and hydroxides are measured via photofragmentation, since the electronically excited states are dissociative [218,301]. Development work on alkali species is summarised in the upper part of Table 5.

Detection limits depend on the species and experimental set-up and measurement conditions. For the alkali species, limits down to 0.1 ppb for Na and K have been reached [148,188,218,303], even in field measurements in technical combustion systems. However, at temperatures above ca. 1500 °C, the detection limits deteriorate markedly as a result of strong glowing of particles and pipe walls, in spite of the spectral and temporal discrimination measures taken. At 1500 °C, limits will be about a factor of ten worse than at 1000 °C [218].

Different *metal atoms* (K, Na etc.) emitting at different wavelengths can be discriminated using beam splitters and

Table 5
Development studies for PFF on alkali and heavy metal species.

Measurement Object	T/°C	Precursor	λ_{ex}, nm	*n* (photon)	λ_{det} nm	Molec. fragments	Depend.[a]	Ref.
Static cell	600–980	NaCl, KCl	193, 210, 230	1	589	–	C	[367]
			193, 205, 219	1	589		C	[367]
Flow cell	<900	NaCl	193	1	330,568,589,818	–	C	[180]
Flow cell	<900	NaCl	193	1	589	–	C	[364]
	<900	NaOH	355	2	589	–	C,E	[304]
Static cell	700/1000	NaCl	193	1	589	–	Q	[183]
		KCl	193	1	767/770	–	Q	[183]
Flame	<2000	NaCl	193	1	589	–	C,E	[305]
	<2000	NaOH	193	1	589	–	C,E	[305]
	<2000	Na_2SO_4	193	1	589	–	C,E	[305]
Static cell	500–950	$NiCl_2$	193	2	300,301,306,338	$NiCl_2$ (460)	C,Q,E	[190]
					349,352,362,440	NiCl (400–440)		
Flame(postflame)	127–227	$NiCl_2$	193	2	300.3, 335–365		C,Q,E	[317]
		$CrCl_2$		2	357.8			
		$PbCl_2/Br_2/(NO_3)_2$/acac		2	403			
		$MnCl_2$		2	405.8			
		$TlCl_3$		2	377.5			
		$BaCl_2$		2	455; 493; 554			
Flame(postflame)	527–627	NiO	193	2	300–361		C,Q,E	[318]
		CrO		2	301–360			
		PbO/$PbCl_2$		2	364,367,406			
		MnO		2	402–404			
Flame (postflame)	527	$Pb(NO3)_2$	193	2	364, 368, 406		C,Q,E	[316]
			193/283.3	2	406			
Static cell	20–23	$HgCl_2$	209.8	3	253.7	HgCl(B-X)	C,Q,E	[311–313]
	440–465							
Flow cell	25	$Hg(CH_3)Cl$	193	2	546, 579	HgCl(B-X)	C,Q,E	[308]
	25	$Hg(CH_3)Cl$	222	2	253, 434			[308]
	87	$HgCl_2$	222	2	253 etc.			[308]
	87	HgI_2	222	2	546,434,405,365	HgI(B-X)		[308]
Flow cell	90	$HgBr_2$	222	2	253 etc.			[309]
	90	$HgBr_2$	222	2	253 etc.			[310]
Static cell	120–250	HgI_2	193	2	366,405,408,463	HgI (B-X)	Q,E	[307]
			248	2	366,405,408,463	HgI (B-X)	Q,E	[307]
Static cell	120–250	$HgBr_2$	193	2	366,405,408,436	HgBr (B-X)	Q,E	[307]
			248	2	366,405,408,436	Rydberg state	Q,E	[307]
Static cell	120–250	$HgCl_2$	193	2	405,408,436	HgCl (B-X)		[307]
			248	2	405,408,436	HgCl (B-X)	Q,E	[307]
Static cell	193	$HgCl_2$	193	2	253, 436, 546	HgCl (B-X)	E[b]	[324]
	200	$HgBr_2$	193	2	253, 436, 546	HgBr (B-X)	E[b]	[324]
	n.s.	HgI_2	193	2	253, 436, 546	HgI (B-X)	E[b]	[324]
CVD Reactor	470–850	GaCl	248	2	245,266,287,294,	GaCl (A-X)	E	[322]
				2	403,417			
CVD Reactor	700	GaCl	193	2	417	GaCl (A-X)	E	[323]
	700	InCl	193	2	451	InCl (A-X)	E	[323]
	552,736	AsH_3	193	2	278; 190-312			[323]
			248	1	AsH_2 (A-X)			[323]
Static cell	n.s.	InCl	193	2	451, 410,326,304	–	E	[324]
	n.s.	InBr	193	2	451, 410,326,304	–	E	[324]

n.s. not stated.
[a] Signal dependence on: C= Concentration, Q = pressure, E = laser energy.
[b] One step probably saturated.

corresponding spectral line filters. Different *types* of molecules such as chlorides and hydroxides can be discriminated using different excitation and/or detection wavelengths, since different molecules have different bond energies [180]. For example, NaCl and NaOH may be discriminated since the bond energy for NaOH (341 kJ/mol) is smaller than for NaCl (408 kJ/mol). This enables the excitation of other transitions (330, 568, 818 nm) that cannot be observed with NaCl, since the emission comes from states significantly above the 2.5 eV corresponding to 193 nm. This was illustrated in Ref. [218] (p.346-7). Excitation of NaCl to states significantly above 2.5 eV would thus require a laser wavelength much shorter than 193 nm.

The above paragraphs refer to single-photon excitation, but alkali species can also be detected by multiphoton-PFF using harmonics of an Nd-YAG-laser [304]. For example, NaOH can be observed via two-photon excitation at 355 nm and fluorescence at 589 nm. However, the achievable detection limits (>5 ppb) are not as low as those for the one-photon excitation with 193 nm radiation (sub-ppb). In addition, much higher energies are required (ca. 300 mJ/cm^2) which means that particles will be vaporised and detected as well as gas phase alkali (s. below). In addition, the wavelength of 355 nm is not short enough to measure NaCl, due to the larger bond energy.

Alkali species on particles: Alkali species in particle and gas phases can be discriminated in two ways. First, PFF operated at low laser intensities (mJ/cm^2-region) detects gaseous species only, whereas at higher energy densities, particles are vaporised and measured as well. Above about 25 mJ/cm^2, both particulate and gaseous NaCl are detected [305]. Thus by raising the laser energy density, alkali species on particles are detected by a mixed photolytic-thermal process. Alternatively, PFF measurements can be compared with data taken for complementary methods (such as PEARLS or surface ionisation, SI), which detect particles as well as gas phase alkali species [148,303].

To understand particle disintegration and production by UV-photofragmentation, nanoscale NaCl particles were irradiated with single and multiple pulses of 193 nm laser light in a constrained air stream [306]. Laser fluences ranged from 0.08 to 0.23 J/cm^2. The resulting particle size distributions were measured with a scanning mobility particle sizer and the morphology analysed qualitatively by scanning electron microscopy (SEM). Photofragmentation of NaCl particles at 193 nm in this way was found to produce gas phase species as well as small solid-phase fragments without significantly heating the particles or creating a plasma. A comparison of SEM images before and after 193-nm irradiation shows that the irradiated particles are less fractal and more spherical than the unirradiated particles.

4.2.3.2. Heavy metals. Photofragmentation fluorescence has been demonstrated for Hg-, Ni-, Cr-, Mn- and Pb-species in laboratory cells [190,307–315] and flames [316–318]. In most cases, metal atoms are excited by a two-photon process, though three-photon schemes also exist [311–313]. For strong transitions, detection limits down to the low ppb region can be achieved. An overview of (small-scale) laboratory investigations for these metals is given in Table 5 and partial energy level diagrams for Hg and Pb are shown in Fig. 7a and b.

Mercury: The first photophysical studies on mercury compounds were performed in the 1920s and 1930s by Terenin [319] and Wieland [320]. These showed the existence of several absorption bands of $HgCl_2$, $HgBr_2$ und HgI_2. In the case of $HgCl_2$, excitation at 185 nm leads to Cl-atoms in the ground state plus excited HgCl*. In contrast, at 227 nm, Cl-Atoms and HgCl in the ground state are formed. In later investigations [321] the green emission (maximum 558 nm) of HgCl* was assigned to the $B^2\Sigma^+ \rightarrow X^2\Sigma^+$ transition (Fig. 8).

In the 1970s and 1980s, photofragmentation and spectroscopy of Hg compounds, particularly halides, was much investigated, as a result of the lasing properties of these compounds. For example, Whitehurst and King [307] reported detailed photophysical studies on the dihalides with excitation at 193 nm. As well as the green B-X fluorescence around 558 nm, emission from various Hg lines can be observed. Dissociative states of $HgCl_2$ and HgCl are involved in the photofragmentation process (Fig. 8a):

$$HgCl_2 + h\nu_{193} \rightarrow HgCl_2^*(1^1\Sigma^+_u) \rightarrow HgCl(B^2\Sigma^+) + Cl$$

$$HgCl(B^2\Sigma^+) + h\nu_{193} \rightarrow HgCl^*(Diss) \rightarrow Hg^* + Cl$$

Later PFF studies, now with a view to developing a mercury monitor for waste incineration, were performed on $HgBr_2$, HgI_2, $HgCH_3Cl$ and $HgCl_2$ [308–310]. These experiments were done in a simple laboratory flow cell and considered signal response as a function of wavelength and precursor concentration as well as fluorescence quenching by nitrogen. An excimer and a YAG-pumped dye laser system, respectively, were used to demonstrate that excited Hg* was formed via a sequential two-photon excitation at 193 and. 222 nm, respectively. These authors give detection limits of 1 ppb in an argon atmosphere.

More recently, a three-photon scheme was developed using a YAG-pumped dye laser, frequency doubled and then tripled to give 207–215 nm radiation [311–313]. The excitation wavelength of 209.8 nm was used preferably, in order to avoid interference with SO_2, a common constituent of flue gas. The longer excitation wavelength of 209.8 nm also has the advantage over 193 nm excitation (2-photon scheme of Ref. [298]) that absorption by gases in the measurement volume (CO_2, O_2 etc.) will be less severe (Section. 4.2.4.2).

In Fig. 8a and b, the two- [307] and three-photon [312–313] schemes for PFF-production of Hg* from $HgCl_2$ are shown side-by-side. In the three-photon scheme, the precursor molecule $HgCl_2$ is fragmented in two stages. In the first stage, two photons excite the molecule to a Rydberg state of $HgCl_2$, which dissociates to form the monohalide in the $B^2\Sigma^+$ state. In the second step, a third photon leads to excited Hg-atoms via highly excited, repulsive states of

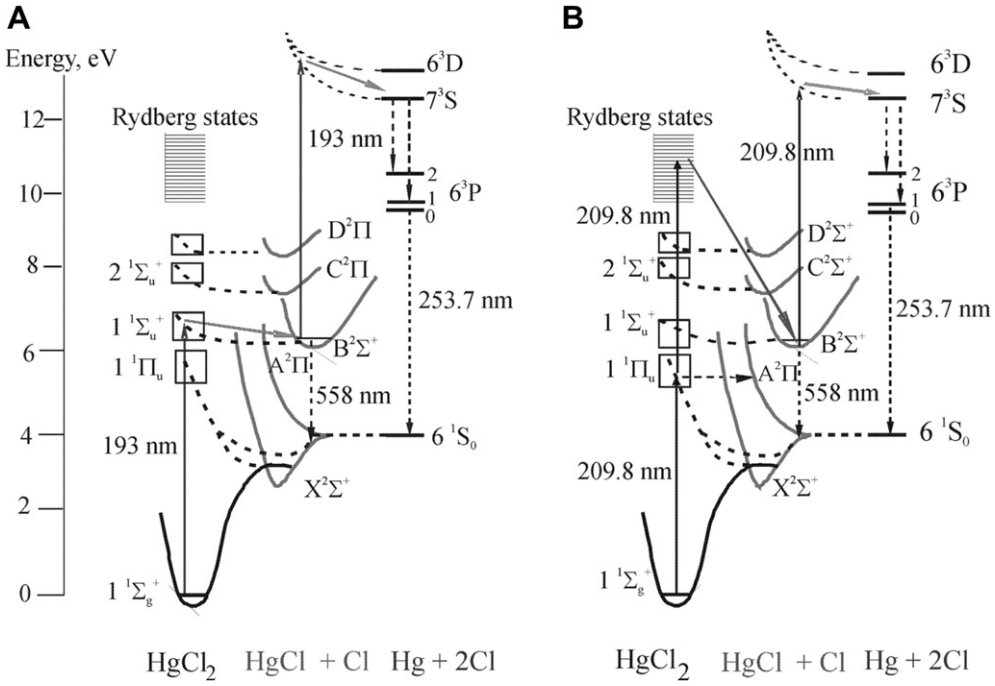

Fig. 8. Schemes for PFF of $HgCl_2$. A) 2-photon $\lambda_{ex} = 193$ nm; B) 3-photon $\lambda_{ex} = 209.8$ nm. The boxes on the left represent the energy regions of the bands given in Ref. [314] and the correlations of states of $HgCl_2$ to those of HgCl are from Ref. [315].

HgCl. As well as spectral characterisation, Refs. [311–313] report important aspects of signal quantification (pulse energy, collision quenching) for the Hg($6^3P_1 \rightarrow 6^1S_0$) emission produced in PFF of $HgCl_2$. Specific estimates of detection limits are not given, but the scheme should have potential for further development into a fieldable measurement system for combustion flue gas.

Other heavy metals. Several other metal species have been the subject of laboratory studies in order to assess potential detection schemes for flue or stack gas monitoring. Buckley et al. [316] describe PFF methods to determine lead in flames and post-flame gases at 1 atm. These schemes all rely on excitation of the $6p^2\ ^3P_0 \rightarrow 7s\ ^3P_1$ transition and detection of fluorescence from the $7s^3P_{1,0}$ to $6p^2\ ^3P_{2,1,0}$ states at wavelengths of 364.0, 368.3 and 405.8 nm (Fig. 7b). Aqueous solutions of lead salts (nitrate, chloride, bromide, acetate) at ppm concentrations were injected into a lean flat flame. In a single-laser experiment, excimer laser excitation at 193 nm (120 mJ in 2 mm) was used to detect gas phase and aerosol lead species via PFF. Here, a single-shot detection limit of 220 ppb for Pb species was determined [316]. In the post-flame temperature region of 600–750 K, a strong rise in PFF-signal from molecular and aerosol forms of Pb was observed and attributed to homogenous nucleation of PbO. Then a two-laser scheme (fragmentation of the lead salt by an excimer laser at 193 nm followed by dye laser excitation of ground state Pb at 283.3 nm) was tested using a variable delay between photofragmentation and Pb atom detection at 405.8 nm. In this way, lead atoms formed in the flame front and concentration profiles in the post-flame gases were determined. A single-shot detection limit at 405.8 nm of ca. 30 ppb was estimated for this second scheme, the lower detection limit being a result of the absence of background signals from O_2, CO^+ and CO_2^+ which occur with excimer laser excitation.

The same group of workers performed similar experiments on Ni, Mn, Cr, Ba, Tl and Pb in atmospheric pressure laboratory flames, here using single-laser excimer excitation at 193 nm [317,318]. As above, salts of these metals were aspirated into the flames. Detection limits (100-shot average) of 50 ppb for Ni (300.3 nm), 70 ppb for Mn (405.8 nm), 100 ppb for Cr (357.8 nm), 10 ppb for Ba (455 nm), 0.5 ppb for Tl (377.5) and 5 ppb for Pb (403 nm) were achieved.

Photofragment experiments on Ni using $NiCl_2$ as precursor have been performed using 193 nm excitation [190] in a heated laboratory cell at 1000 °C. The $NiCl_2$ molecule was used as precursor for photofragmentation since it is one of the main Ni species in combustion of solid fuels. Emission spectra, taken in the range 300–550 nm showed a variety of Ni atomic lines as well as molecular bands from excited $NiCl_2$ and NiCl. For emission at 440 nm ($3d^84s5s - 3d^84s4p$ transition) and 362 nm ($3d^84p - 3d^84s$ transition), the energy dependency was found to be quadratic, corresponding to a two-photon excitation process. The Ni atomic emission line at 440 nm was chosen initially for field studies, but later studies showed that the 362 nm transition may be a better choice, since it was free of background from molecular emissions. Quenching effects in nitrogen and air were measured by time-resolved PFF; results show only a small effect for N_2 but for air, the lifetime fell from 293 ns to 52 ns after filling the cell to atmospheric pressure. A detection limit of about 50 ppb for a typical flue gas at atmospheric pressure was estimated for a laser fluence of 10 mJ/cm^2 and averaging over 500 laser shots.

Finally, since the availability of UV-lasers, a considerable amount of research has been done on the elements Ga, As and In. At the time, this work was associated partly with lasing properties of the halides of the respective halides and partly with the development of chemical vapour deposition (CVD). Alfano and Benard [322] used a 248 nm excimer laser to study PFF of GaCl. The power dependence of the atomic Ga* PFF-signal corresponded to a two-photon excitation, the first photon producing ground-state Ga, the second photon Ga*. On the other hand, Donnelly and Karliceck [323] excited GaCl with a 193 nm excimer laser. Here, the two-photon process gave first ground-state Ga; the second photon ionised the Ga atom. The Ga^+ ion then recombined with an electron to give a recombination emission. The same type of mechanism was proposed for PFF of InCl [324]. In contrast, photofragmentation AsH_3 with 193 nm radiation [323] gave molecular emission of AsH_2(A-X) plus atomic emission from excited As* states in the region 190–312 nm. The authors believe these emissions are produced by the process.

$$AsH_3 + 2\ h\nu \rightarrow As(5s^2P_{3/2}) + H + H_2$$

This reaction requires 10.9 eV, accessible via two-photon excitation at 193 nm (6.4 eV/photon). However, it was pointed out that As* detection may not be a quantitative measure of arsine concentrations, due to the high degree of fragmentation; detection of molecular emission was preferred in this respect. Similar work on InCl and InBr has been performed using 248 nm radiation [324], where spectra showed strong emissions from several In* transitions.

4.2.4. Quantification of measured fluorescence data

In the simplest interpretation, the signal detected (normally the measured voltage) can be given as.

$$I_F = C_{det} \cdot h\nu / N_2 A_{21} \quad (8)$$

where N_2 represents the population of the upper state of the transition of interest ($N_2 \rightarrow N_1$) of frequency ν and A_{21} is the Einstein coefficient for spontaneous emission. To relate N_2 to the total number density of species N_0 ($=N_1+N_2$), rate equations for the two energy levels have to be solved, as discussed in standard texts on LIF (such as [325]). The factor C_{det} accounts for geometrical and optical factors as well as electronic settings and can be determined in the course of a calibration under standardised conditions (Section 3.1.4.).

The raw signal (whether induced fluorescence or spontaneous emission) at first represents only a relative measure of the amount of metal species in the measurement volume. To obtain absolute metal concentrations, several factors need to be considered:

1) In induced fluorescence measurements, the average laser energy C_{AE} in the measurement volume has to be included in the equation. However, depending on the wavelength of the light source, a correction for absorption of the light beam by gases in the environment (CO_2, O_2 etc.) and, if particles are present, a correction for extinction may also be needed. In the case of UV-light below 200 nm and of pressures above atmospheric and for temperatures above 1000 °C, this correction can be several orders of magnitude, as shown below in Section 4.2.4.1
2) In realistic i.e. pressurised systems, signals are reduced by collisional quenching due to gaseous molecules (N_2, O_2, CO_2 etc.) in the environment. Therefore a value for the effective lifetime of the excited metal atom has to be obtained. Since it is unlikely in practice that one can measure this value directly (sophisticated equipment including picosecond laser required), this correction is normally calculated from low-pressure data and extrapolated to the required conditions of temperature and pressure. This procedure is discussed below in Section 4.2.4.2.
3) Depending on the concentration range to be measured, laser energy densities used and other factors, several non-linearities of signal may have to be accounted for (Section 4.2.4.3.)

4) An allowance (C_{det}) for the optical geometry, optical elements and the electronic settings (Boxcar integrator etc.). This factor is essentially independent of pressure and temperature in the measurement volume. Ways of characterising (calibrating) this factor were discussed in Section 3.1.4.

Thus the simple equation above has to be modified to include these factors:

$$I_F = C_{det} \cdot C_{AE} \cdot n_{MX} \cdot a_{abs} \cdot q_{korr} \quad \text{where } C_{AE} = \int A(x) \cdot E(x) dx \tag{9}$$

Here, $A(x)$ is the optical image efficiency, $E(x)$ the effective laser energy at position x, n_{MX} the concentration of the metal compound of interest MX, a_{abs} the absorption cross section for the production of M* and q_{korr} the collisional quenching factor.

It should further be noted that if the *detection* wavelength is also at a UV wavelength below ca. 250 nm, similar corrections for attenuation by gases and particles in the environment will also be required.

4.2.4.1. Optical transmission. Preferably, the optical transmission should be determined continuously and simultaneously with the analyte signal, in order to facilitate the corrections required. However, it is necessary to estimate the strength of the absorption effect using suitable data (absorption coefficients, gas composition) *before* designing an optical access and planning experimental work. For UV-wavelengths below about 250 nm, beam absorption can be severe at high-temperatures, pressures and/or for larger dimensions [218,326] and, as the discussion below shows, may lead to limitations of conditions under which fluorescence measurements can be carried out.

The direct measurement of transmission will cover both absorption by gases in the measurement environment and scattering by particles, if present. However, the transmission due to absorption can be estimated if the relevant absorption coefficients at the wavelength of interest as well as gas composition data are available. If particles are absent, then the calculated transmission should correspond to the measured transmission. The effective transmission is then used to calculate the effective energy of the light in the measurement volume and can be estimated using the Lambert–Beer Law:

$$I = I_0 \exp(-k_i l) \tag{10}$$

where I_0 is the intensity of light falling into the measurement region, I the intensity leaving the region after a distance of l (cm) and k_i (cm^{-1}) the absorption coefficient. Values of k_i are calculated as the product of absorber concentration (c_i(cm^{-3})) and the absorption cross section σ_i (cm^2):

$$k_i = \sigma_i^* \cdot c_i \tag{10a}$$

To obtain the effective transmission ($T_{eff} = I/I_0$) for a particular gas composition, the total coefficient k_{tot} has to be determined and placed in eq. (10) instead of k_i. This is done by calculating the individual contributions k_i and summing them:

$$k_{tot} = \sum k_i = \sum \sigma_i^* c_i \tag{10b}$$

The total coefficients are then used to obtain relative intensities according to eq. (10).

This approach assumes that the gases of interest absorb in a broadband manner in the emission region of the light source (e.g. for an ArF-excimer laser ca. 1 nm), i.e. the k_i values do not vary strongly. In the case of CO_2, H_2O, NH_3 this condition is fulfilled for 193 nm laser light [326–330], but not for O_2, which shows a pronounced fine structure in its UV-absorption spectrum [331]. In the latter case, a modified form of the Lambert–Beer law has to be used [329].

For a typical combustion flue gas, N_2, O_2, CO_2 and H_2O are the main species in the flue gas, whereas for gasification conditions they are N_2, CO, CO_2, H_2 and CH_4 with traces of H_2S, NH_3 and several other species. Even at 193 nm, N_2, H_2 and CH_4 show negligible absorption. Thus for a combustion environment, absorption by O_2, CO_2 and H_2O have to be accounted for. In the case of gasification, CO, CO_2 plus those trace species with very large absorption coefficients have to be included.

A review of the literature on absorption coefficients for 193–250 nm shows that sufficient data are available over a wide temperature range for O_2, CO_2, H_2O and NH_3 up to 3000 K [328,331–336]. For these gases, except NH_3, absorption coefficients increase strongly with temperature. Fig. 9 shows absorption coefficients for these four molecules at 193 nm. The parameterisations in these studies can be used to calculate k_i values for the required temperature range. For CO on the other hand, very little pertinent information is available for the weak absorption in the Cameron bands. An early study [337] suggests its absorption coefficient is about two orders of magnitude below that of CO_2.

A detailed study of absorption by CO_2 and H_2O over the wavelength range 190–320 nm has been performed for temperatures from 900 K to 3050 K [326]. The results show significant to strong absorption for all wavelengths below 250 nm. However, the absorption in the range 200–250 nm is much weaker than at 193 nm. For example, for a mixture of CO_2, H_2O and N_2.at 13 bar, 2400 K and 5 cm distance, an attenuation of more than a factor of 10^5 at 193 nm, as against 85% at 226 nm and about 40% at 248 nm can be calculated [326]. Thus if the metal species of interest can be excited by light of a longer wavelength, this is obviously to be preferred.

For gasification environments, H_2S could be a major problem. Absorption coefficients for this molecule exist only in the range 170–370 K [338]. This study gives 6×10^{-18} cm^2 at 193 nm and 370 K, much larger than, for example, that for CO_2. Although the amount of H_2S in the flue gas is normally in sub-percent region, a cross section of this magnitude would swamp all the other components.

4.2.4.2. Quenching and energy transfer. Realistic (industrial) reactive systems are operated at atmospheric or higher pressures. This

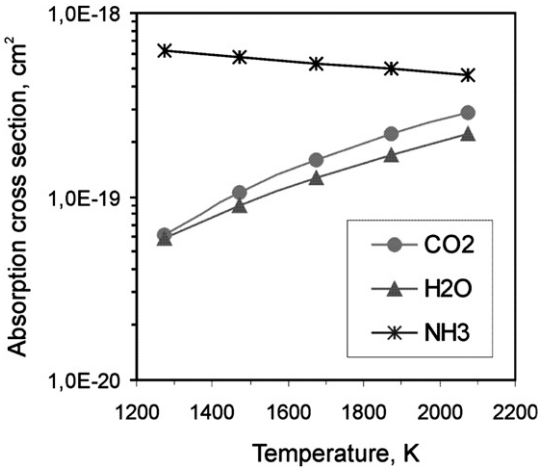

Fig. 9. Absorption cross sections for some important combustion gases at 193 nm. Curves for CO_2 and H_2O follow the parameterisation of Ref. [326]; the curve for NH_3 follows that of Ref. [330].

means that the intensity of emitted light is reduced by deactivating collisions of the excited analyte species with molecules in the environment. This non-radiative process is termed *collisional quenching* and requires correcting when evaluating recorded data. In theory, the simplest method would be to determine the effective collisional lifetime of the excited metal atom using time-resolved fluorescence of the excited state; then the value of q can be determined directly. However, to perform such measurements under conditions of technical interest (total pressure = 1 bar), a picosecond excitation pulse with ultrafast detection would be required, since the effective lifetimes are on the order of nanoseconds or less. Such measurements have been made for atmospheric pressure flames [339,340], but sophisticated equipment is required that would be impractical for use at industrial combustors/gasifiers.

Thus when evaluating measured data, the usual practice is to use cross sections for quenching for the major colliders from the literature and the corresponding concentrations to calculate the effective quenching rate and hence the effective lifetime of the excited state of interest. Ideally, these data should be known as a function of temperature. Fortunately, the quenching of sodium and potassium atoms is reasonably well-characterised [183,339–342] for all important colliders relevant to combustion (H_2O, CO_2, N_2, O_2). In contrast, the corresponding data for many important heavy metals are very sparse. Some data exist for Zn [344–345] Cd [346,347], Hg [348,349], Pb [350–352], Ga [353], Ge [354–356], Fe [357]. For Ni* [190], a very small quenching effect is observed for emission from the quintet state at 440 nm, but a large (tens of Å^2) effect for the singlet emission at 362 nm. Differences in quenching efficiency have also been observed for Zn and Cd; cross sections for the singlet states are on the order of several tens of Å^2, whereas those for the triplet states are one to two orders of magnitude smaller [344–347].

Quenching mechanisms: collisional quenching can be a) non-reactive or b) reactive

a) $M^* + XR \rightarrow M + XR(^{\dagger})$
b) $M^* + XR \rightarrow MX(^{*,\dagger}) + R$

In case b), the excited atom is incorporated into the product molecule. Typical collision pairs for this case are Hg, Na or K + (O_2, N_2O) and Zn, Cd, Pb or Sn + (O_2, N_2O, H_2). The quenching cross sections tend to be large i.e. several tens of square angstroms, corresponding to rate constants in the range 10^{-11}–10^{-10} cm^{3}molec^{-1}s^{-1}. In such reactive collisions, molecular emissions from excited metal oxides or hydrides may also be observed. In case a), the main quenching mechanisms are i) direct crossing between potential surfaces of the entrance and exit channels; ii) indirect crossing via an ion-pair intermediate; iii) systems where bound potentials (long-lived complexes) exist; iv) dipole–dipole and related interactions. It should be noted that combinations of mechanisms may operate in particular collision pairs. For instance, a reactive collision may proceed via an ion-pair curve:

$$M* + RX \rightarrow M^+ + (RX)^- \rightarrow M^+X^- + R$$

If R is a large polyatomic group, the ion pair may rearrange and form a longer lived complex. A well-known example of the charge-transfer mechanism is the pair $Na^* + N_2$, although here the collision belongs to class a), i.e. is non-reactive.

Some quenching data can be correlated with the long-range forces C_6-parameter, i.e. a plot log σ_i again log C_6 is linear. This has been shown for quenching of singlet states of Zn and Cd, for which data have been measured for colliders from H_2 to i–C_4H_{10}. [343–347] The C_6-parameters are calculated using the Slater–Kirkwood approximation [358] and are proportional to the polarizabilities of the collider molecules. Thus small non-polar colliders (such as Ar, H_2) have cross sections between 10 and 30 Å^2, whereas the corresponding values for isobutane are more than 100 Å^2.

Quenching correction for flue gas mixtures: To obtain the actual number densities in the system concerned, the effective quantum yield q ($=A_{21}/(A_{21} + Q_{21})$ has to be calculated, where A_{21} is the Einstein coefficient for spontaneous emission and Q_{21} is the total quenching rate for a particular environment, determined by:

$$Q_{21} = \sum n_i \sigma_i v_i \tag{11}$$

where n_i are the number densities of the individual collider species, σ_i the corresponding quenching cross sections and v_i the average relative velocities of the collision pair (excited metal atom M* + species i.)

For *direct* excitation of atoms or molecules, the fluorescence signal is related to the total species number density N_0 ($= N_1 + N_2$) by:

$$I_{fl} = C_{det} \cdot N_0 \cdot B_{12} \cdot I_v \cdot q \tag{12}$$

with the Einstein coefficient for absorption B_{12} and the laser intensity I_v.

In the case of PFF, the fluorescence signal is related to the number density of the precursor compound MX by:

$$I_{PFF} = C_{det} \cdot N_{MX} \cdot a_{abs} \cdot I_v \cdot q \tag{13}$$

with the absorption cross section for production of excited metal atoms M*, a_{abs} the absorption coefficient for production of M*.

If the concentrations of major species (N_2, O_2, CO_2 etc) in the measurement environment are known and collisional quenching data are available, the factor q can be calculated as shown above. As an example, the main quenching partners in the PFBC flue gas are N_2, CO_2, O_2 and H_2O with typical mole fractions of 0.76, 0.14, 0.05, and 0.04 respectively. From the calculation of Q_{21} using Eq. (10), a value of $q = 400$ is obtained for the Na-D-line emission in a typical industrial flue gas at 10 bar. The precision in this case is around 10%, but for other species and spectroscopic transitions, less quenching data is available and hence the precision will not always be as good.

Other collisional effects, such as mixing between states may also be of importance. In the case of atoms, transitions between closely lying fine-structure states can be induced by collisions with species in the environment. In process gas, typical pressures are atmospheric and upward, so that transfer and mixing is usually very rapid and thermal equilibrium is likely to be reached before quenching processes take place. For example, for alkali atoms, the ^2P_J doublet states mix with cross sections, typically of 100 Å^2 or more [359,360]. Similar studies have been performed for Hg [297,298] as well as Ga and Tl [361]. Nevertheless, in some situations, fine-structure splitting and collisional transfer can play a role in the selection of detection schemes.

For molecules, vibrational and rotational energy transfer also have to be considered in devising detection schemes and evaluating data. The influence of pressure and temperature has been described for molecules such as PbO [362] and HgCl [363], but so far, there is little quantitative data in the literature.

4.2.4.3. Non-linearities of signals.

a) *Optical saturation of excited transition*: If a single-photon transition is excited, the signal should be linear with pulse energy up to the onset of optical saturation. When saturation occurs, the population of the lower laser-excited level is significantly depleted. This leads to a non-linear dependence of signal on

laser energy. However, due to temporal, spatial and spectral variations in the laser intensity, complete saturation of a transition is hard to achieve in an experiment. Thus saturation may occur in some regions of these three domains, but not at the edges of the intensity distribution, leading to so-called "wing effects". Because of their generally larger transition probabilities, atoms are more prone to saturation than molecular species. Various models have been proposed to describe saturation behaviour, which include treatments of accompanying energy transfer processes with various degrees of complexity [325]. If measurements are to be performed in the saturation regime, laser density dependence of the transitions to be measured should be determined first, under the conditions of temperature and pressure of interest.

For multiphoton processes, the dependence on laser energy density is non-linear at sufficiently low energy densities. For example, excitation of NaOH with 355 nm radiation follows approximately a quadratic relation up to 300 mJ/cm^2 [304], corresponding to a two-photon process involving a virtual intermediate electronic state. Optical saturation was not observed in this regime and was expected to occur at about 3 J/cm^2.

b) *Radiation trapping*: For strong transitions that emit to the electronic ground state, such as the Na D-Line or the 254 nm line of Hg, the fluorescence signal becomes non-linear with species concentration above a certain value. This is a result of re-absorption of radiation by ground state atoms. The onset of the effect depends, in the first instance, on the strength of the transition observed and, if performing photofragmentation fluorescence, the degree of photodissociation of the precursor molecule. In addition, the competition between photon emission and collisional quenching has to be considered. The trapping effect can be corrected with the aid of Monte–Carlo modelling [364,365]. The simulation tracks the excitation energy of the excited species as it is transferred by successive emission events and calculates the net probability of photons escaping from the measurement volume, where it may then be detected. A more refined model was later developed and applied to radiation trapping of the Hg resonance line at 254 nm to predict effective decay rates of Hg (6^3P_1) atoms [366]. This model included Voigt profiles to account for line broadening processes (radiative, Doppler, buffer gas) as well as hyperfine and isotope structure and partial frequency redistribution. The results of trapping simulations were then compared with time-resolved LIF measurements of decay rates of Hg (6^3P_1) atoms in argon, for the Hg density range $(5–700) \times 10^{13}$ cm^3. The agreement was mostly good, but at high Hg densities, the experimental decay rates were slightly higher, due to small quenching effects of Hg and Ar. Similar calculations were performed for the case of PFF of NaCl at 193 nm, where the simulations lead to a limit of linearity of 20 ppm, on the basis of a photodissociation rate of 0.7% [364].

c) *Detector saturation*: This can be avoided by using appropriate neutral density filters for the dynamic intensity range of the experiments.

d) *Dimer formation*: At high analyte concentrations, dimers or even trimers of the metal species can form. Thermodynamic equilibrium calculations [118,119] show that in typical reactor flue gases, dimers of alkali species are unlikely to be present. In addition, Oldenburg et al. [367] show that in the concentration and pressure range of interest (at least up to ppm range), dimers make a negligible contribution to the fluorescence signal. These authors also find that the ease of photofragmentation for monomers is greater than for dimers by about a factor of two for sodium and a factor of 8–9 for potassium.

4.3. Plasma spectroscopies (with optical detection)

This section considers a group of on-line plasma techniques that employ *optical* detection.

- Intracavity plasma (ICP) spectroscopy
- Microwave plasma (MIP) spectroscopy
- DC-Plasma spectroscopy (PEARLS = Plasma enhanced atomic resonance line spectroscopy and HEAMON = Heavy metal monitor)
- Spark induced breakdown spectroscopy (SIBS)
- Laser induced breakdown spectroscopy (LIBS), also known as laser induced plasma spectroscopy (LIPS)

These techniques use different methods of plasma generation to atomise and excite species of interest. They all employ AES (OES) for detection, with the exception of PEARLS/HEAMON, where detection is by AAS, and ICP, which can alternatively be coupled to mass spectrometry (MS) (Section 4.4.3) or atomic absorption (AAS, Section 4.1.1 or CRDS, Section 4.1.3) detection.

Several fundamental aspects of plasma spectroscopy had been considered on P.344-6 of Ref. [218], including temporal behaviour of emissions, spectral discrimination, dependence on excitation wavelength, self-absorption of emission lines and matrix effects. This section reviews some contributions to development of the above techniques, mostly from the past few years.

4.3.1. Intracavity plasma – atomic emission spectroscopy (ICP-AES)

The ICP-AES method (also known as ICP-OES) is one of the most commonly applied plasma spectroscopies and there are a number of commercial devices on the market. In recent years, several groups have invested much effort to develop further and quantify various aspects of the on-line technique [368–376]. In an ICP-AES system, the process gas is extracted (Section 3.2.5) and led via a suitable interface (of which there are several variants) to a radio-frequency operated argon plasma (Fig. 10). At plasma temperatures on the order of 1000 °C or more, the various elements in the sample are atomised and excited electronically. The emissions are then analysed, using appropriate time delays, by either a polychromator system or a simple detector with selective atomic line filters.

Poole et al. [368–371] have setup a mobile continuous emissions monitoring laboratory, based on ICP-AES technology, to study temporal variations in metal concentrations in realistic flue gases. Samples were taken isokinetically from the process using a heated (200 °C) sample line, sub-sampled via a secondary sampling stage and then mixed with argon before being introduced to the ICP-AES system. The concentrations of over 30 elements were monitored prior to flue gas clean-up. In the incinerator [368,370], detection limits in the range 0.007–0.06 mg/m^3 were achieved under realistic combustion conditions. The system was calibrated using multi-element aqueous standard solutions introduced into the gas stream as a dry aerosol using an ultrasonic nebuliser. Calibrations were performed for a number of gas mixtures; full details of statistics for different metals are given in Ref. [369]. A particular effect observed in the calibration measurements was that signal sensitivities at elevated CO_2-levels differed from those determined in atmospheric air; for Al and Ni they were increased, whereas for V the sensitivity was lower. Such an effect could result either from a change in plasma temperature and hence in Boltzmann energy distribution or from changes in ionic species generated, such as C^+. If elements

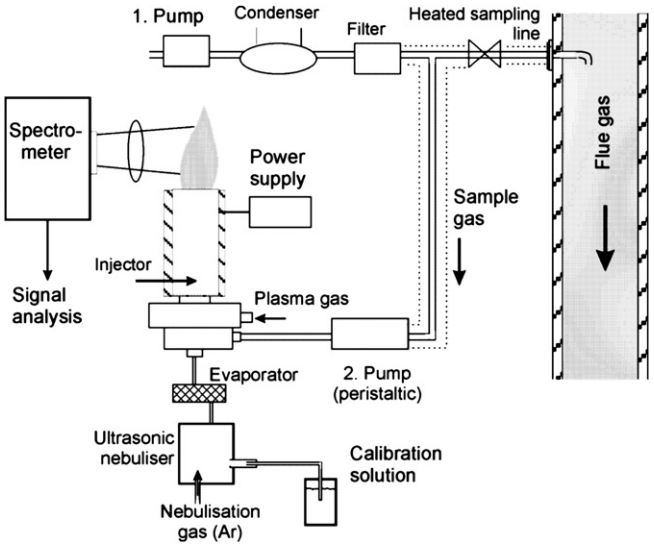

Fig. 10. On-line flue gas analysis by ICP-AESs.

being detected have ionisation energies lower than these ions, ionisation may be enhanced.

Ludwig et al. [372] and Gauthier et al. [373,374] each developed their own ICP-AES systems to measure vaporisation rates of heavy metal species in real time in thermochemical processes, though their respective approaches differ. The Swiss group [372] coupled their ICP-AES system to a thermogravimeter (TGA) using a condensation interface [213] (mentioned in Section 3.2.5), which transforms gaseous high-boiling substances into aerosols. This device allows the study of evaporation behaviour of metal species under different thermochemical conditions. The method is suitable for use in industrial processes since relatively large samples in liquid or solid form (up to 500 mg) can be analysed. The TGA-CI/ICP-AES system allows quantitative data to be obtained, so the emission intensities could be directly related to gravimetrically determined evaporation rates of the compounds of interest. First tests were performed on $CdCl_2$, a key volatile heavy metal species.

In the method of Gauthier et al. [373,374], an ICP spectrometer, modified to allow direct injection of gas into the argon plasma was employed. The interface consisted of two sampling stages: first the gas was first aspirated through a membrane pump and then passed through a peristaltic pump. The sample was then sent through a heated line and injected into the ICP. In the specific application, metal species vaporising from a fluidised bed incinerator were sampled from burning organic matrices without directly sampling the fluidised solids. Emission intensities were monitored as a function of time and used to validate an inverse model [373], which predicts the global rate of release of metal species from the combustion process, so that rates of vaporisation can then be determined from any matrix following on-line measurements of metals from flue gas.

To allow the introduction of molecular gas samples as well as higher water and particle loadings, an air-ICP system was developed at Iowa State University. Emission spectra observed in an air-ICP include not only the metal spectra of interest in the region 200–350 nm, but also interfering molecular bands (N_2^+, NO, OH). Thus a much higher spectral resolution is needed to isolate the atomic lines of interest. Initially, a conventional 1 m monochromator/CCD combination was used to analyse the ICP emissions, but this was later replaced by an échelle/acousto-optic filter (AOTF) spectrometer system [375] for better spectral resolution and coverage as well as multiple element detection capability and suppression of plasma background emissions.

A similar system was constructed by modifying a commercial argon-ICP device to facilitate introduction of sample air [376] and to extract continuously from gas stack or ducts. Using a multichannel vacuum spectrometer, simultaneous analysis on up to 61 different wavelengths allowed measurements of many species including As, Cd, Cr, Hg, Pb. The instrument was capable of a measurement frequency of 30–60 measurements/hour and detection limits between 0.1 and 20 $\mu g/Nm^3$. Nevertheless, interferences in the incinerator stack gas lead to overlapping atomic lines and various molecular emissions. In addition, the combustion product CO_2 was found to suppress plasma excitation. After laboratory tests, the system was linked to a rotary kiln incinerator simulator and was further developed into a prototype commercial system (Section 5.4).

4.3.2. Microwave induced plasma – atomic emission spectroscopy (MIP-AES)

Where analytes are carried by molecular gases (as in combustion analysis) MIP-AES may represent a good alternative to the argon ICP-AES system. The excitation power of the IC-Plasma is reduced by the presence of even small amounts of molecular gases. Air and N_2-ICP-systems are available, but these require relatively high powers (>3 kW), making the equipment much less compact. Timmermans et al. [377] investigated and compared MIP systems based on the axial injection torch (TIA) and on the microwave plasma torch (MPT). The TIA (=Torche à l'injection axiale [378]) is the less sensitive of the two techniques, but is more compact, requiring lower powers for stable plasma generation and lower gas flows.

Recent developments in AES with microwave-induced plasmas (MIPs) are presented by Broekaert and Siemens [379], including production of MP discharges, miniaturised systems and sample introduction, including pneumatic and ultrasonic nebulisation. Developments in the generation of gaseous analyte species and spark and laser ablation are discussed, as well as the application to trace element (Pb, Hg, Se, Sn etc.) monitoring and particle sizing for different types of analytes.

Woskov et al. [380] designed a continuously operating atmospheric microwave plasma monitor and applied it for measurements of trace metals in-stack exhaust. The plasma, powered at 1.5 kW and 2.45 GHz, was sustained in a shorted graphite waveguide attached to the stack pipe by a short sample line (<50 cm). Stack gas was drawn isokinetically into the plasma by suction. Measurements at a RKIS simulator were made on lead, chromium, and beryllium and were referenced to EPA Method-29. Tests were made at high (40–60 mg/m^3) and low (10–15 mg/m^3) concentration levels. The instrument was calibrated by injecting known concentrations of metal solutions as required. The MP monitor achieved relative accuracies of ca. 20% for Pb and Be 40% for Cr with a detection limit <3 mg/m^3 for a time response of ca. 1 min. Further metals could be monitored, but Hg and As present problems because the plasma is less efficient in exciting Hg and because absorption by O_2 and by other species in the UV interferes with detection of As. This difficulty is also common to air-ICP and in-situ spark plasma methods for continuous monitoring of metal species.

4.3.3. DC-plasma spectroscopy

This method, in the form of PEARLS (=plasma excited atomic resonance line spectroscopy), was developed at Tampere University of Technology/Finland and applied for alkali measurements in combustion facilities operating under industrial conditions where optical ports equipped with windows are installed in the flue gas pipe [148,381]. A sample flow is taken through a short, electrically heated (850–900 °C) sampling line and turbulently mixed in a nitrogen DC-plasma jet, which heats the gas to 2100–2500 °C.

Alkali species bound in compound form atomise in the plasma and the alkali atoms are detected by AAS or AES. Optical signals are then transferred to a remote computer/spectrometer unit by an optical fibre. Measurements were quantified using the calibration system and procedure described in Ref. [184].

A modification of the PEARLS instrument, HEAMON (HEAvy Metal MONitor) has been demonstrated for heavy metal detection [382–384]. In this case, detection of metal species was by AAS only, making use of the Zeeman background correction [223,385] method using magnetic fields of up to 0.88 T to remove background interferences.

Since alkali species are measured here via atomic spectroscopy, application of the PEARLS/HEAMON method requires that the atomisation rate of metal compounds in the measurement volume be estimated. This is done by performing equilibrium calculations for the relevant gas composition using HSC chemistry [184,386]. Results show that the optimum atomisation temperature lies between 2000 and 3000 K. The rate differs for different species, for example, at 2300 K, nearly 100% dissociation is achieved for Cd, whereas for Pb, the corresponding rate is only about 50%. Temperatures reached in the DC-plasma are much lower than in other types of plasma discussed here and the residence time of the sample gas is short. Under these conditions, heat transfer calculations give an upper size limit for vaporisation of particles of ca. 3 μm.

Details of the atomisation and excitation mechanism for this technique can be found in Ref. [386a].

4.3.4. Laser induced breakdown spectroscopy (LIBS)

As an analytical method, LIBS can be traced back to the 1960s [387]. Its development and the diversity of its application for both off- and on-line measurements can be judged from several reviews and books [388–390]. Some fundamental aspects of the technique (temporal behaviour, spectral discrimination, wavelength dependence, calibration, matrix effects) were described briefly in the previous review [218, p. 344-6]; these and some further aspects are considered below. Section 5.6.3 then considers applications of LIBS in glass furnaces and mineral melts as well as in the flue gas of combustion and gasification plants.

Of all the on-line plasma methods, LIBS is the only one that can be operated *in-situ*. It can be considered non-intrusive, since only a microplasma is generated. The experimental setup is similar to LIF and PFF, but high laser densities (several J/cm^2) are required to generate the microplasma in the measurement volume (Fig. 11). In this way, particles up to a certain size are vaporised, atomised and then measured together with the gaseous metal atoms already present. Thus gaseous and particulate phases cannot be discriminated. In addition, the strong focussing of the laser beam leads to small measurement volumes, typically only about 100–200 μm in size and this limits the sensitivity of the method. Typical detection limits lie in the range 10–100 ppb, depending on the element, conditions and optical arrangement. Typical precision (as given by relative standard deviation) for LIBS is in the range 5–20%. Shot-to-shot fluctuations cause differences in the plasma, influence signal intensities and hence lead to poorer precision. It is therefore usual to average spectra as needed to achieve an acceptable statistical error. Accuracy on the other hand depends on factors such as sample matrix, homogeneity, particle size, chemical composition and can be very variable. Some typical figures are given in the relevant sections of Chapter 5.

At short times (up to a few μs after plasma generation), temperatures reached in laser induced plasmas are in the range of 10,000–25,000 °C. This allows atomisation of molecules and excitation of the electrons in the neutral atoms and ions formed in the plasma out of the ground state and into excited electronic states. As

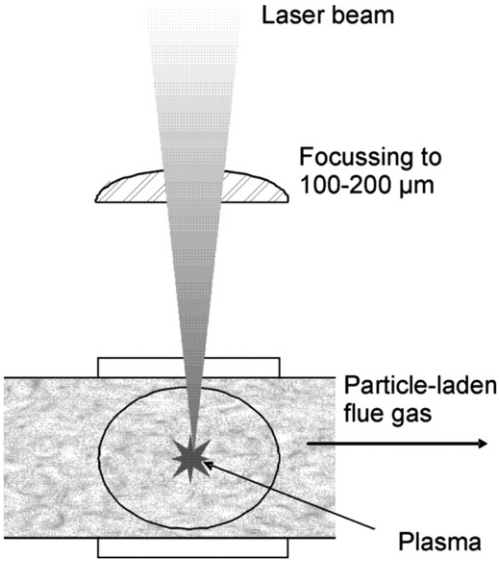

Fig. 11. LIBS – principle.

the plasma cools, excited electrons and ions relax into their ground states, emitting light at characteristic atomic frequencies, which are then detected by AES.

Several authors have performed kinetic modelling of the LIBS process. Casavola et al. [391] studied the expansion of the plume produced by a nanosecond laser pulse interacting with a metallic titanium target in a nitrogen environment. The model was based on a 2D fluid dynamic code and was coupled with either a local thermodynamic equilibrium (LTE) or a chemical non-equilibrium model. These workers showed that the role of chemistry and particularly the interaction between the plasma and the background gas strongly affects the gas dynamic behaviour of the induced plasma. Vidal et al. [392] used a 1D fluid dynamics model to investigate plasma expansion following ablation of aluminium by ultrashort pulses.

Babushok et al. [393] developed a chemical model for the LIBS plume from metallic lead, while working towards a CFD model of LIBS phenomena. The model, which assumes a high-temperature mixture of air and water vapour, contains 38 species and 220 reactions and includes air and ion chemistry as well as steps corresponding to oxidation, excitation and ionisation of Pb atoms. The neutral atomic Pb species, nine distinct electronic states, include the upper and lower levels of the levels most observed. Other Pb species are Pb^+, PbO, PbO_2 and Pb_2. Initial plasma temperatures are taken to be 10,000–18,000 K and the gas temperature decayed exponentially in times of 2–30 μs. The model was used to calculate the temporal evolution of major air and Pb species in the ns to μs range. In addition, lifetimes of Pb transitions in the LIBS plume determined experimentally by time-resolved emission were consistent with those calculated for an assumed temperature decay time of 25 μs. Air and water vapour decreased the amounts of excited Pb atoms in the plume compared to those measured in an inert atmosphere (such as N_2). Part of this decrease should result from collisional quenching and energy transfer (point 5 below), but chemical processes resulting from ionisation and dissociation of gas molecules also play a role.

In performing and evaluating LIBS measurements, a number of factors and procedures have to be considered:

1. Detection timing. Investigations of temporal gating for several metals show differing decay rates between the continuum

plasma emission and atomic emissions, which means that maximum S/N ratios were observed at different times [395,396]. For example, a relatively short delay of 12 μs was found suitable for Ar, Cd, Hg and Be, whereas for Cr and Pb, a delay time of 50 μs gave the best results. The temporal characteristics observed are related to the associated energy levels of the respective transitions. The lower emission intensities at longer delay times can be compensated by wider gate widths.

2. Pulse energy/spark size. Beyond a certain threshold pulse energy, a constant percentage of the laser energy, corresponding to a certain energy density, is coupled into the plasma [396,397]. As the laser pulse power is increased, the volumetric energy density remains the same while the size of the plasma itself increases. Now the temporal character of the plasma depends both on the initial energy and on the size of the plasma (affecting the radiative properties of the plasma), so each chemical species in the plasma will have its optimum detection timing.
3. Particle size. Quantification of LIBS-signals essentially requires that particles in the measurement volume vaporise completely. Partial vaporisation may result in a non-representative sample and hence only a semi-quantitative measurement. However, one cannot define any particular size that can be fully vaporised, since each particle has its own threshold for vaporisation, dependent on its composition. Thus a specific amount of energy is needed vaporise a particular type of particle. For example, Carranza and Hahn [398] measured emission of Si microspheres at 288.16 nm and obtained a linear relation of LIBS signal to particle size up to nearly 10 μm.
4. Determination of peak area for the transition of interest and division by a representative baseline area. For an optically thin plasma, the peak area is approximately proportional to the elemental concentration and the laser power, whereas the baseline is proportional to the laser power. Thus the ratio of the two areas is proportional to the analyte concentration only. At low concentrations (about 50 ppm by mass), the evaluated ratios are usually linear.
5. Effects of measurement environment (bath gas)
   a. Collisional quenching and energy transfer of excited states. Oxygen, generally one of the most efficient quenchers in combustion environments, can reduce the LIBS signal significantly, particularly at longer delay and gate times. Again the magnitude of the effect differs for each element. For example, for the Pb transition at 405.8 nm and the Be transition at 234.9 nm, quenching by oxygen can be significant, but minimal for Be at 313.1 nm. In contrast, O_2 causes an *increase* in emission signal for Cr measured at the 429 nm line. For Hg emission at 254 nm (6p state), a strong quenching effect has been observed, with a nearly 85% fall in the LIBS signal when changing the environment from N_2 to air for a delay and integrations times of 25 μs and 20 μs, respectively [399]. However, for two other transitions of Hg at 365 and 436 nm (from the 7s and 6d states respectively, Fig. 7a) the corresponding fall in LIBS signal was only 18%. Thus the strong quenching effect is specific to the 6p state of Hg. On the other hand, at short delay times (<20 μs), where the plasma temperature is high and the mole fraction of O_2 is small enough, the LIBS signal at 254 nm is not substantially affected. The strength of quenching effects for Hg (and also for Be and Pb) may be associated with the closeness of energy levels of the Schumman-Runge bands of O_2 and the atomic levels [394]. In contrast, the Cr transition at 429 nm lacks energy levels close to the O_2 transition energies.
   b. Other bath gas effects. The intensity and time evolution of LIBS signals from Na, Ca and Mg in different bath gases was studied at 10 μs delay and 50 μs gate width [400]. Results showed that the presence of CO_2 in the bath gas leads to increased peak areas and background levels for emission lines of neutral atoms compared to pure nitrogen bath gas. For Na, peak areas at 589 nm were 27% higher. On the other hand, decreased values were observed for ionic Mg and Ca lines. These effects were interpreted as resulting from an increase in free electron number density for this delay time. Equilibrium calculations showed that this increase in free electron density is to be expected for atomic and molecular species with low ionisation energies in the presence of CO_2. In contrast, similar studies for short delay times (0.35–2 μs) showed only minor changes in electron number density with bath gas composition [401].
6. Effects of analyte phase on calibration response. In Section 3.1.4, general aspects of signal calibration were discussed. For actual combustion effluent streams, calibration of LIBS signals becomes more complex, since mixtures of gas phase and particulate-phase species are invariably present and both are detectable by LIBS. However, it should not be assumed that LIBS signals are generated with the same efficiency from solid and gas phases. Hohreiter and Hahn [401a] showed that at constant electron density and plasma temperature, a far larger signal can be generated from particulate carbon than from gaseous molecules such as CO_2, CO and CH_4. These workers proposed a physical model whereby solid-phase analyte species are accumulated and dissociated preferentially within the plasma, resulting in larger emission signals than with gas phase analytes. A key role appears to be played here by the relative inertial effects when the analyte species interacts with the expanding plasma.
7. Optical effects. The position in the plasma with respect to the collection optics has a significant effect on the signal collected from particles. Lithgow and Buckley [402] showed that the scatter in LIBS particle data can to a large extent be corrected with a transfer function related to the collection optics.
8. Self-absorption of strong emission lines linked to the ground state. Reabsorption by ground state atoms leads to non-linearity of the dependence of line emission intensity on element concentration. This problem can be circumvented by determining correlation coefficients between measured LIBS concentrations and certified concentrations for known samples and for a given experimental arrangement. Using these coefficients, the concentrations of elements in samples of unknown composition can be obtained [403,404].

4.3.5. Spark induced breakdown spectroscopy (SIBS)

This method is one of the two plasma techniques not requiring a sampling line. The plasma is generated by spark electrodes (1–5 J discharge energy, 1 Hz) inserted into the flue gas. Thus SIBS is both on-line and in-situ, but is intrusive [405–407]. To make measurements on a gas stream, the spark gap is arranged so that the stream flows between the electrodes. The spark discharge heats the gas between the electrodes to temperatures in excess of 5000 K. The sample molecules are thus vaporised, ionised and excited. Spectral resolution is achieved with a spectrometer/OMA combination. Analyte signals are separated from broadband plasma emission by delaying detection 20–50 μs and are collected radiometrically by filtered photomultiplier tubes. Using AES for detection, the SIBS monitor detects heavy metals in gases, aerosols and as particulate species. To check for possible spectral interferences, stack gas-equivalent concentrations (>1000 $\mu g/m^3$) of the

main ash components (Fe, Ca, Mg, Al) were generated and sampled. No spectral interferences were found from these elements in the wavelength regions at the bandwidth (1 nm FWHM) of the radiometer filters. Metals detected include Pb, Cd, Cr, Hg, U238, Tc99, Se, Sb and As. An accuracy of ±10% of reading is claimed with ±5% repeatability. Detection limits for Pb and Cr are estimated to be about 10 μg/m^3.

4.4. Ionisation/mass spectrometric methods

An extensive review of mass spectrometric methods (specifically addressing aerosol detection covers developments up to the end of the 1990s [408]. The methods discussed below are selected to represent those that have undergone further recent development and have been applied in combustive environments.

4.4.1. Surface ionisation (SI)

Surface ionisation was developed and refined in the 1990s specifically for measuring alkali species in combustion systems. The method was described in the previous review [218], but the basic working principle is as follows: after impinging on a heated platinum filament, adsorbed alkali salt particles from the gas stream melt, the molecules dissociate and alkali atoms are evaporated as either positively charged ions or neutral atoms. The probability for the formation of ions is dependent on the work function of the surface and the ionisation potential of the atom. For most elements, the ionisation potential is larger than the work function of platinum, resulting in a very low probability for ionisation. However, if the ionisation potential is low, the probability for ionisation becomes large. Alkali metals have very low ionisation potentials, leading to an ionisation probability close to unity.

The SI detector is equipped with a hot sampling line to extract flue gas for continuous alkali measurements at pressures up to 30 bar. The instrument and its support system is described in detail [127,409]. Time resolutions of seconds and a lower detection limit of about 1 ppb can be achieved. Raw SI signals can be converted to absolute concentrations by calibration in one of two different ways [409]: a) evaporation of a known amount of crystalline alkali salt and b) detection of an aerosol of submicron monodisperse alkali salt particles generated by a constant output atomiser. The factor to be determined is the *detection probability*; for method a) a value of $(1.1 \pm 0.3) \times 10^{-3}$, was obtained at atmospheric pressure whereas at 11 bar the corresponding value was $(4 \pm 1) \times 10^{-4}$. For method b) the measured probability was $(1.2 \pm 0.3) \times 10^{-3}$, in good agreement with method a).

The SI technique has been applied extensively to coal and biomass combustion [127,409–411] and also for investigating the capture of alkali by minerals [412]. These applications and others are discussed in Section 5.7.1.

A new system, combining SI with an aerosol mass spectrometer is described below in Section 4.4.4.

4.4.2. Molecular beam mass spectrometry (MBMS)

In MBMS, the sampled gas is led to a high-pressure mass spectrometer (HPMS), where free jet expansion occurs, leading to formation of a molecular beam. This procedure minimises chemical reactions and condensation of the gaseous molecules. Mass resolution allows a variety of chemical species to be determined with sensitivities down to about 20 ppb in real-time [153,413,414]. The technique is suitable for condensable and non-condensable species in the gas phase. The MBMS method has been used on various combustion and gasification plants at temperatures up to 1500 °C and pressures up to 15 bar. A number of applications are considered in Section 5.7.2.

4.4.3. Inductively coupled plasma – mass spectrometry (ICP-MS)

The coupling of ICP and MS is now well established in many areas of analysis and commercial instruments are available. Technology exists that allows chemical analyses in time frames suitable for transient inlet systems [415]. Real-time multielement monitoring of airborne particulates was demonstrated recently by Nichigushi et al. [416] using ICP-MS equipped with a gas converter facility. This allowed direct introduction of particles into the ICP-MS instrument. A series of metals, including Cd, Sn, Sb, and Pb, was measured with a time resolution of 8 min over a time period of 77 h.

4.4.4. Single-particle mass spectrometry (SPMS)

Aerosol particles from industrial sources usually contain a mixture of chemical species and it is the mixing of particles that obscures their original chemical distribution. Conventional particle analysis systems, of which a broad range is on the market, may be able to size-select particles but the chemical analysis gives only average properties. The only way to obtain the full chemical distribution is by single-particle analysis (SPA). The development of fast digital converters and higher computational capabilities as well as optical and laser technology in the past 1–2 decades has allowed the construction of new instruments for real-time measurements of size-selected (single) particles. For details of the essential features and functioning of real-time SPA systems the reader is referred to the article of Wexler and Johnston [200]. These systems are able to determine not only particle size but also provide information on the chemical composition of individual particles. The tasks of ionisation, mass analysis, particle sizing and detection may be performed in a variety of ways, but the common feature of SPA-instruments is an inlet system (usually containing three differentially pumped vacuum chambers) that forms a particle beam and reduces the pressure to the nPa level needed for admission to the mass spectrometer. Three of these instruments will be described briefly here to illustrate their capabilities.

Surface ionisation-mass spectrometry was developed at the University of Göteborg [417–419]. The instrument consists of an aerosol inlet system, an SI unit, and an MS unit. The vacuum system is pumped by one mechanical and two turbomolecular pumps, and a pressure of 10^{-5} mbar is maintained in the main chamber during operation. Aerosol particles are drawn into the mass spectrometer through the particle inlet consisting of a critical orifice (100 μm diameter) and an aerodynamic lens system. The orifice controls the pressure drop and flow rate. The aerodynamic lens system consists of six orifice lenses in a stainless steel tube [420,421]. As a result of successive compressions and expansions of the aerosol on its way through the lens system, the particles form a narrow collimated beam. The sharply focused particle beam is directed onto a resistively heated platinum surface in the detection chamber. The Pt surface is made as a box of platinum foil (25 μm thickness), which limits particle bounce on the hot (1500 K) surface [417,418]. On contact with the Pt surface, particles decompose and the alkali content of the particles is transformed into a burst of alkali ions during (typically) a few hundred microseconds.

The first version of this instrument used a quadrupole mass spectrometer [417] and measured one element at a time, but a more recent version combines the SI device with an orthogonal acceleration time-of-flight mass spectrometer (OA-TOFMS) [419]. In this setup, the ions emitted from the Pt surface enter a deflector unit, which at a certain time accelerates them into the flight tube of the OA-TOFMS. The new version of the instrument produces a mass spectrum for each detected particle. After characterizing the instrument in laboratory experiments and determining alkali metal content for particle diameters in the range 50–500 nm, ambient air measurements were made at an urban background site. In addition,

particles from sea spray and from biomass burning could be identified from their Na and K content.

Atmospheric time-of-flight mass spectrometry ATOFMS [422,423], developed at the University of California at Riverside. Particles from the sampled gas entering the measurement system are desorbed and ionised in the mass spectrometer using a pulsed laser (excimer or tripled- or quadrupled-YAG-laser). The ions formed are separated by time-of-flight i.e. ions with different m/z-ratios reach the detector at different times. As well as performing chemical analysis by laser desorption mass spectrometry, the ATOFMS instrument includes a particle-sizing region, where particles are sized using light scattering of a 50 mW, cw-diode laser pumped YAG-laser at 532 nm. The original ATOFMS [422] had a converging nozzle inlet but this has been replaced by an aerodynamic lens focussing system [423]. The light scattering region was also improved by replacing several optical components with precision lenses and mirrors and including a fast amplifier with noise filter in the detection system. The improved ATOFMS can now analyse ultrafine particles down to about 90 nm.

A third SPA-system [424] also uses an aerodynamic inlet and TOFMS analysis, but in the source region, ions are formed by a high-powered Nd:YAG laser. This allows particles down to ca. 10 nm size to be ionised, i.e. down to the nuclei mode. Positive ions formed by multiphoton laser ionisation are accelerated along the TOF tube and detected with an MCP.

An aerosol mass spectrometric system that combines three different laser-based methods for on-line analysis of particles has enabled a wide range of organic and inorganic species to be detected [425]. The three techniques were one-step laser desorption/ionisation (LDI), two-step laser desorption/photoionisation (LDPI) and thermal desorption/photoionisation (TDPI). Of these, LDI is especially suitable for the detection of inorganic compounds and the determination of elemental carbon content.

5. Applications

This section describes field applications of several methods presented in chapter 4 under a variety of industrial or near-industrial conditions. Some areas of application had already been identified in Section 2.6. Other methods, which may have potential for development, but have so far only been demonstrated in small, bench-scale laboratory experiments, are not considered further here.

5.1. Conventional absorption

Following development of the absorption monitoring system described in Section 4.1.2 [240], field measurements of Hg emissions were performed on a rotary kiln incinerator simulator (RKIS), where various gases (NO_2, SO_2, HCl etc.) were injected as potential interferants. These measurements were compared with data from the Ontario-Hydro method and a commercial CEM as references. The instrument showed sufficiently fast response to changes in gas conditions, as demonstrated by corresponding spikes in the signal. The pyrolysis tube was employed successfully to convert molecular Hg to elemental Hg prior to analysis. Total Hg concentrations up to about 20 ppb (by volume) were measured and detection limits near 0.6 ppb achieved. Comparison with the data from the other two analysers showed reasonable agreement, so long as the pyrolysis tube was kept at a high enough temperature (1100 °C), in order to atomise all the Hg that had been in molecular form. Relative accuracies are then given as 2–3%. Compared to most (commercial) CEM systems, this instrument is compact and requires relatively low maintenance, since no chemical solutions or traps are used. This also means that losses of Hg are minimised.

As mentioned in Section 4.1.2, commercial extractive CEMs have been developed [237–239] and some are already approved by national authorities (e.g. TÜV in Germany) for flue gas measurements and have produced many hours of data at larger scale power plants.

The new *in-situ* AAS monitor for atomic Hg [242, Section 4.1.2.], using LED-absorption for background correction of SO_2, has been tested in the stack gas of a commercial (230 MW) coal-fired power plant. The monitor was installed just after the electrostatic precipitator, where particle loads were low. Hg- and SO_2-concentrations were determined simultaneously and continuously for several hours from start-up of the plant burners. Internal quantification of the measured Hg data gave concentrations in the expected range of 1–30 $\mu g/m^3$.and variations in Hg concentrations were observed to correspond to various plant operations such as start-up or switching from natural gas to coal firing. However, although SO_2-concentrations could be verified by a standard measurement method, an equivalent method for Hg was not available for these first tests. Thus full evaluation of this technique awaits further tests, including comparison with an accepted standard method and measuring experience under different operational conditions.

5.2. TDLAS

Alkali species: The TDLAS method, applied to potassium, rubidium and caesium, has been employed in several measurement series at industrial power plants [226,227]. Simultaneously, O_2-concentrations were monitored, so that correlations between K and O_2 could be investigated.

a) 250 kW Atmospheric pressure PCC [226]. In the atmospheric pressure combustor, quantitative measurements of K concentrations gave values in the range 50 ng/m^3–30 $\mu g/m^3$, although typical values were about 2 $\mu g/Nm^3$, corresponding to 8×10^9 atoms/cm^3. The detection limit attained was 4×10^7 atoms/cm^3 (10 ng/m^3 or 7.5 ppt by weight). The corresponding minimum absorptions were in the range 10^{-3}–10^{-4} for a path length of 30 cm. The O_2 concentration, measured in this experiment by an extractive probe, was anti-correlated with that of K, i.e. under reducing conditions K can rapidly increase by a factor of 100 or more and lead to complete absorption of the laser beam. A similar effect of increasing metal emission with decreasing O_2 concentration has been observed in glass furnaces during detection of Na by LIBS (Section 5.6.3).
b) 1000 kW Pressurised PCC [226]. The optical access to the flue gas was located downstream of the liquid ash separator. Many hours of continuous data were taken. Averaging over 100 scans per measurement point, a time resolution of 1.7 s was achieved. In the initial stages, oil was used as fuel and the low alkali content is reflected in the amount released during combustion, approximately 20 ng/m^3. As soon as combustion was stable and the temperature sufficiently high (around 1450 K), the fuel was changed to pulverised coal. The K concentration then rose steadily up to 1.5 $\mu g/m^3$.

The DL chosen for this work was the VCSEL, because of the wide continuous tuning range of 30 cm^{-1}, and was used to scan over both K and O_2 lines. Pressure broadening leads to reduced sensitivity and accuracy: the minimum detectable fractional absorption was on the order of 10^{-4} (at a path length of 14 cm) for the O_2 absorption lines and 10^{-3} for the strongly broadened K lines. The D1 line was selected because it interferes less with neighbouring oxygen lines, in spite of having only half the line strength.

c) Test combustor for batch incineration and pilot-scale (1.5 MW) rotary kiln with post-combustion chamber [227]. As well as concentration measurements, TDLAS can be applied to determine residence times of flue gas in combustion environments. In this work, rubidium and potassium were used as tracer to follow the gas flow, using an FPDL or ECDL and VCSEL, respectively. An aqueous solution containing KCl and RbCl was injected over an 836 ms period and the passage of the two elements through the flue gas monitored at two different locations: Rb was monitored 8.5 m after the injection site but before the post-combustion chamber, whereas K was detected 8.6 m further downstream. The residence times measured in the rotary kiln were 15 s for Rb and 26 s for K. Peak concentrations of K were about 2×10^{14} atoms/m^3, those of Rb ca. 1.5×10^{15} atoms/m^3. However, K was present in the fuel of the kiln, therefore it had an offset compared to Rb. This background K concentration was between 1 ng/m^3 (ca. 3.5×10^{12}) and 1 μg/m^3, depending on the fuel, temperature and oxygen concentration. Detection limits of about 0.1 ng/m^3 (80 ppq = 80×10^{-15}) were achieved for K and standard deviations for K measurements, derived from residuals are typically in the region of 5–10% for an average of 100 scans.

Mercury: The TDLAS UV-sensor described in Section 4.1.3 was applied for measurements of atomic mercury in both in-situ and extractive modes in a laboratory-scale 29.3 kW (thermal power) coal combustor and *in-situ* measurements in a flow reactor [265]. Measurements by TDLAS were compared to measurements from a commercial mercury analyser (CMA). Extractive sampling was performed to improve the detection limit of the sensor and demonstrate the feasibility of total Hg concentration measurements in the future through extractive sampling. Significant variation in the atomic mercury concentration of coal-combustion exhaust was observed over short time periods during the *in-situ* measurements. Detection limits obtained for in-situ and extractive modes of measurement were of 0.3 and 0.1 ppb, respectively, over a 1 m path length. Concentrations of Hg measured with the TDLAS method were nearly a factor of two higher than those determined using the commercial analyser. This was attributed to adsorption of mercury on the sampling lines of the extraction system.

5.3. DOAS

The DOAS technique (as IACM), has been applied extensively for gas phase alkali measurements up to commercial scale [282–285]. The typical position of the instrumentation in a PFB plant is downstream of the main boiler and just upstream of the convection pass. The main application to date is to monitor the progress of the "ChlorOut" process [426]. In this process, ammonium sulphate is sprayed into the hot combustion gases to convert the highly corrosive alkali chlorides into the less troublesome alkali sulphate. Plants where this process is used include the 105 MW BFB CHP-boiler at Nyköping [284] and the 96 MW boiler at Munksund, both in Sweden [282,285]. In the former case, the fuel mixture consisted of wood chips, demolition wood and coal, in the latter case, mainly bark (<80%), but also sawdust, wood chips and plastic waste material (ca. 6%) were fired. The signal from the IACM system was used to control the amount of ammonium sulphate introduced into the boiler. Data taken on several days gave alkali chloride quantities varying from 0.5 to 1.9 ppm with ChlorOut and 14–19 ppm without. In this way, the effectiveness of the ChlorOut-process could be verified.

A typical measurement in the Munksund CFB boiler is shown in Fig. 12 [282]; the IACM instrument was positioned after the second superheater. A combination of operational and IACM data shows the prompt response on injecting the additive ammonium sulphate. A mixture of biomass (bark) and waste was fired, the waste fraction being 3–4%. The IACM measurement shows that the KCl concentration decreased from 15 ppm to about 2 ppm Fig. 12 also shows that emissions of NO were reduced by 50–60%, since NO reacts with the ammonia formed in the process to form nitrogen and water.

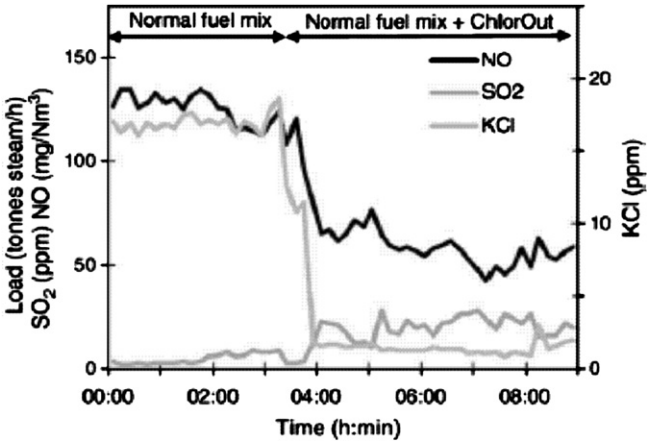

Fig. 12. Operating conditions and flue gas emissions, showing application of ICAM to the measurement of KCl and SO_2; concentrations of NO obtained from operational data. Reproduced from [282] with permission.

In a smaller (12 MW) scale CFB boiler at Chalmers University, Sweden, the dependence of the ratio of biomass to coal at different feed rates of limestone was studied [283]. Again IACM measured the alkali chlorides upstream of the convection section of the boiler. In addition, deposits in the boiler were analysed by SEM-EDX. Results showed increased amounts of alkali both in the gas phase and in the collected deposits.

5.4. Conventional emission

For mercury, commercial continuous emission monitoring systems have been evaluated (Section 4.2.1, [287,288]) at different coal combustion utilities (PPC, CFB) over several months operating time and results compared to values obtained using reference techniques, here the Ontario-Hydro (OH)-Method [205] and Method 30A, a conceptual protocol proposed by EPA as a reference for CEM systems [204]. Procedures specified by US Federal Regulations were followed. All detectors were based on atomic fluorescence, half of them using gold traps to capture elemental mercury to form an amalgam. Aspects considered included linearity, response time, day-to-day stability and efficiency of the Hg speciation. Detailed relative accuracy (RA) and bias tests were performed. Two of the CEM systems gave RA values less than 20%, but the other field tests were also considered acceptable because the deviations from the OH-method values were less than 1.0 μg/cm^3 (dry basis).

The multimetal monitoring system based on X-ray fluorescence (XRF) [289, Section 4.2.1] has been evaluated in detail [290]. Field measurements were made at a diesel-fired combustor for incinerating decommissioned munition. The furnace end temperature was 538 °C, the stack temperature 260 °C and the stack gas velocity 14 m/s. The system was tested for its ability to measure Sb, Se, Ag, Tl, As, Hg, Ni and Zn in the feed stream and Pb in the stack gas. Measurements in the stack gas were also attempted for the other metals, though here spiking was needed to ensure sufficient concentrations. All results were correlated with data obtained using the EPA M29 method. For Ni, Pb, Sb and Zn, r^2-values were

better than 0.95, but for Hg, r^2 was only 0.39. Possibly, chemical reactions or deposition had occurred in the sampling lines.

Systems for on-line analysis of sampled process gas by atomic flame emission also exist and these were described in the previous review [218,p.361].

5.5. Photofragment fluorescence (PFF)

5.5.1. Solid fuel combustion (PCC, FBC)

Alkali species: The PFF method, described in Section 4.2.3, has been applied extensively for real-time monitoring in the area of solid fuel combustion, following development of the technique at the Physical Chemistry Institute in Heidelberg. Measurements of Na and K species have been made in pulverised [151,427,428] and fluidised bed (FB) [124,148,188,303,429–432] coal combustion as well as FB biomass combustion [123]. Table 6 gives an overview. In this work, an excimer laser at 193 nm was employed for photofragmentation, so the method is referred to as ELIF, excimer laser fragmentation fluorescence. Potassium and sodium species were detected simultaneously at 769 nm and 589 nm, respectively, in a two-channel system. Sodium species have also been detected by ELIF in an atmospheric bench-scale reactor under conditions that simulated those of gasification [180], where a two-wavelength detection scheme allowed discrimination of NaCl and NaOH (Section 4.2.3.1). However, there has not yet been a demonstration of alkali detection by ELIF in an actual gasifier at semi-technical level or higher.

In the above work, it was shown that alkali species can be monitored continuously, in-situ (i.e. avoiding sampling of the process gas), with high sensitivity (0.1 ppb) and temporal resolution down to seconds over complete reactor operation periods. Typical uncertainties in ELIF alkali measurements are between 30% and 50%, including statistical errors in the signal (5–10%), calibration factor for optical geometry (ca. 10%), uncertainty in the quenching rate (max. 10% for the $K4^2P$ and $Na3^2$ P states)) and uncertainties in the measurement of laser beam absorption by the flue gas (variable, depends on the amount of ash, typically 10–20%).

The PFF method (here ELIF) can furthermore be operated as a method specific to gas phase species, provided that laser energy densities are kept below a level corresponding to the vaporisation energy (around 10 mJ/cm^2 for the alkali chlorides). This feature was exploited in order to obtain information about the gas-/particle-phase partitioning in the flue gas of a PFBC pilot facility [148,303]. In that work, ELIF data were compared with results obtained simultaneously by two complementary techniques, plasma emission spectroscopy (PEARLS)(Section 4.3.3) and surface ionisation (SI)(Section 4.4.1). The latter two methods measure both aerosols and gas phase alkali and consequently the values obtained by PEARLS and SI were mostly higher than those measured by ELIF.

As well as real-time measurements, parametric studies under specific sets of conditions have been performed to determine the dependence on chlorine, sulphur, water, alkali and mineral (particularly clay mineral) content of the fuel on alkali release. Effects of stoichiometry, residence time and temperature have also been investigated. In this case, time-resolved signals recorded for 15–30 min under a constant set of conditions were averaged. For pulverised fuel combustion conditions (drop tube reactor), fuel composition effects have been investigated systematically at atmospheric pressure [427,428]. A hard coal was fired in the range 1000–1300 °C, for residence times in the range 3–5 s and for air numbers (air/fuel ratios) from 1.15 to 1.50. In addition, the amount of chlorine, water vapour and sulphur, respectively, was increased in known amounts by controlled dosing of HCl, H_2O and SO_2 into the combustion gas to determine effects of these components on release or capture of the alkali species. The experimental results are also compared with values calculated using ash/fuel analyses and sequential extraction. The comparison showed that the potassium release expected on the basis of sequential extraction corresponded closely to that observed in the measurements. In the hard coal, K is to a large extent bound up in the clay minerals. The extraction results for Na gave much higher concentrations than the measurements; this is probably a result of Na uptake in slag phases, leading to lower amounts being present in the gas phase and hence measurable.

Similar results on varying fuel compositions have been reported for coal combustion under PFB conditions. One of these experiments [124], performed at 10 bar pressure, considered the effects of varying chlorine and alkali content in the system. The addition of chlorine only (in form of methylene chloride in the air feed) leads to overproportional increases in the alkali concentration, whereas addition of sodium only (in the form of sodium acetate in the fuel) gave moderate, under proportional increases in the flue gas. In contrast, clay minerals such as kaolin in the coal or in the fluidised bed strongly suppressed alkali release by chemisorption, whereby alkali is incorporated into the aluminosilicate structure. Another study [430] was performed at atmospheric pressure, where similar effects were observed as those at 10 bar. In addition, measurements were made after a hot gas filter, whereby a significant reduction (from 20 to 25 ppb to less than 10 ppb) was observed.

In the course of ELIF measurements in an atmospheric CFB combustor, biomass and coal were fired (either alone or in co-firing mode) [123]. Fuels used were four types of straw, selected for their different alkali, chlorine and silica contents and a Colombian black coal. Typical results are shown in Fig. 13. The release of gaseous alkali species were shown to depend particularly on the K/Cl and K/Si ratios in the fuels, but Ca also played a role, since this element competes with alkali for sulphur and chlorine. The highest release was found for the straw fuels with both high K and Cl contents, but co-firing with coal did help to mitigate the release of alkali. Equilibrium calculations confirmed the observed trends of fuel composition and gave more information on sequestering of alkali species by minerals.

Nickel: Real-time monitoring of nickel species in a FB combustion flue gas has been demonstrated, simultaneously with

Table 6
Application of PFF in semitechnical to pilot-scale combustors (all at $\lambda_{ex} = 193$ nm).

Refs.	Measurement object	Main Precursor	λ_{det}, nm	Main aspect considered
[151]	Pulverised coal combustion	NaCl, KCl	589, 766	Real time measurement, varying conditions
[427,428]				Parametric study (T,p, O_2 etc.)
[152,428]				Sorbent effectiveness
[148,303, 430–432]	FB coal combustion	NaCl, KCl	589, 766	Real time measurement, varying conditions
[124,430]				Parametric study (T,p, O_2 etc.)
[124,430]				Sorbent effectiveness
[148,303]				Discrim. Particle/gas
[429]	FB coal combustion	NiCl2	440	Real time measurement, varying conditions
[123]	FB cofiring coal/ biomass combustion	NaCl, KCl	589, 766	Real time measurement, varying conditions
[123]				Sorbent effectiveness
[434]	Glass furnace	NaOH	589	Real time measurement, varying conditions

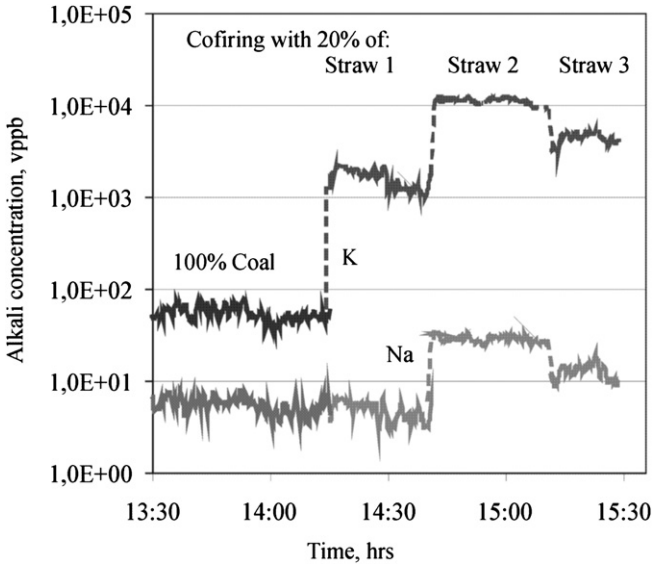

Fig. 13. Alkali concentrations in the flue gas of FB combustion on firing coal and cofiring coal with 20% straw fuels of different composition. The figure is a composite of time-resolved data, average values of which were published in Ref. [123]. Examination of results shows that not only the amounts of alkali are important in deciding the amount of its release; Cl, S, Si and Ca also play significant roles. The highest alkali release, from straw 2, is largely due to the high calcium content; calcium competes e.g. for available sulphur, which would otherwise react with alkali to form the less volatile sulphate. On the other hand, alkali release from coal is low, as a result of the presence of aluminosilicates, which effectively sequester alkali.

potassium species, using two detection channels [429]. Molecular species (in this case mainly KCl, $NiCl_2$) were photofragmented at 193 nm and fluorescence from Ni* and K* atom fragments detected at 440 and 769 nm, respectively. Absolute concentrations were evaluated for K, but for Ni the results were semi-quantitative, since insufficient data on collisional quenching were available for detailed quantitative evaluation. The Ni signals were low compared to those of K, partly due to the very small amount of Ni in the gas phase (<1%) at the flue gas temperatures (ca. 800 °C) and partly to the low laser energy densities (a few mJ/cm^2) used, and hence very low probability of the two-photon excitation process.

For Ni detection at 440 nm, a sensitivity of 50 ppb would be feasible were the laser energy density raised to 10 mJ/cm^2 and the number of laser shots average increased from 50 (as used in those experiments) to 500 (giving 1.25 min resolution at 6.4 Hz). On the other hand, for future work, detection at 362 nm may be preferable, since signal losses by quenching are smaller as a result of the much shorter lifetime of the upper electronic state (56 ns for 362 nm emission as against (293 ns for 440 nm emission) [190]). Also, background at 362 nm is likely to be less than at 440 nm due to the absence of underlying molecular states. For quantitative work, collisional energy transfer and potential spectral background interferences need to be investigated in more detail. In addition, field measurements by ELIF in conjunction with other complementary techniques, such as plasma methods, would be useful as well as analysis of the coal and ash.

Nevertheless, even in the limited study of Ref. [429], it could be shown that the gas phase concentrations of both K and Ni are affected by the amount of chlorine in the system. Both metals have an affinity for chlorine; on the other hand, K and Ni both interact strongly with clay minerals [124,433]. Depending on the situation, if chlorine is added to the system two effects may occur a) if hydroxide is still present, more of it can be converted to chloride and b) the extra chlorine can shift the equilibrium of alkali species (for example contained in aluminosilicates) towards chloride release [429,430,433]. For the case of Ni, extremely little will be in the gas phase at all and considering the vapour pressures of Ni species, this can only be the chloride; everything else is condensed.

Since the vaporisation of Ni compounds at FB temperatures is typically <1% [132] and most of the Ni will be present on ash particles in the flue gas, the application of ELIF to Ni, as described here, will be of more interest to plants operating at temperatures substantially above about 1000 °C, such as pulverised coal combustors and incinerators. However, a greater proportion of the Ni content would be detectable were the laser energy density raised by 2–3 orders of magnitude, i.e. causing laser vaporisation of particles, though signal analysis would then be more complex. On the other hand, compounds of metals such as Pb and Hg are present in gaseous form in much greater amounts and will be of more general interest for fuel conversion facilities and it is on these species that future efforts should be concentrated. A scheme for Hg detection by PFF has now been developed (Section 4.2.3.2, [312,313]), which appears promising for application in combustion flue gases.

5.5.2. Glass furnace

Knowledge of gas phase alkali species concentrations is also of importance in refractory glass furnaces as a result of corrosion problems and particulate emissions to the environment. In particular, information is needed concerning the relation between tank operating conditions and tank atmosphere alkali concentrations. Thus the ELIF method has also found application in an oxygen-fuel glass furnace, to determine amounts of volatilised NaOH under high-temperature conditions [434]. The setup is similar in some respects to that described above for application in solid fuel conversion plants. However there are some differences, such as the use of a smaller excimer laser, operated at 100 Hz, but with pulse energies of typically 100 μJ (rather than mJ at 6.4 Hz [427,432]). A spectrometer was used to isolate atomic lines of Na and K. Field tests were conducted in the oxy-fuel mode at a temperature of 1500 °C and atmospheric pressure. Feed mixtures, including waste materials, were added in batches containing known quantities of sodium carbonate to increase the NaOH concentration in the furnace. The rise and decay of the ELIF signal was followed over periods of about 100 s following addition of each batch of fuel. Signals were converted to NaOH concentrations using a calibration curve generated in a small test furnace. Maximum concentrations up to ca. 250 ppm appear to have been measured, however it is not clear whether and how non-linearities such as radiation trapping were accounted for. The main constraint for this measuring system is that when the furnace is running at 1500 °C, the system cannot be operated in places where the air temperature is 90 °C or more.

5.6. Plasma spectroscopies

5.6.1. ICP-AES

Waste-to-energy-plant. Using their mobile ICP-AES system, Poole et al. made on-line measurements at a commercial scale waste-to-energy, reverse reciprocating grate plant [368–370]. Furnace temperatures were regulated between 850 °C and 1100 °C, with further waste being added in response to falling temperature, which was measured using two thermocouples in the radiation shaft. The plant was operated with excess air, giving an oxygen level in the combustion chamber between 6% and 14%. The flue gas was treated with hydrated lime and an activated carbon dry scrubbing system. Fabric filters collected the fly ash and scrubber products, and were designed to remove particulate matter down to a minimum of 5 μm. The gas clean-up system was preceded by an economiser, which reduced the flue gas temperature to 130 °C at the bag filters. Access of the ICP-AES system to the flue gas was via

a sampling port in a vertical section of the duct just before the scrubber, but some data were also taken at a sampling port immediately after the bag filter system. The particle loadings in the uncleaned gas were very high (ca. 1 g/m^3) and the sampling train was designed to sample particles of max.10 μm size as well as gases. Larger particles were removed using a small cyclone. For some metals, significant variations (4–18 mg/m^3 for Na, 0–0.18 mg/m^3 for Cd) were observed, and were linked to properties of the metal in question, to incinerator operating conditions, and to variations in the waste feed charge. The concentrations of some metals were attributable to specific sources in the waste.

Gasification. Poole et al. [371] also used their ICP-AES system for continuous analysis of elemental emissions from an air-blown fluidized-bed gasification rig of 0.15 m diameter, fired with biofuel (Miscanthus). Flue gas at 250–300 °C was sampled just downstream of the two cyclones, was cooled 200 °C and then passed via a doubly bended pipe (to minimise tar flow) to the ICP-AES system. The flue gas line also included a condensation pot to collect tar. Nevertheless, occasional blockages still occurred, requiring replacement of sampling lines. The gasification gas also affected the shape and colour of the plasma. To be able to monitor the analytical performance and standardise the measurement scale, elements of the plasma bulk gases (Ar, C, N, O) were recorded continuously during all measurements. In this way one could ensure that sufficient gas from the gasifier was being sampled and was reaching the ICP for analysis. The carbon emission was also used to indicate the progress of gasification. Emissions of K, Na, Fe and Ca, all in the concentration range of tens to hundreds of mg/m^3, were observed shortly after the start of gasification, and which decayed with time. Later, Zn was observed (tens of mg/m^3) and still later further emissions of K and Na, indicating a second phase of gasification. Accuracies and standard deviations were calculated for all metals detected and were based on the introducing calibration standards during continuous monitoring. These standards were spiked in relatively high concentrations (several mg/m^3) so as to be distinguishable from the gasifier emissions. For most elements (Al, Ba, Be, Ca, Cd, Co, Cr, Cu, Fe, Mg, Mn, Ni, P, Pb, Sn, V, Zn) accuracies were found to be within 20%. In the case of B, K, Na and Si they were significantly larger, due to actual emissions from the gasifier occurring during the period of the calibration check.

The temporal behaviour of the emissions indicated the relative rates and extent of volatilisation, though quantitative comparisons are not made. The time resolution available shows that even if the time-averaged quantities of released metals are small, short-term (minutes or less) rises can be large and lead, for example, to corrosion effects or environmental problems.

Other work. The ICP-AES device of Seltzer and Meyer [376] has been linked to a rotary kiln incinerator simulator. The system was then further developed into a prototype instrument TJA TraceAIR Multimetals continuous monitor and installed at the Waste Technologies Industries (WTI) commercial waste incinerator in East Liverpool, Ohio for field tests [435].

A promising alternative solution to the problem of sampling for on-line ICP-AES measurements is the condensation interface [213,372]. In the CI, the process gas is rapidly quenched with a cold-water aerosol vapour mixed in a counter current. In this way, a constant fraction of the heavy metals in the carrier gas is transferred to the ICP-AES instrument. The method has been applied to the thermal treatment of filter ash from municipal solid waste incinerators, where the evaporation rates of several elements can be determined on-line in time intervals typically less than 1 min. The method was also adapted to determine total trace amounts of Cd, Zn, Cu, Pb, and K in materials such as contaminated soil, galvanic sludge, scrap metal and bottom or filter ash as well as in thermal recycling of metals from batteries [436] and analysing process gas from wood gasification [437].

5.6.2. DC-plasma

Operation of the PEARLS DC-plasma instrument described in Section 4.3.3 has been demonstrated for on-line determination of sodium and potassium in a 20 kW BFB at VTT, while firing biomass and mixtures of biomass (pine bark or forest residue) and bituminous coal or lignite, respectively [381]. Measurements were made directly in the particle-laden flue gas at a temperature of 880 °C, at the upper port of the freeboard, 2–3 s after the tertiary air inlet. Data taken over periods of ca. 20 min were averaged for each measurement condition. Then it could be shown, in a similar way to the work done by ELIF [123], that firing coal or lignite with the biomass can reduce alkali concentrations in the flue gas substantially by converting chlorides or hydroxides to either sulphates or aluminosilicates. For example, addition of 30% coal to pine bark reduced K release by 59% and Na release by 64%. In general, sulphur and aluminosilicate will compete for the alkali, but the dominance of one mechanism or the other is likely to depend on the relative amounts of these two components in the fuels being fired.

The above BFB combustor was also operated for field measurements of heavy metals using the modified instrument, known as HEAMON. In this case, a mixture of wood (spruce heartwood or bark) and waste was co-combusted [381]. Cadmium and lead were measured by AAS using Zeeman background correction [385] At the cyclone outlet, measured flue gas concentrations were in the range 0.04–0.74 mg/m^3 for cadmium and <0.6–4 mg/m^3 for lead. In the freeboard, concentrations determined for Cd were 0.042–0.54 mg/m^3 and for Pb were <0.6–5.9 mg/m^3. On-line measurements were compared with elemental analysis of ashes collected from the freeboard walls (70–250 μm), the cyclone (10–70 μm) and the baghouse filter (below 10 μm).

A further set of measurements was made in a pilot-scale (2 MW) BFB during co-combustion of wood chips and plastic waste [384]. In this case, the HEAMON instrument was mounted onto the wall of the combustion chamber and the sampling line inserted into the chamber about 7 m above the bed surface. The sampling temperature was 750 °C. Cadmium concentrations of about 0.4 mg/m^3 were measured and Pb concentrations were approximately 4 mg/m^3 when firing wood/waste mixtures.

Under the conditions of the field measurements, detection limits of 0.04 mg/m^3 were achieved for Cd; the corresponding limits for Pb were 0.4 mg/m^3. However, with further development, the method is expected to reach detection limits of 0.01 mg/m^3 or less for several metals that are regulated by EU legislation [14,15].

5.6.3. Laser induced breakdown spectroscopy (LIBS)

An overview of applications to date (not claimed to be exhaustive) is given in Table 7. Most of the facilities were operated at atmospheric pressure, but the temperature at the measurement point ranged from 332 K in the stack of a waste processor to 2550 K in an MHD facility. Except for two investigations employing sampling by a moving band filter, all measurements were performed by direct optical access. Spectral and temporal discrimination was achieved in a variety of ways, ranging from the compact PMT/filter-type system to the more sophisticated ICCD/spectrometer combinations (Section 3.2.3). In many cases, reference measurements were performed by sampling and analysis using XRF, EPA Method 29 or other methods.

5.6.3.1. Combustion of solid fuels. Grate combustor: With a view to investigating slagging potential of various fuels, LIBS measurements were made in a stoker-fired travelling grate combustor of 10 MW electrical power in which biomass (bagasse, fibre cane) and coal were co-fired [438]. The optical access was positioned near the superheater tubes, 0.6 m from the furnace wall. Temperature at the measurement point was about 900 °C. The plasma was created

Table 7
Overview of on-line LIBS applications.

Ref.	Measurement object	Metal Species detected	T*(K)	P*(MPa)	v (m/s)	Other analysis
[438]	Grate boiler (coal/biom.)	Si, Al, Ti, Fe, Ca, Na, K	1170	0.1	12 to 18	Superh. deposits
[438]	Recovery boilers (Black liquor)	Na, K, Si, Mn, Fe, Ca	1230	0.1	10 or 11	n.a.
[441]	Blast furnace, top gas	Na, K, Zn, Pb, Fe	453	0.23	10 to 20	n.a
[442]	Blast furnace, top gas	Na, K, Zn, Pb, Ca, Fe	453	0.23	10 to 20	n.a
[443]	Cement plant (pulverised coal kiln)	Na, K	380	0.1	n.a	JIS-K8808/K0095
[187]	Coal-fired MHD-Facility	Ca, Fe, Ti, Sr, Al	2550	0.36	1089	n.a
[439]	Prototype FB coal gasifier	Na, K	350	1	n.a	n.a
[440]	HT, HP Furnace (gasif.cond.)	Ca, Mg, Fe, Si, Al	350–750	0.1–3.0	n.a.	n.a
[446]	TSCA Incinerator	Cd, Cr, Fe, Be, Y	355	0.1	6	EPA M29
[446]	Simulated incinerator (RKIS)	Cd, Cr, Fe, Be, Y	500	0.1	1.8 to 2.9	EPA M29
[444]	Simulated incinerator (RKIS)	Cr, Cd, Pb, Be	500	0.1	1.8 to 2.9	EPA M29
[445]	Simulated incinerator (RKIS)	Be,Cd, Cr,Hg,Pb,Sb,As	500	0.1	1.8 to 2.9	EPA M29
[447]	Mixed waste surrogate/Plasma hearth	Cr, Mn, Fe, Pb, Ca, Al	n.a.	n.a.	n.a.	EPA M29
[448]	Waste incinerator – filter band	Ni, Cu, As, Sn, Sb, Tl, Pb	n.a.	n.a.	n.a.	TRXRF
[449]	Waste incinerator – filter band	V, Cr, Mn, Cd, Co	n.a.	n.a.	n.a.	TRXRF
[446]	Contained rocket burn facility	Pb	350	0.1	n.a.	n.a.
[453]	NG/O2 glass furnace	Na	620	0.1	29 (down)	
[450]	NG/O2 glass furnace	Ca, K, Na	720/1380	0.1	0.8 (up) 31 (down)	
[451]	NG/O2 glass furnace (air infiltration)	Na	720/1380	0.1	0.8 (up) 31 (down)	TSD/CV
[452]	NG/O2 glass furnace (carryover, volatil.)	Na, Ca, Si, Mg, Al	720/1380	0.1	0.8 (up) 31 (down)	TSD/CV
[400]	NG/O2 glass furnace	Mg, Ca, Na	720/1380	0.1	0.8 (up) 31 (down)	
[438]	NG/O2 glass furnace	Ca, K, Na	1450	0.1	0.5 (up)	n.a.
[454]	NG Engine exhaust	Ca, Mg, Na, Fe	600–720	0.1	30 to 37	
[455]	NG Engine exhaust	Na, Si, Ca	600–720	0.1	30 to 37	EPA M5
[455]	NG-fired steam generator	Na, Si, Ca	430	0.1	10	EPA M5
[455]	NG-fired el. turbine generator	Si, Fe	420	0.1	30	EPA M5
[456]	NG-fired, pyrolytic waste processor	Cr, Mn, Fe	332	0,1	n.a.	EPA M29
[457]	Mineral melt/direct access	Te, Fe, Mn, Mg, Ca, Na, Al	1673–1873	0.1	n.a.	XRF
[458]	Electroplating facility - direct access	Cr	316–340[a]	0.1	n.a.	Filter analysis with ICP-AAS
[459]	Technical polymers/flame retardants	Cd, Cr, Pb, Hg, Sb,Sr	Ambient	0.1	n.a.	n.a.

*T = Temperature and pressure at measurement point; n.a. - not stated in paper.

using an Nd:YAG-later at 1064 nm and 5 Hz and metal elements were detected by an échelle grating spectrometer/ICCD camera system. Spectral resolution ($\lambda/\Delta\lambda$) was 4000. In this way, Ca, Mg, Al, Si, Ti, Fe, Na and K could be detected simultaneously. In the combustor, real-time concentration profiles of these elements were recorded over periods of several hours and then averaged for the different sets of conditions. For example, average K concentrations were about 8 ppm when firing coal/oil and 90–100 ppm when firing mixtures of biomass, coal and oil. Sodium concentrations were about 40 ppm. The LIBS signals fluctuated considerably when biomass was fired, as a result of the high water content in the fuel. The fuel analyses are not given, but one can assume that the large increase in K concentrations stems from a high K content in the biomass as well as the ease of release from biomass compared to coal.

Recovery boilers: LIBS spectra were taken in two black liquor recovery boilers, just upstream of the first superheaters, 1.8 m from the furnace wall [438]. Fume particle loadings were 10–20 g/m^3 and soot blowers were in operation, so the measurement duration was limited before fouling of the optics occurred. In one set of measurements, a linear spectrometer and ICCD camera was used to detect the metals K, Si, Mn and Mg and an OMA to detect Na, both in single-shot mode. In a second set, the combination of échelle spectrometer and ICCD was used to record spectra (1000 shot) and Na, K, Tl and Rb were observed.

Blast furnace: Brysch et al. and Sturm et al.[441,442] demonstrated continuous and simultaneous monitoring by LIBS of Na, K, Zn, Pb and Fe in the top gas (and dust particles carried therein) in a blast furnace. This was done by firing the laser through an optical access at the end of the top gas tube. A lance that contains the optical measuring head with focussing optics and multi-fibre optics to collect the LIBS signals can be moved into the dust stream inside the top gas tube to make measurements at different positions across the tube diameter. The lance works under the conditions of the top gas: average temperature of 180 °C, gas velocities of 10–20 m/s and an average gas overpressure of 2.3 bar. The laser pulses had to be temporally modulated to suppress the effects of pressure on the measured spectra. The top gas pressure affects the LIBS spectra by enhancing particle–particle interactions, increasing the line width and decreasing the line height of the element specific emission. The high CO content of the top gas necessitated monitoring the absence of O_2 inside and CO outside the top gas tube as a safety measure. The instrumentation was installed for measuring campaigns at blast furnace sites in Germany, Finland and Spain. Measurements were made for up to 10 h a day at a time resolution of 10 s. First correlations of on-line top gas measurements with blast furnace parameters were made.

Cement plant: A further LIBS system has been installed at a commercial cement plant with a pulverised coal kiln burner [443]. Concentrations of Na and K were determined in the optically accessed exhaust duct (380 K) over a period of one year. LIBS signals (at 589 nm and 767 nm, respectively) were collected in the back-scatter mode (Fig. 1c) and transmitted to the data acquisition system by an optical fibre. Signals corresponding to Na, K, N and noise from continuous background emissions) were separated by optical filters and detected by gated photomultipliers. Signals were also normalized to correct for plasma temperature effects. Typical Na and K concentrations in the exhaust gas, measured with a resolution of 1 min, were 10–50 ppb, although several sharp peaks (up to 180 ppb), corresponding to changes in operating conditions, were observed. The main source of Na and K was fine particles of cement material, which contained similar amounts of Na and K. The general level of Na and K concentrations determined by LIBS was in good agreement with that obtained from conventional sampling measurements (Japanese industrial standards JIS-K8808 and JIS-K0095). However, the fast response (1 min) of the

LIBS measurements allowed sudden changes to be observed, whereas the conventional sampling methods required several hours sampling time to detect ppb levels of alkali and averaged out short-term peaks.

Magnetohydrodynamics (MHD) test facility: LIBS spectra in the range 387 nm–407 nm were taken from the aerodynamic duct of a coal-fired MHD facility at 2950 K combustion temperature and a total pressure of 4.5 bar [187]. Here the LIBS signals were detected in the forward scattering direction (Fig. 1a), for which opposing windows had been installed in the duct. In addition, the receiving optics contained dichroic mirrors and a notch filter to separate the LIBS signal from the high-intensity laser beam. Major peaks of the spectra were Ca and Al with smaller peaks from Fe, Mn and Ti. Absorption dips close to the 404.58 nm line of Fe were also observed, which were assigned to the 404.41 nm and 404.72 nm lines of K.

Waste incineration: Zhang et al. applied LIBS for detection of metallic elements in a rotary kiln incineration simulator (RKIS), employing a single-window optical access to the measurement volume (cf. Fig. 1c) for laser excitation and detection [444,445]. Results of field tests show that LIBS has sufficient capability as a multimetal continuous monitor for As, Be, Cd, Cr, Hg, Pb and Sb.Time resolution down to 10 s was obtained when averaging over 100 laser pulses. Time-averaged results for the four metals were mostly in reasonable agreement with data obtained concurrently by the EPA M29 reference method. For the reference measurements, samples were collected over 2 h and analysed separately by AAS or ICP-AES. These workers also describe their calibration methods using open or closed calibration setups, both using an ultrasonic nebuliser to produce aerosols of the metal species of interest. In addition, accuracy and precision data are presented for all metals detected. For example, relative accuracies in the range 19% (Cr) to 78% (Cd) were obtained for the low metal concentration field tests (15 μg/m^3) tests [445].

Further LIBS studies done on an RKIS facility as well as a TSCA (=toxic substances control act) incinerator [446] measured Be, Ca, Cr, Fe and Y. On a time-averaged basis, the average difference between LIBS data and the reference method 29 data was 63% for all species. If Be was excluded, the average deviation was 37%.

Similar field simulation measurements were also performed in the off gas of a plasma hearth test stand, into which a surrogate waste mixture had been introduced [447]. Metals detected were Cr, Mn, Fe, Pb, Ca and Al. Simultaneously, analysis was performed by the EPA M29 method and for chromium, detection by laser opto-galvanic spectroscopy (LOGS) was also feasible. The LOGS technique is on-line, but requires sampling, as the OGS-signal is generated in an out-of-pipe flame. Chromium concentrations were significantly higher than those determined by LIBS, largely as a result of interference by a two-photon transition of Na at the detection wavelength of 520.87 nm.

A rather different approach was made by the group at TU Munich, where the measurement volume was accessed using an automated, in-line filter-sampling interface [448,449]. Aerosols from the incineration process were collected on the filter band and analysed by LIBS. Fibre optics was used to transport laser radiation and LIBS signals to and from the filter band, respectively. In this way, quasi-on-line data on the elemental composition of the deposited aerosols was acquired with detection limits for Cu, Co, Cr, Mn, Ni, Sn in the range 0.03–1.2 μg/m^3, for a sampling volume of 1 m^3 and a loaded filter area of 3 cm^2.

Rocket control burn facility [446]: In a prototype process, the solid propellant-fired rocket engine in an anti-tank missile fired into a sealed chamber. This type of engine is a jet engine that uses only propellant mass for forming its high speed propulsive jet. These usually work by internal combustion and obtain thrust in accordance with Newton's third law. The propellant in this case contained lead, so particulate filters were employed to remove the gaseous and particulate emissions generated. The LIBS system was mounted in a duct at the entrance to the filtration system to determine the total airborne lead generated by the burn using the 405.8 nm emission line. When the tank was vented, the Pb concentration rose to 30–40 ppm but decreased slightly before the blower was turned on. The concentrations then rose to a maximum of 40–60 ppm and decayed by three orders of magnitude over the next 20 min while the tank was flushed with air. Typical measurements of lead concentrations as a function of time after firing the motor are shown in Fig. 14 for four individual rocket motor burns, where one data point was taken every 30 s, giving an ensemble average of 150 laser shots.

5.6.3.2. Glass furnaces. Modern fuel-oxygen fired glass melting furnaces are able to reduce NO_x and particulate emissions and improve furnace energy efficiency relative to the more conventional fuel-air fired technology. However, to fully optimize furnace operation, a number of problems need to be solved, including crown refractory corrosion and the effects of operating conditions on metal vaporisation and of batch carryover as well as the formation of gaseous air pollutants such as SO_2.

Blevins et al. used LIBS to measure Na, K and Ca vaporising from molten glass and material from batch dust [438]. The measurement position was about 10 m downstream of the furnace exit port, 0.2 m from the wall in a 3.6 m wide duct. The gas temperature near the furnace exit was ca. 1140 °C. On following Na concentrations in real-time over several days, a clear increase with wall temperature in the range 1250–1290 °C was observed from about 180 to 350 ppm.

A further study aimed to determine relative quantities of alkali species and calcium in the high-temperature exhaust of a commercial glass furnace [450]. Measurements were made a) 15 m from the furnace outlet at a temperature of 1380 K and b) in the flue duct at a typical gas temperature of 715 K. For measurements in the high-temperature gas, an external water jacket and internal water cooling of the probe were needed and purge jets had to be used to keep optics clean at small flows. The glass furnace was usually operated slightly fuel lean, occasionally also fuel rich. Lower limits for the concentration levels were 18 ppm (K), 114 ppm (Na), and 5 ppm (Ca). The results show variations in LIBS peak areas as

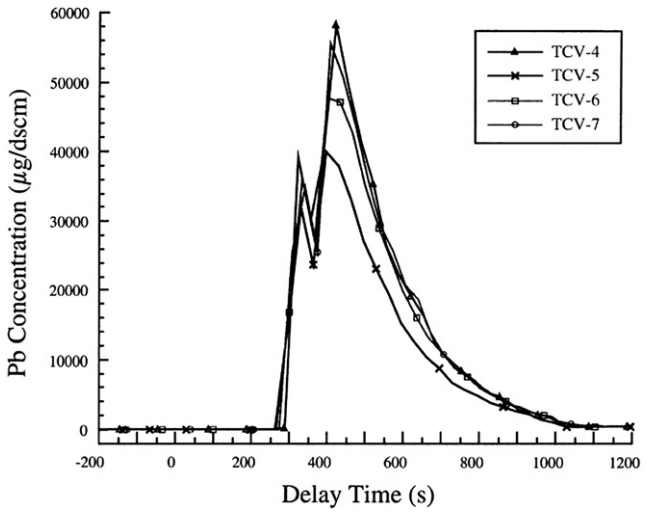

Fig. 14. Time series of Pb concentration measurements in the CBF during a Shillelagh rocket motor burn. TCV-4 – TCV-7 are individual rocket motor burns over a period of a month. Reprinted from [446] with permission.

a function of time over several hours, simultaneously with corresponding O_2 and CO concentrations. However, no absolute calibration was made, so the results are semi-quantitative. For detection of the D-lines of Na and K, strong attenuation of the LIBS signal was found below about 2.5% oxygen concentration. Radiation absorption (see 4.2.4.3) by ground-state Na atoms can be held responsible for this effect at atom number densities above ca. 10^{11} cm^{-3}. Spectrally resolved emissions of Na at 589 nm for O_2 concentrations in the range 0–4.3% vary strongly both in emission intensity and spectrum shape. In contrast, on detecting Na at the alternative wavelength of 818 nm, the intensity and shape of the spectrum changed little with stoichiometry. This is because the 818 nm transition falls, not to the 3s ground state, as the 589 transitions does, but from a 3d to a 3p state of low population (cf. ref. [218, p. 347]) and so is much less affected by radiation absorption. Thus detection of Na at 818 nm has a clear advantage in this respect. On the other hand, at high-temperatures, detection at this wavelength will suffer from much higher background from glowing pipe walls and particles etc.

In the glass furnace studied, diurnal variations in ambient air temperature occurred and lead to changes in exhaust gas composition [451]. This complicated data interpretation, since the apparent exhaust stoichiometry then corresponded neither to the as-fired nor to the in-furnace stoichiometry. At the highest temperatures, concentrations of O_2, N_2 and NO were at a minimum, whereas those of glass-related species (such as SO_2) were at their maximum. Therefore N_2-, CO_2 and O_2-concentrations were determined by micro-GC. A detailed mass balance then showed that air infiltration could account for 30 wt-% of the total gaseous input to the furnace. The sensible heat associated with the N_2 in the infiltrated air represents 6% of the total specific energy input, so reducing the amount of air infiltration would improve furnace efficiency and reduce crown refractory corrosion.

To establish parameters affecting alkali vaporisation, LIBS measurements of Na and K, concentrations in the exhaust of the same O_2/natural gas-fired glass furnace were related to measurements of flue gases, pressure and temperature [452]. The burner stoichiometry was varied while maintaining normal glass production. A trend towards increased alkali concentrations is found with SO_2 whereas Na and K decrease with O_2-concentration. No correlation of alkali with NO_x-concentration was found and only very weak positive correlations with temperature. To detect particle carryover, single-shot LIBS measurements were made; data analysis shows that carryover particles contain Ca, Si, Mg and Al from limestone, sand, dolomite and contaminants, respectively. In addition, batch carryover was found to decrease strongly on reducing furnace differential pressure.

Concentrations of sodium species have also been determined at various locations in an oxygen-natural gas-fired soda-lime-silica glass melting furnace [453]. The objectives of the work were a) to determine mechanisms of sodium volatilization, transport, and deposition, b) provide data for validation of numerical models and c) identify operating conditions under which sodium volatilization could be minimized. Ten hours of measurements in the flue gas from the melting furnace were made, which gave Na concentrations in the range 60 ± 10 ppm. Potassium, magnesium, calcium, and silicon were also observed.

5.6.3.3. Other NG-fired processes. Further applications of LIBS have concerned the determination of metals in the exhausts of a 342-Bhp rich-burn SI engine [454,455], a 22.5 MW (electric) turbine generator [455] and a 50 million Btu/h steam generator [455], all fired using natural gas. Separate measurements were also made in the ambient air near to the respective combustion air inlets. In the steam generator exhaust, Ca, Na and Si were measured at concentrations similar to those in the ambient air near the inlet to the burner. In the engine exhaust, the main metallic element observed was Ca, a component of the lubricating oil, at 11.6 $\mu g/m^3$. The elements Na and Si were also observed, at levels a factor of four higher than those in the air. In the exhaust of the turbine generator, LIBS measurements during start-up following a shut-down to wash the turbine, gave Si and Fe as major species, at concentrations of 6.4 and 16.2 $\mu g/m^3$, respectively. The silicon could have originated from water injected into the turbine for NO_x control whereas Fe-containing particles were thought to be scale from ferrous metals.

5.6.3.4. Other processes. On-line analysis of metals in a mineral melt at 1600 °C for production of mineral wool (mineral fibres made from natural or synthetic minerals or metal oxides with industrial applications in, for example, thermal insulation, filtration and soundproofing) has been performed with a LIBS system based on an Nd:YAG-laser for plasma production and an échelle spectrometer/ICCD camera for detection [457]. Metals detected were Ti, Fe, Mn, Ca, Si, Na and Al over periods of 80 and 130 min, which covered the times of load changes. Measurements were qualitative but were of sufficient temporal resolution to detect the load changes. Simultaneously, independent manual sampling from the melt and XRF analysis was performed, setting a sampling interval of 60 s, in order to synchronise with the LIBS measurements. Overall, a qualitatively good correlation of sampling with LIBS measurements was obtained for most elements.

Another mobile, LIBS-based CEM was developed for measurement of Cr aerosols and installed at an electroplating facility to monitor particle emissions [458]. The intention was to provide instant feedback for process control. Measurements were made along the stack (raw gas) and in the stack gas purification system (clean gas) by sampling using heated steel tubes inserted perpendicular to the stack gas flow and a heated quartz flow cell. LIBS emission was imaged from the cell onto the spectrograph, which was coupled to a gateable intensified diode array. In the raw gas, concentrations were variable in the range 150–600 $\mu g/m^3$, whereas in the clean gas Cr levels were at a relatively stable level around 50 $\mu g/m^3$. The system achieved the required time resolution (minutes) and detection limits (14 $\mu g/m^3$) for emission monitoring below the legal threshold (1 mg/m^3) values. A good correlation was found between the on-line LIPS measurement and the independent conventional filter-based reference analysis with ICP-AAS detection.

Recycling of electronic equipment: To assist sorting of EOL-WEEE waste, LIBS has been used to detect heavy metals in a multi-sensor system in an automatic sorting line [459]. The sensor system contained LIBS, MIR and NIR modules. The EOL-WEEE pieces moved along a belt conveyor. The work focussed on detecting Pb (405.6 nm), Cr (425.4 nm)), Cd (228.8 nm) and Hg (253.7 nm) present in pigments, heat stabilisers and nucleating agents. In addition, Sb (259.8 nm) was detected from Sb_2O_3, used as a synergist for flame retardants in these materials. Concentrations up to 2000 ppmw were measured and reference analyses were performed using ICP-OES.

5.6.4. SIBS

The SIBS method is based on generating a high energy electrical spark (1–5 J discharge energy, 1 Hz) between two electrodes [405,406]. The sample to be measured is thereby vaporised, ionised and excited. To make measurements on a gas stream, the spark gap is arranged to allow the stream to flow between the electrodes. So far, the SIBS monitor has been field tested as a continuous emissions monitor for lead and chromium in stack gases at a joint EPA/DOE field test, in industrial hygiene monitoring tests for lead at a firing range, in monitoring of chromium at a hard chrome plating

facility and at a rotary kiln industrial simulator [405]. Detection limits for Pb and Cr are estimated to be about 10 μg/m^3.

5.7. Ionisation/mass spectrometry

5.7.1. Surface ionisation (SI)

The SI detector developed at Göteborg University [127,409,410,Section 4.4.1] is equipped with a hot sampling line to extract flue gas for continuous alkali measurements at pressures up to 30 bar. Field measurements with the instrument have been performed at fluidized-bed combustion facilities operating under pressurized and atmospheric conditions and firing coal, biomass, and/or demolition waste under particle-laden conditions [127,409,410]. The measured alkali concentration corresponds to the concentration of alkali components present as vapours and fine-mode particles. In systems with high levels of fluidized-bed material or fly ash, alkali bound to coarse particles is also expected to contribute. Under these conditions, the instrument is operated preferably in a pulse counting mode where the concentration of coarse particles can be estimated. With a time resolution of seconds and a lower detection limit of about 1 ppb, the SI system is suitable for a wide range of applications.

A typical measurement using SI is shown in Fig. 15, where alkali vaporised during pyrolysis of untreated and washed wheat straw is shown. Relative amounts of vaporised alkali can be obtained by integrating the signal curves [410]. A large part of the alkali release occurs between 200 and 500 °C. In this region, the differences between the profiles for samples washed in water and untreated samples are relatively small, whereas the release from the acid-washed sample is significantly lower that for the other samples. About 600 °C, where the signal for the untreated sample rises, larger differences are observed: for the sample washed in 5 ml of water, only a small rise in signal is observed whereas for those washed in 20 ml water or in acid no alkali emission at all is seen. The low-temperature peak can be attributed to the decomposition of organic alkali species, whereas the high-temperature emission can be ascribed to inorganic alkali salts, here mostly KCl.

An independent SI detector has been applied in conjunction with a thermogravimetric analyser with a condensation interface [411] and was the first study of the thermochemical behaviour of different biomass samples using such a combination. In general, bimodal release patterns similar to those in Ref. [410] were observed, with alkali emission peaks in low and high-temperature regions. For biomass with low organic content, alkali emission was observed only in the higher temperature region above 500 °C, where inorganic alkali species are volatilized.

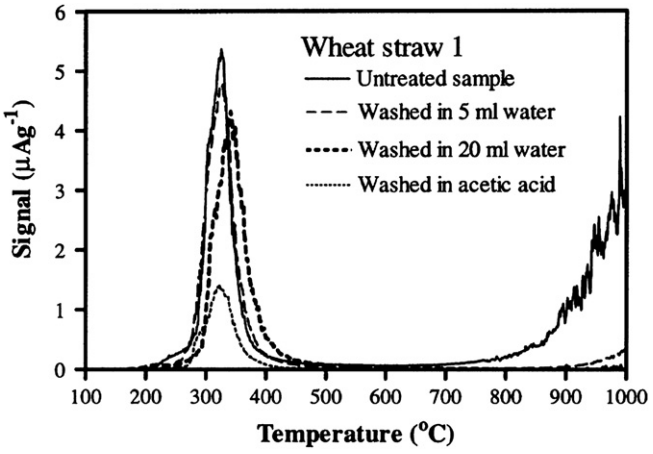

Fig. 15. The release of alkali compounds during pyrolysis of untreated and washed wheat straw WS1, measured by the SI method. Reproduced from [410] with permission.

5.7.2. Molecular beam mass spectrometry (MBMS)

Several research groups have linked their MBMS systems to high-temperature (1000–1400 °C) reactors to study the release of chlorine, sulphur and alkali species during combustion of coal and biomass under varying conditions as well as the capture of alkali species by various sorbents. In one study [460] the combustion products of black liquor, combusted in helium containing 5% oxygen, were monitored in real time in a flow reactor at 1100 °C. Different phases of the combustion process could be identified (volatilisation, char combustion etc.) from time profiles for specific m/z values. For each phase, mass spectra were obtained showing peaks from the oxides of N, C, and S as well as alkali species. The amounts of gas phase NaCl and KCl measured were quantified by vaporising known amounts of these salts under the same conditions as for the combustion experiments. Results showed that NaCl was the most abundant gaseous alkali species present although NaOH was also observed for both wet and dry samples and additionally, Na_2SO_4 was measured during combustion of the dry black liquor. As discussed in Section 2.4.2, a recent detailed model [114] confirms that the sulphate is stable enough to be detectable in combustion (i.e. under oxidising conditions). However, under gasification conditions where oxygen is lacking, the sulphate is probably not detectable [413]

In a later investigation [65], biomass (oak, straw), coal and blends thereof were co-combusted to study the effect of coal minerals on alkali release. The mass spectrometer was scanned continuously at about 100 amu/s, so that complete mass spectra ($m/z = 20$–180) could be recorded at a time resolution of seconds. Both gas phase combustion products and transient species were detected, so that the initial heating, devolatilisation and char combustion of injected solid fuel particles could be followed. From the results, predicted values for pure fuels against measured values) were plotted on parity diagrams. For NaCl, all points were close to the parity line, indicating little or no interactions between the blends. In contrast, those for KCl lay below the parity line, suggesting that mixing the high alkali metal- and chlorine-containing straws with coal affects the partitioning of chlorine in the gas phase.

On-line analysis of combustion products including alkali chlorides and sulphates was performed during combustion of Rheinish brown coals using high-pressure mass spectrometry (HPMS) [154], an MBMS-system similar to that of Dayton et al. [65,460]. Intensity profiles of a range of species as a function of time are shown on the minute timescale, which allowed differences in devolatilisation behaviour to be observed.

French and Milne [66] also measured alkali vapour species with MBMS, coupled to a flow-tube reactor for simulating batch combustion of solid and liquid biomass fuels. The real-time sampling and fast-scanning MS yielded a complete record of the gaseous species evolution as the material combusted. The primary aim was to show the time scale of evolution of different species during combustion of switchgrass (solid and oil) in an 1100 °C He/O_2(20%) atmosphere. Three different phases were observed: volatile combustion, char combustion and finally an ash "cooking" phase. Potassium was released in the latter two phases. Based on previous work (cited in Ref. [66]), the authors assumed that the K^+ signals originate mainly from KCl (g). In this way their salt calibration gave estimates of several hundred and a few tens of ppm (by weight), for potassium release from 1100 °C combustion of solid and liquid switchgrass, respectively.

A mobile mass spectrometer combining optical selectivity of resonance enhanced multiphoton ionisation (REMPI) with time-of-

Table 8
Overview of main features of on-line methods for metal species.

Method	Form present[c]	Detection	Species	Gas/Particle discrim.	In-situ[g]
Photofragment fluoresc. (PFF/ELIF)	Molecule	At. Fluoresc.	Single species[d]	Gas or (Gas + Particle)[b], dep. on laser energy[h]	√
Diff. absorption spectrosc. (DOAS)	Molecule	Molec. Abs.	Single species[e]	Gas phase specific	√
Flame spectroscopy[a]	Atom/Molec.	AES/AAS	Single species[d]	None → (Gas + Particles)[b]	X
Direct atom detection	Atom	AES/AAS/TDLAS	Single species[d]	Gas phase specific	√
Plasma spectroscopy[a] (e.g. ICP, PEARLS, LIBS)	At. + Molec.	AAS/AES/MS etc.	Single species[d]	None → (Gas + Particles)[b]	X (expt. LIBS)
Surface ionisation (SI)	Molecule	Atomic ions	Sum (K + Na)	None → (Gas + Particles)[b]	Difficult
MBMS/TOFMS	At. + Molec	At.-/Molec. Ions	Single species[f]	Gas phase or Particles[b] accd. method	X

[a] Molecules present in the flue gas are atomised thermally (flame) or by plasma and then detected by AES, AAS, TDLAS or MS.
[b] Particles are measured up to a certain size (depending on method).
[c] Form present in the measurement volume (atom, molecule).
[d] Corresponding to the spectral resolution or filtering.
[e] So far developed for chloride detection and known as "In-situ alkali chloride monitor (IACM)"; K and Na so far measured as sum, though discrimination may be feasible.
[f] Corresponding to mass resolution.
[g] Requirement: optical access (window). Otherwise sampling required.
[h] Up to Ca. 20 mJ/cm^2 gas phase only.

flight mass analysis was developed by Heger et al. [461] and applied to measurements in the flue gas of a (grate) incineration pilot plant, operated in either the gasification or the combustion mode. Flue gas was sampled either from the post-combustion chamber or further downstream between the dust filter and the activated coke filter. For on-line measurements, the mass spectrometric system was linked to the flue gas by an effusive molecular beam inlet. Measurements are calibrated using gas standards prepared dynamically with permeation and diffusion devices linked to the inlet of the laser mass spectrometer. From this and similar investigations it can be shown that trace compounds in the ppt (by volume) range will be detectable.

Capture of metal species by minerals: Monitoring the effectivity of sequestering materials can also be performed using an MBMS interfaced to a high-temperature reactor [154,153]. Detailed studies on a variety of aluminosilicate sorbents have been reported for pulverised coal combustion conditions (about 1400 °C). An alkali chloride-laden gas stream was passed through a bed of mineral sorbent using a flow channel reactor. The measured ion signals were quantified by comparing intensities of known concentrations of the species of interest in the carrier gas in blank tests with the corresponding intensities in the mass spectra during the sorption experiments.

5.7.3. Single-particle mass spectrometry (SPMS)

The aerosol mass spectrometer (SI-MS) [417] has been linked to a 12 MW CFB combustor at Chalmers University of Technology [462], firing wood chips and pellets with an air excess ratio of 1.2. The main purpose was to follow alkali processes in the CFB combustor using Cs as a tracer. This was done by adding caesium carbonate to the fuel feed of the furnace for several hours and following Cs concentrations in the flue gas for 70 h. Particles were collected after the primary cyclone exit at 800 °C and the post-convection pass at 160 °C. The SI-MS instrument was combined with a low pressure impactor and a scanning mobility particle sizer to cover the full size range of a few nm to tens of μm. Sampling was then performed perpendicular to the flue gas flow. The hot gas (initially at 800 °C) was cooled in the sampling probe, so that gaseous components condensed on particles or formed new particles. The short residence time of less than 0.2 s ensured that only limited losses to the pipe walls occurred. A cyclone in the sampling line removed particles larger than 5 μm, and the sampled flue gas was diluted a factor of 350 to reduce the high particle concentration. The gas was then led to the SI-MS, where as well as Cs, the metals Na, K and Rb were detected (though in the quadrupole-MS not simultaneously). Since potassium concentrations were approximately constant, Cs concentrations were normalised to the K values to minimise boiler operational effects. The rise in Cs/K ratio after carbonate addition (about a 1000-fold) and the subsequent gradual decay over the following days could readily be followed. Similar decreases in Cs concentration were observed in the analyses of ash taken at different sampling points over the same measurement period. For AMS measurements (all particles), AMS (150 nm particles) and baghouse filter ash, rate coefficients of 0.024 ± 0.001, 0.039 ± 0.012, and 0.037 ± 0.003 per hour, respectively, were obtained. These values correspond to a half-life of Cs in the boiler in the range 15–30 h.

Table 9
Optical in-situ methods – Properties/figures of merit.

Criterium	PFF	LIBS	TDLAS	DOAS
Measurement principle	Photofragment fluorescence	Plasma emission	Atomic absorption	Molecular absorption
Detection limits[a]	0.1 ppb–10 ppb	ppb–100 ppb	ppt–ppb	1 ppm[c]
Usual max. concentration	20–30 ppm (extendable)	ca. 100 ppm (incl. particles)	20–30 ppm	ca. 50 ppm[b]
Time resolution achievable	Seconds	Seconds	Seconds	Minutes
Applications to date	PC, AFBC, PFBC, Pyrolysis Glass furnace	PFBC, PFBG, PC Glass furnaces, Waste incin.	PCC, ACC, Waste incin. CVD	AFBC, PFBC

[a] According to wavelength.
[b] 5 m path length.

With ATOFMS, alkali species from ambient air have been detected [422] while from car exhaust various species could be analysed, including the metals Ca, K, Na [463]. Lead (Pb) in individual aerosol particles was measured using ATOFMS after sampling from urban air [464] and was found in 3% of particles with diameters in the range 0.1–2.0 μm. Single particle data were analysed, focussing on the particles with high Pb content which were mostly submicron. From the size distribution, temporal variation of number density, chemical composition and correlations between chemical species for each particle class, the three major emission sources were identified. Lead-rich particles containing 45% organic or elemental carbon were assigned to coal combustion whereas particles with a good correlation between Cl and Pb content were attributed mostly to waste incineration. A third class featured strongly phosphate and Pb and was assigned to the phosphate industry. Other Pb-rich particles included aged sea salt and particles from metallurgical processes.

The SPA-system described in [424] analysed diesel particulates from a running diesel engine [465]. Of particular interest was the

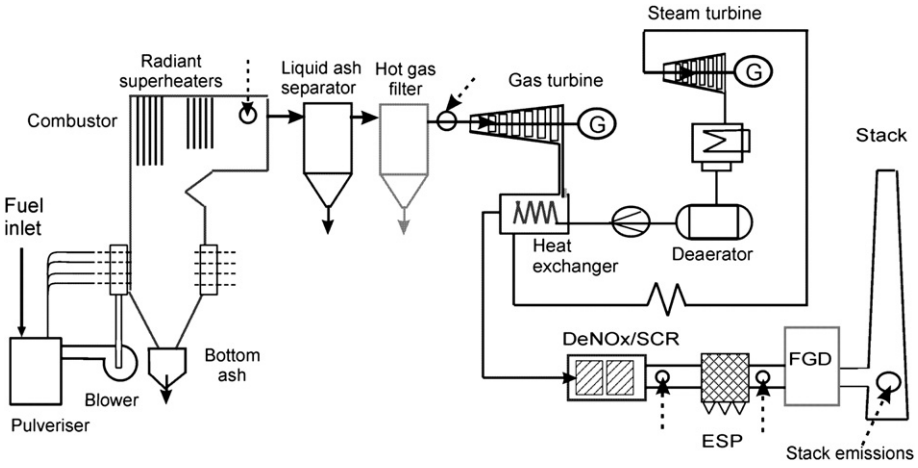

Fig. 16. Application of diagnostics/analysis at a pulverised fuel combustion plant with steam- and gas–turbine cycles (combined-cycle plant). SCR = Selective catalytic reduction of NO_x; FGD = Flue gas desulphurisation, ESP = Electrostatic precipitator: ----▶possible positions for sampling and/or optical access.

origin of trace metals and size preferences of metals originating from fuel oil as well as fuel additives such as ferrocene. Particles down to ca. 10 nm size, corresponding to the nuclei mode, were analysed.

So far, most of the applications of SPMS have sampled from ambient environments. However, the application of ATOFMS at a 0.5 MW incineration pilot plant firing wood has also been demonstrated [466]. Particles were sampled directly from the stoker system at two different heights over the feed bed in the third air supply zone. The collected particles were re-aerosolized by a powder-dispersing unit. Chemical species from the particles are then laser desorbed/ionized by Nd:YAG-laser pulses at 266 nm and analysed by TOFMS, providing information on bulk inorganic composition of the individual particles.

The aerosol mass spectrometric system that combines three laser-based methods for on-line analysis of particles is able to detect a wide range of organic and inorganic species [425]. The three techniques were one-step laser desorption/ionisation (LDI), two-step laser desorption/photoionisation (LDPI) and thermal desorption/photoionisation (TDPI). The LDI method is especially suitable for the detection of inorganic compounds as well as the determination of elemental carbon content. Particles were sampled from spruce wood ash generated by a residential heating system and exhaust gases from a gasoline passenger car. Positive LDI mass spectra showed metal cations such as potassium and iron, whereas carbon clusters were detected in the negative mode. Using LD-REMPI and TD-REMPI, polyaromatic species such as phenanthrene and pyrene were observed.

6. Conclusions and outlook

The review of progress so far on measurement techniques (chapter 4) shows that a fair range of methods have been developed that have applicability in certain types of industrial environment. Indeed, significant progress on some techniques has been made and/or new applications demonstrated since the previous review [218]. However, Chapter 5 shows that only a limited number have been applied for detailed real-time measurements at the high-temperatures and/or pressures of combustion and gasification systems. Of the methods involving sampling, conventional (flame) absorption and emission, ICP-AES, PEARLS/HEAMON, SI and MBMS fall into this category. Of the *in-situ* methods, one may include LIBS, PFF, DOAS, TDLAS and a recent variant of AAS. The general features of these methods are compared in Table 8; the first four in-situ methods are further compared in Table 9. It may be noted that many researchers favour absorption methods, for example, because they do not normally require independent calibration and also because with fluorescence methods, collisional quenching of fluorescing species is an issue to be solved. On the other hand, broadening effects, to a large extent also caused by collisions at higher pressures, are still an important issue for atomic absorption methods. For all optical methods, problems of spectral interferences have to be combated, either by temporal or spectral discrimination, as indicated in the relevant sections of the review.

As shown in chapters 2 and 5, real-time monitoring during plant operation is important for optimising furnace conditions (temperature, pressure, residence time, stoichiometry etc.) with respect to metal release, especially during start-up or changing fuels (TDLAS [226,227], DOAS [282–285], LIBS [438–459]; ICP-AES [368–372], ELIF [148,303,427–432,434], PEARLS/HEAMON [148,382–385], SI [127,303,409,410]). The methods named above are able to monitor gas quality with respect to metal species in post-combustion gases, especially following hot gas filters [148,188,303,430]. Gas quality assurance is also relevant to preventing deactivation of NO_x-catalysts by alkali or other metals as well as in systems combining combustion/gasification with fuel cells of type MCFC or SOFC.

Fig. 16 shows a combustion plant scheme with steam and gas turbine cycles, indicating positions where monitoring of metals could be of importance. Obviously, if a full assessment of metal partitioning (speciation, phase discrimination) is aimed for, a whole series of ports for sampling or optical access will be required. Also, two or three complementary methods should be selected, since as Tables 8 and 9 show, each method offers different advantages and limitations. Other investigations may concentrate on one specific aspect, such as alkali concentrations prior to a gas turbine inlet or final stack gas concentrations, where conditions (temperature, pressure and particle loading etc.) differ enormously, necessitating different choices of measuring techniques.

A word of warning should be given when comparing different measurement techniques. Apparent differences in flue gas metal concentrations can, on one hand, be a result of measurement errors. On the other hand, differences can result, for example, from different sampling efficiencies or discrimination against specific species or phases (gas, solid) due to the nature of the method. An example of the latter case was described in Section 5.5.1.

Process control: One major aim of control strategies is to optimise system performance with respect to efficiency, specific

emissions, temperature, fuel feed rate, air flow or, in vapour deposition work to control rates of deposition. Process control may also be used to minimise instabilities/oscillations of important parameters. An extensive review on this subject has been presented by Docquier and Candel [467], focussing on sensor systems already in use or on those offering potential for control tasks. Specific examples are described in Refs. [253] (vapour deposition), [468] (afterburner of an incinerator) and [469] (sputter deposition of coatings). For application of on-line methods in process control using closed-loop systems, the determination of absolute concentrations is not necessarily the primary aim. Rather, the essential requirement is a response on the timescale of interest. So far, diode lasers have received much attention in this area [253,468], as a result of their practical advantages, including compactness, ease of operation, ability to couple with fibre optics, as discussed in Section 4.1.3. Large cumbersome equipment is less suitable for control tasks and tends to remain in the domain of monitoring and diagnostic investigations.

Other applications in solid fuel conversion discussed in this review are:

- Fuel screening (especially for biomass/waste conversion or co-firing) with respect to metal release (ELIF; PEARLS, LIBS, SI, MBMS)
- Monitoring the effectivity of sorbents and other sequestering materials (e.g. minerals): (ELIF, SI, MBMS)
- Kinetics of vaporisation or deposition for different metal species (TDLAS, ICP-AES)
- Gas-/particle partitioning, where combinations of methods could be used (ELIF/SI)

Applications in other areas:

- Engine exhaust (ATOFMS)
- Glass furnaces (LIBS, SIBS, ELIF)
- Mineral melts (LIBS, ICP-AES)
- Electroplating (SIBS)
- Vapour deposition (ELIF, TDLAS)

Needless to say, only a few of the monitoring systems described in this review are offered on the commercial market. Nevertheless, most of those developed in the course of research projects have proved to be sufficiently robust to work in harsh environments under realistic industrial conditions and have generated substantial amounts of data that contribute to the understanding of metals release and suppression under a wide variety of conditions.

Acknowledgements

Thanks are due to all those who assisted in the preparation of this article, especially M. Aho (VTT) for detailed reading of chapter 2 as well as M. Bröström (U. Umeå), K.O. Davidsson (Swedish Testing & Research Institute)), C. Ludwig (PSI/Villigen), M. Müller (Forschungszentrum Jülich) and B. Chadwick (U. South Australia) for answering diverse queries and/or supplying recent literature.

References

[1] Vassilev SV, Vassileva CG. Energy Fuels 2005;19(3):1084–98.
[2] Barman BN, Cebolla VL, Mehrotra AK, Mansfield CT. Anal Chem 2001;73:2791–804 [refs. therein].
[3] Maciejewska A, Veringa H, Sanders J, Peteves SD. EU report EUR 22461, DG JRC – Institute for energy, 2006.
[4] Ashton S, Cassidy P. Energy basics, fact sheet 5.8. In: Hubbard W, Biles, Mayfield S, Ashton S, editors. Sustainable forestry for bioenergy and bio-based products. Athens, GA, USA: Southern Forest Research Partnership, Inc.; 2007. p. 189–92.
[5] Raveendran K, Anuradda G. Fuel 1996;75:1715–20.
[6] Han J, Xu M, Yao H, Furunchi M, Sakano T, Kanchanapiya P, et al. Energy Fuels 2007;20:583–90.
[7] Nelson PF. Energy Fuels 2007;21(2):L:477–84.
[8] Gibbs BM, Thompson D, Argent BB. Fuel 2008;7(87):1217–29.
[9] Wang Q, Zhang L, Sato A, Ninomiya Y, Yamashita T. Energy Fuels 2007;21 (2):756–65.
[10] Zhang L, Wang Q, Sato A, Ninomiya Y, Yamashita T. Energy Fuels 2007;21 (2):766–77.
[11] Holt N, Findsen J. Science applications international corporation, report: best practices in environmental monitoring for coal-fired power plants: lessons for developing Asian APEC economies of the APEC energy working group, expert group on clean fossil energy; Nov. 30, 2008.
[12] Technical guidance note (monitoring) Environment Agency. Monitoring of stack emissions to air; Nov. 2002.
[13] Environmental health and safety guidelines: base metal smelting and refining. Int. Finance Corporation; April 30th, 2007.
[14] EU-directive 2000/76/EU Official K. Eur Commun 2000;L322:4–14.
[15] Hazardous waste combustor rule (HWC MACT Standard). Federal register, http://www.epa.gov/osw/index.htm; February 13, 2002.
[16] Pacyna JM, Pacyna EG, Aas W. Atmos Environ 2009;43:117–27.
[17] European Environment Agency, Environment in the European Union at the turn of the century, Waste generation and management, Report 2000, Chapter 3.7.
[18] Moffet RC, Desyaterik Yu, Hopkins RJ, Tivanski AV, Gilles MK, Wang Y, et al. Environ Sci Technol 2008;42(19):7091–7.
[19] Geagea ML, Stille P, Gauthier-Lafaye F, Millet M. Environ Sci Technol 2008;42 (3):692–8.
[20] Gallon C, Tessier A, Gobeil A. Environ Sci Technol 2008;40(3):741–7.
[21] Wangberg I, Edner H, Ferrara R, Lanzillotta E, Munthe J, Sommar J, et al. Sci Total Environ 2003;304(1–3):29–41.
[22] Hylander LD, Herbert RB. Environ Sci Technol 2008;42(19):5971–7.
[23] Ettler V, Šebek O, Grygar T, Klementová M, Bezdička P, Slaviková H. Environ Sci Technol 2008;42(21):7878–84.
[24] Ettler V, Johan Z, Baronnet A, Jankovsky F, Gilles C, Mihaljevič M, et al. Environ Sci Technol 2005;39(23):9309–16.
[25] Directive 2001/80/EC. Off J Europ Comm 27.11.2001;L309/1.
[26] Health risks of heavy metals from long-range transboundary air pollution. Brochure World Health Organsation; 2007. ISBN 978 92 890 7179 6.
[27] Dreher K, Jaskot R, Richards JH, Lehmann JR, Winsett D, Hoffman A, et al. Amer J Respir Crit Care Med 1996;153:A15.
[28] Dreher K, Jaskot R, Lehmann JR, Richards JH, McGee JK, Ghio AJ, et al. J Toxicol Environ Health 1997;50:285–305.
[29] Block C, Dam R. Water Air Soil Pollut 2004;5:207–11.
[30] Bryers RW. Prog Energy Comb Sci 1996;22:29–120.
[31] Yan R, Liang DT, Laursen K, Li Y, Tsen L, Tay JH. Fuel 2003;82:843–51.
[32] Xiong S, Burvall J, Örberg H, Kalen G, Thyrel M, Öhman M, et al. Energy Fuels 2008;22:3465–70.
[33] Sidhu TS, Prakash S, Agrawal RD. Curr Sci 2006;90(1):41–7.
[34] Rezaie A, Headrick WL, Fahrenholtz WG, Moore RE, Velez M, Davis WA. Refractories Appl News 2004;9(5):26–31.
[35] Oakey J, Simms N, Kilgallon P. Mater Res 2004;7(1):17–25.
[36] Forster MEC. Int J Energy Technol Policy 2007;5(3):383–90.
[37] Khan AA, de Jong W, Jansens PJ, Spliethoff H. Fuel Proc Technol 2009;90:21–50.
[38] Rubow L, Zaharchuk R. Proceedings, 2nd Annual Contractors meeting on contaminant control in hot coal-derived gas streams. Morgantown, WV: U.S. Dept. Energy; 1982. p. 60–74.
[39] Osborn GA. Fuel 1992;71:131–42.
[40] Salmenoja M, Mäkelä K, Hupa M, Backman RJ. Inst Energy 1996;69:155–62.
[41] Lee SHD, Natesan K, Swift WM. Report ANL/FE-95–01. Argonne Nat. Lab; 1995.
[42] Gagliano MS, Hack H, Stanko G. 34th International Technical Conference on Coal Utilization & Fuel Systems. Clearwater, FL, USA; May 31–June 4, 2009.
[43] Montgomery M, Vilhelmsen T, Jensen SA. Mater Corrosion 2008;59(10): 783–93.
[44] Wada K, Yan L, Takahashi M, Takaishi K, Furukawa T. Mater High Temp 2001;18(2):131–8.
[45] Nielsen HP, Frandsen FJ, Dam-Johansen K, Baxter LL. Prog Energy Comb Sci 2000;26:283–98.
[46] Tillman Da, Duong D, Miller B. Energy Fuels 2009;23(7):3379–91.
[47] Kobayashi H, Wu KT, Tuson GB, Dumoulin F, Kiewall HP. Ceramic Bull 2005;2:14–9. 3: 24–27.
[48] Bartels M, Lin W, Nijenhuis J, Kapteijn F, van Ommen JRund. Prog Energy Comb Sci 2008;34:633–66.
[49] Dam-Johansen K, Lin W, Frandsen F. Chem Eng J 2003;96:171–85.
[50] Beck J, Brandenstein J, Unterberger S, Hein KRG. Appl Catal B 2004;49 (1):15–25.
[51] Lisi L, Lasorella G, Malloggi S, Russo G. Appl Catal B 2004;50(4):251–8.
[52] Moradi F, Brandin J, Sohrabi M, Faghihi M, Sanati M. Appl Catal B 2003;46 (1):65–76.
[53] Larsson A-C, Einvall J, Sanati M. Aeros Sci Techn 2007;41(4):369–79.
[54] Larsson A-C, Einvall J, Andersson A, Sanati M. Energy Fuels 2006;20: 1398–405.
[55] Neyestanaki AK, Klingstedt F, Salmi T, Murzin DYu. Fuel 2004;83(4–5): 395–408.

[56] Bartholomew CH. Appl Catal A 2001;212(1–2):17–60.
[57] Norheim A, Lindberg D, Hustad JE, Backman R. Energy Fuels 2009;23:920–5.
[58] Tomasi C, Barattieri M, Bosio B, Arato E, Baggio P. J Power Sources 2006;157 (2):765–74.
[59] Iaquaniello G, Mangiapane A. Int J Hydrogen Energy 2006;31:399–404.
[60] Hancock P. Mater Sci Technol 1987;3:536–44.
[61] Bankiewicz D, Yrjas P, Hupa M. Energy Fuels 2009;23(7):3469–74.
[62] Andrade Korn MdG, Santana Sodré dos Santos D, Welz B, Rodrigues Vale MG, Paixao Teixera A, de Castro Lima D, et al. Talanta 2007;73:1–11.
[63] Rodushkin I, Axelsson MD, Burman E. Talanta 2000;51:743–59.
[64] www.sciro.au/resources/Fluorine-in-export-coals.html#1, update 1.12.08.
[65] Dayton DC, Belle-Oudry D, Nordin A. Energy Fuels 1999;13:1203–11.
[66] French RJ, Milne TA. Biomass Bioenergy 1994;7:315–25.
[67] Werther J, Saneger M, Hartge E-U, Ogada T, Siagi Z. Proc Energy Comb Sci 2000;26:1–27.
[68] Galbreath KC, Zygarlicke CJ, Huggins FE, Huffman GP. Energy Fuels 1998;12: 818–22.
[69] Municipal solid waste incinerator residues, Report of the International Ash Working Group, 1997.
[70] Joutsenoja T, Sternberg J, Hernberg R. Comb Sci Tech 1996;121:123–32.
[71] Joutsenoja T, Sternberg J, Hernberg R. Appl Opt 1997;36:1525–35.
[72] Davidovits P, McFadden DL, editors. Alkali halide vapors, structure, spectra and reaction dynamics. N. York: Acad. Press; 1979.
[73] Husain D, Plane JMC. J Chem Soc Faraday Trans 2 1982;78:163–78.
[74] Husain D, Plane JMC, Xiang CC. Faraday Trans 1984;80:1465–83.
[75] Husain D, Lee YH, Marshall P. Combust Flame 1987;68:143.
[76] Plane JMC. J Phys Chem 1987;91:6552–7.
[77] Plane JMC, Rajasekhar B. J Chem Soc Faraday Trans 2 1988;84:273–85.
[78] Plane JMC, Rajasekhar B. J Phys Chem 1988;92:3884–90.
[79] Plane JMC, Rajasekhar B. J Phys Chem 1989;93:3140–315.
[80] Marshall P, Narayan AS, Fontijn A. J Phys Chem 1990;94:2998–3004.
[81] Rajasekhar B, Plane JMC, Bartolotti LJ. Phys Chem 1989;93:7399–404.
[82] Cox RM, Plane JMC. Phys Chem Chem Phys 1999;1:4713–20.
[83] Goumri A, Rocha J-DR, Misra A, Marshall P. J Phys Chem A 1999;103:9252.
[84] Shi Y, Marshall P. J Phys Chem 1991;95:1654.
[85] Goumri A, Laakso D, Rocha J-DR, Francis E, Marshall P. J Phys Chem 1993;97: 5295–7.
[86] Srinivasachar S, Helble JJ, Ham DO, Domazetis G. Prog Energy Combust Sci 1990;16:303–9.
[87] Hynes AJ, Steinberg M, Schofield K. J Phys Chem 1984;80:2585–97.
[88] Slack M, Cox JW, Grillo A, Ryan R, Smith O. Comb Flame 1989;77:311–20.
[89] Steinberg M, Schofield K. Comb Flame 2002;129:453–70.
[90] Steinberg M, Schofield K. Prog Energy Comb Sci 1990;16:311–7.
[91] Fontijn A. Pure Appl Chem 1998;70:469–76. Fontijn A. Proceedings. In: Spear KE, editor. High-temperature materials chemistry IX, Vol. 97–39. Pennington: The Electrochemical Society, Inc.; 1997. p. 617.
[92] Cosic B, Fontijn A. J Phys Chem A 2000;104:5517–24.
[93] Hransiavljevic J, Fontijn AJ. Phys Chem 1997;101:2323–6.
[94] Blue AS, Fontijn A. J Phys Chem A 2001;115:179–83.
[95] Cosic B, Belyung DP, Hranisavljevic J, Fontijn A. J Phys Chem A 2003;107:9132–6.
[96] Cosic B, Fontijn A. Z Phys Chem 2000;214(11):1521–31.
[97] Takahasi K, Giesen A, Roth P. Phys Chem Chem Phys 2001;3:4296–300.
[98] McClean RE. J Phys Chem A 2000;104:8723–9.
[99] McClean RE, Norris L. Phys Chem Chem Phys 2005;7:2489–97.
[100] Campbell ML, Plane JMC. J Phys Chem A 2003;107(19):3747–51.
[101] Campbell ML. J Phys Chem A 2003;107(17):3048–53.
[102] Campbell ML. Chem Phys Lett 2002;365:361–5.
[103] Campbell ML, Kölsch EJ, Hooper KL. J Phys Chem A 2000;104(47):11147–53.
[104] Qiao Y, Xu M, Yao H, Wang C, Gonh X, Chen H, et al. Asia-Pacific J Chem Eng 2007;2:158–64.
[105] Schofield K. Environ Sci Technol 2008;42(24):9014–30.
[106] Taylor PH, Mallipeddi R, Yamada T. Chemosphere 2005;61:685–92.
[107] Ariya PA, Khalizov A, Gidas A. J Phys Chem 2002;A 106(106):7310–20.
[108] Donohoue DL, Bauer D, Hynes AJ. J Phys Chem 2005;109:7732.
[109] Xu M, Qiao Y, Zheng C, Li L, Liu J. Comb Flame 2003;132:208–18.
[110] Wilcox J, Robles J, Marsden DCJ, Blowers P. Env Sci Techn 2003;37:4199–204.
[111] Edwards JR, Srivastava RK, Kilgroe JD. J Air Waste Manage Assoc 2001;51: 869–77.
[112] Niksa S, Helble JJ, Fujiwara N. Env Sci Techn 2001;35:3701–6.
[113] Glarborg P. Proc Comb Inst 2007;31:77–98.
[114] Glarborg P, Marshall P. Comb Flame 2005;141:22–39.
[115] Mojtahedi W, Kurkela E, Nieminen M. J Inst Energy 1990;63:95–100.
[116] Niksa S, Helble J, Harada M, Ando T, Shigeta J, Kajigaya I. Comb Sci Technol 2001;165:229–37.
[117] Thambimuthi KV. Gas cleaning for advanced coal-based power generation. IEA/53 Report. London: IEA Coal Research; March 1993.
[118] Wall TF. Proc Comb Symp 1992;24:1119–26.
[119] Wibberley LJ, Wall TF. Fuel 1982;61:87–92.
[120] Iisa K, Lu Y, Salmenoja K. Energy Fuels 1999;13:1184.
[121] Hansen LA, Michaelsen HP, Dam-Johansen K. Fluidised-bed combustion. ASME 1995;1:39–48.
[122] Wornat MJ, Hurt RH, Nancy YC, Yang NYC, Headley TH. Comb Flame 1995;100:131–43.
[123] Glazer M, Khan MP, Schürmann H, Monkhouse P, de Jong W, Spliethoff H. Energy Fuels 1889;2005:19.
[124] Gottwald U, Monkhouse P, Bonn B. Fuel 2001;80:1893–9.
[125] Laatikainen J, Nieminen M, Hippinen I, Proceedings,12th Fluidized Bed Combustion Conference. San Diego, California; May 9–13, 1993. p. 1369-1374.
[126] Lee SHD, Teats FG, Swift WM, Banerjee DD. Combust Sci Techn 1992;86:327–36.
[127] Korsgren JG, Hald P, Davidsson KO, Pettersson JBC. Proceedings, 15th Conference on FB Combustion. Savannah/Georgia, USA; May 16, 1999, Paper No. FBC99–0125.
[128] Lundholm K, Nordin A, Backman AR. Fuel Proc Technol 2007;88 (11–12):1061–70.
[129] Linak WP, Wendt JOL. Prog Energy Comb Sci 1993;19:145–85.
[130] Helble JJ. Fuel Proc Technol 2000;63:125–47.
[131] Yan R, Gauthier D, Flamant G. Fuel 2001;80:2217–26.
[132] Verhulst D, Buekens A, Spencer PJ, Eriksson G. Environ Sci Technol 1996;30:50–66.
[133] Senior CL, Bool III LE, Srinivasachar S, Pease PR, Porle K. Fuel Proc Technol 2000;63:149–65.
[134] Senior CL, Helble J, Sarofim AF. Fuel Proc.Technol 2000;65–66:264–88.
[135] Galbreath KC, Toman DL, Zygarlicke CJ, Pavlish JH. Energy Fuels 2000;14:1265–79.
[136] Reed GP, Dugwell DR, Kandiyoti R. Energy Fuels 2001;15:794–800.
[137] Richaud R, Lachas H, Healey AE, Reed GP, Haines J, Jarvis KE, Herod AA, Dugwell DR, Kandiyoti R. Fuel 2000;79:1077–87.
[138] Lind T, Valmari T, Kauppinen E. Proc Inst Combust 2000;28:2287–95.
[139] Lind T, Kauppinen E, Nilsson K, Sfiris G, Maenhaut W. Environ Sci Technol 1999;33:496–502.
[140] Lind T, Kauppinen EI, Jokiniemei JK, Maenhaut W. Proc Comb Inst 1994;25:201–9.
[141] Kauppinen EI, Pakkonen TA. Environ Sci Tech 1990;24:1811–8.
[142] Yao H, Mkilaha ISN, Naruse I. Fuel 2008;83(7–8):1001–7.
[143] Yao H, Naruse I. Control of trace metal emissions by sorbents during sewage sludge combustion. Proc Comb Inst 2005;30(2):3009–16.
[144] Wendt JOL, Lee SJ. Fuel 2010;89(4):894–903.
[145] Jeong SK, Kim SB, Kim SS, Chen X, Biswas P. J Ind Eng Chem 2007;13 (7):1154–61.
[146] Hofstetter TB, Schwarzenback RP, Haderlein SB. Environ Sci Technol 2003;37 (3):519–28.
[147] Daijou Y, Lee SHD, Suzuki K, Ishimori T, Yanaisawa T, Tsumita Y. In: Schmidt E, Gäng P, Piltz T, Dittler A, editors. High temperature gas cleaning. Institut für Mechanische Verfahrenstechnik & Mechanik der Universität Karlsruhe; 1996. p. 664–83.
[148] Häyrinen V, Hernberg R, Oikari R, Gottwald UA, Monkhouse PB, Davidsson K, Lönn B, Engvall K, Pettersson JBC, Lehtonen P, Kuivalainen K. Proceedings of the 6th International Conference on Circulating Fluidized Beds. Würzburg; 1999, p. 873–878.
[149] Aho M. Fuel 2001;80:1943–51.
[150] Kyi S, Chadwick BL. Fuel 1999;78:845–65.
[151] Schürmann H, Unterberger S, Hein KRG, Monkhouse PB, Gottwald UA. Faraday Discuss 2001;119:433–44.
[152] Willenborg W, Müller M, Hilpert K. Energy Fuels 2006;20:2593–8.
[153] Escobar I, Müller M. Energy Fuels 2007;21(2):735–43.
[154] Oleschko H, Schimroszyk A, Lippert H, Müller M. Fuel; 2007:2275–83.
[155] Davidsson KO, Steenari B-M, Eriksson D. Energy Fuels 2007;21(2): 1959–66.
[156] Tran K-Q, Iisa K, Steenari B-M, Lindqvist O. Fuel 2005;84(2–3):169–75.
[157] Dou B, Shen W, Gao J, Sha X. Fuel Proc Technol 2003;82(1):51–60.
[158] Davidsson K, Amand L-E, Steenari B-M, Elled A-L, Eslilsson D, Leckner B. Chem Eng Sci 2008;63:5314–29.
[159] Lundholm K, Nordin A, Öhmann M, Boström D. Energy Fuels 2005;19: 2274–8.
[160] NIST Atomic Database, Version 3.0 Beta, October 2004. Also in Morton DC, Atomic database for resonance absorption lines, Part II. Astrophys J Suppl Ser 2000;130:403, physics.nist.gov./cgibin/At-Data;
Part III. Astrophys J 2003;149:205.
[161] Bernath PF. Annu Rep Prog Chem Sect.C 2000;96:177–224.
[162] Merer AJ. Ann Rev Phys Chem 1989;40:407–38.
[163] Pugh J, Shen KK, Winstead, Gole JL. Chem Phys 1996;202:129–38.
[164] Little AM, Corlett GK, Ellis AM. Chem Phys Lett 1998;286:439–45.
[165] Joo J, Worsnop DR, Kolb CE, Kim SK, Herschbach DR. J Phys Chem A 1999;103:3193–9.
[166] O'Brien LC, Borchert BA, Farquhar A, Shaji S, O'Brien JJ, Field RW. J Mol Spec 2008;252:136–42.
[167] Appelblad O, Lagerqvist A, Renhorn I, Field RW. Physica Scripta 1981;22: 603–8.
[168] Zhang S, Zhen J, Zhang Q, Yang C. J Mol Spec 2008;252(1):77–80.
[169] Ziebarth K, Setzer KD, Shestakov O, Fink EH. J Mol Spectrosc 1998;191:108.
[170] Brom JM, Beattie WH. J Mol Spec; 1980:445–54.
[171] Lei J, Dagdigian PJ. J Mol Spec 2000;203:345–8.
[172] Ram RS, Bernath PF. J Mol Spec 2003;221(2):261–8.
[173] Ram RS, Bernath PF. J Mol Spec 2005;229:57–62.
[174] Ram RS, Bernath PF, Davis SP. J Chem Phys 2001;114(10):4457–60.
[175] NiCl Poclet A, Krouti Y, Hirao T, Hirao T, Pinchemel B, Bernath PF. J Mol Spec 2000;204:125–32.
[176] NiCl Dufour C, Pinchemel B, Bernath PF. J Mol Spec 2000;202:53–8.
[177] NiCl2 Ashworth SH, Grieman FJ, Brown JM. J Chem Phys 1996;104:48–63.
[178] Liu H, O'Brien LC, Shaji S, O'Brien JJ. J Mol Spec 2009;253:73–6.

[179] HITRAN Molecular database. Version12.0, http://www.cfa.harvard.edu/hitran/Download/HITRAN04paper.pdf; 2004 [last accessed March 2010].
[180] Chadwick B, Domazetis G, Morrison RJS. Anal Chem 1995;67:710.
[181] Stepowski D. Proc Symp Comb 1990;23:1839.
[182] Clark CD, Campuzano-Jost P, Covert DS, Richter RC, Maring H, Hynes AJ, et al. Aerosol Sci 2001;32:765–78.
[183] Hartinger KT, Nord S, Monkhouse P. Appl Phys B 1997;64:363–7.
[184] Häyrinen V. Gas standards generator for calibration of combustion process alkali monitors. Tampere/Finnland: Tampere University of Technology, Publication Nr. 451; 2003.
[185] Chase Jr M, Davis CA, Downey Jr JR, Frurip DJ, McDonald RA, Syverud AN. NIST Thermochemical tables. Monograph 9. 4th ed. American Chemical Society/American Institute of Physics; 1998.
[186] Colin TB. Validation of CEM system accuracy and reliability. Ch. 3. In: Down RD, Lehr JH, editors. Environmental instrumentation and analysis handbook. J. Wiley & Sons; 2005. p. 49–60.
[187] Zhang H, Singh JP, Yueh F-Y, Cook RL. LIBS in a coal-fired MHD facility. Appl Spectrosc 1995;48:1617–23.
[188] Gottwald U, Monkhouse P. Appl Phys B 1999;69:151.
[189] Farnsworth PB, Smith BW, Ommenetto N. Spectrochim Acta B 1990;458:1151–66.
[190] Gottwald U, Monkhouse P. Appl Spectrosc 2003;57:117–23.
[191] Bates SC. SAE Technical paper series; 1988. Nr. 880520.
[192] Roeloffs N, Taranto N. NASA Technical Memorandum 106783; May 1995.
[193] Carranza JE, Gibb E, Smith BW, Hahn DW, Winefordner JD. Appl Opt 2003;42:6016–21.
[194] Sabsadi M, Heon R, St-Onge L. Spectrochim Acta B 2005;60:1211–6.
[195] Müller M, Gornushkin IB, Florek S, Mory D, Panne U. Anal Chem 2007;79:4419–26.
[196] Jimenenz S, Ballester J. Aerosol Sci Technol 2005;39:811–21.
[197] Fantom IR. Proceedings of the 2nd International Symposium on Gas Cleaning at High Temperatures, Guildford, UK, September 27–29, 1993. Blackie Academic & Professional. Glasgow, p. 541–555.
[198] Lee SHD, Carls EL. Proceedings of the 10th Fluidized Bed Combustion Conference, San Francisco, California, Apr. 30-May 3, 1989. p. 977-985. 200.
[199] Eliot P. Chem Eng Prog 2001;87(2):75–91.
[200] Wexler AS, Johnston MV. In: Willeke K, Baron P, editors. Aerosol measurement: principles, techniques and applications. Von Nostrand Rheinhold; 2001.
[201] Hippinen I, Lu Y, Laatikainen J, Nieminen M, Jahkola A. J Inst Energy 1992;65:154–9.
[202] Reed GP, Brain S, Cahill P, Fantom I. Proceedings of the 14th International Conference on FB combustion. ASME Book No. G1052B; 1997. p. 1285–1293.
[203] Cauch B, Silcox GD, Lighty JS, Wendt JOL, Fry A, Senior CL. Environ Sci Technol 2008;42:2594–9.
[204] US EPA Standard test methods, www.epa.gov/ttn/emc/promgate.html.
[205] ASTM, 2002. Method D 6784-02 (Standard test method for elemental, oxidized, particle-bound, and total mercury in flue gas generated from coal-fired stationary sources (Ontario–Hydro Method). American Society for Testing and Materials; 2002.
[206] European Standard EN 13211. Manual method of determination of the concentration of total mercury; 2001.
[207] European Standard BS EN 14385:2004 (multimetal) for stationary source emissions. Method implementation document (MID 14385). Environ Agency. Available from, www.mcerts.net; May 2006.
[208] Punjak WA, Uberoi M, Shadman F. ALChE J 1989;35:1184–6.
[209] Lee SHD, Johnson IJ. Eng Power 1980;102:397–402.
[210] Lee SHD, Swift WM. Proceedings of the ASME 10th Fluidized Bed Combustion Conference. Montreal, Canada; Apr. 21–24, 1991. p. 1095–1103.
[211] Lee SHD, Swift WM. 9th Annual Coal-Fueled Heat Engines Contractors Review Meeting. Morgantown, West Virginia; October 27–29, 1992, 7 p.
[212] Hallgren AL. Proceedings of the 29th Intersociety Energy Conversion Engineering Conference. Monterey, CA, USA, AIAA-94-400-CP, Vol 4; 7–11 Aug. 1994. p. 1566–1571.
[213] Ludwig C, Schuler AJ, Wochele J, Stucki S. J Water Sci Technol 2000;42:209–16;
Recovery, recycling, re-integration, 4th World Congress. Geneva, Switzerland, Vol. II; February 2–5, 1999. p. 205–210.
[214] Lee SHD, Carls EL. J Inst Energy 1990;63:203–10.
[215] Kurkela E, Stählberg P, Laatikainen J, Nieminen M. Proceedings of the Conference on Energy from Biomass Wastes XV. Washington; 1991;March 25–29, 24 p.
[216] Hippinen I, Lu Y, Jahkola A, Laatikainen J, Nieminen M. Proceedings of the Conference on Fluidised Bed Combustion. London; Dec. 1991. p. 281–292.
[217] Pavageau M-P, Pécheyran C, Krupp EM, Morin A, Donard OFX. Environ Sci Technol 2002;36:1561–73.
[218] Monkhouse P, Prog. Energy Comb Sci 2002;28:331–81.
[219] Ebert V, Wolfrum J. Chapter 14. In: Mayinger F, editor. Optical measurement techniques and applications. 2nd ed. Heidelberg, München: Springer; 2000. p. 273–312.
[220] Demtröder W. Laser spectroscopy, basic principles. 4th ed. Berlin: Springer; 2008.
[221] Nishimoto T, Kato Y, Somey R, Sato J, Nakamur T, Yamaguchi S, et al. Rev Laser Eng; 2008:1276–8.
[222] Silver JA. Appl Opt 2005;44(31):8545–56.
[223] Koizumi H, Yamada K, Yasada K, Uchino K, Oishi K. Spectrochim Acta 1981;36B:603–14.
[224] Allard N, Kielkopf J. Rev Mod Phys 1982;54:1103–82.
[225] Matsui M, Komurasaki K, Ogawa S, Yoshihiro Arakawa Y. J Appl Phys 2006;100:063102.
[226] Schlosser E, Fernholz T, Teichert H, Ebert V. Spectrochim Acta A 2002;58:2347–59.
[227] Schlosser E, J. Wolfrum J, Hildebrandt L, Seifert H, Oser B, Ebert V. Appl Phys B 2002;75:237–47.
[228] Gustafsson J, Axner O. Spectrochim Acta 1998;53:1895–905.
[229] Sanders ST, Mattison DW, Ma L, Jeffries JB, Hanson RK. Opt Express 2002;10:505–14.
[230] Affolderbach C, Nagel A, Knappe S, Jung C, Wiedenmann D, Wynands R. Appl Phys B 2000;70:407–13.
[231] Nefedov AP, Sinel'shchikov, Usachev AD. Phys Scripta 1999;59:432–42.
[232] Olivares IE, Duarte AE, Lokajczyk T, Dinklage, Duarte FJ. J Opt Soc Am B 1998;15(7):1932–9.
[233] Horvatic V, Veza D, Movre M, Niemax K, Vadla C. Spectrochim Acta B 2008;63:652–6.
[234] Franzke J, Wizemann HD, Niemax K, Vadla C. Eur Phys J D 2000;8:23–8.
[235] Jacobs JP, Warrington RB. Phys Rev A 2003;9(3):032722.
[236] Makdisi Y. Opt Commun 1997;147:215–9.
[237] Mercury information clearing house quarterly report. Canadian Electricity Association; April 2004.
[238] Schmid V. Continuous monitoring of Mercury emissions from Stationary Sources. Report of Clean Air Engineering; 2002.
[239] http://www.umweltbundesamt.de/luft-e/messeinrichtungen/index.htm [last accessed March 2010].
[240] Zamzow DS, Bajic SJ, Eckels DE, Baldwin DP. Rev Sci Instrum 2003;74:3774–83.
[241] Tao S, Miller GP. J Anal at Spectrom 2002;17:1344–8.
[242] Thiebaud J, Thomson MJ, Mani R, Morrow WH, Morris EA, Jia CQ. Environ Sci Technol 2009;43(24):9294–9.
[243] Zybin A, Koch J, Wizemann HD, Franzke J, Niemax K. Spectrochim Acta B 2005;60:1–11.
[244] Wizemann HD. Spectrochim Acta B 2008;63:539–60.
[245] Allen M, Meas. Sci Technol 1998;9:545–62.
[246] Friedrichs G, Zeitschr. Physikalische Chem 2008;222:1–30.
[247] Sanders ST, Baldwin JA, Jenkins TP, Baer DS, Hanson RK. Proc Comb Inst 2000;28:587–94.
[248] Ebert V, Fernholz T, Giesemann, Pitz H, Teichert H, Wolfrum J, et al. Proc Comb Inst 2000;28:423–30.
[249] Oh DB, Paige ME, Bomse DS. Appl Opt 1998;37:2499.
[250] Groll H, Niemax K. Spectrochim Acta B 1993;48:633–41.
[251] Gustafsson U, Somesfalen G, Alnis J, Svanberg S. Appl Opt 2000;39:3774 [Pb, K].
[252] Wizemann HD, Haas U. Spectrochim Acta B 2003;58:931–47.
[253] Wang W, Hammond RH, Fejer MM, Ahn CH, Beasley MR, Levenson MD, et al. Appl Phys Lett 1995;67:1375–7.
[254] Groll H, Schnürer-Patschan, Niemax K. Spectrochim Acta B 1994;49:1463–72.
[255] Niemax K, Zybin A, Eger D. Anal Chem 2001;73:134A–9A.
[256] Leinen H, Glässner D, Metcalf H, Wynands R, Haubrich D, Eschede D. Appl Phys B 2000;70:567–71.
[257] Hildebrandt L, Knispel R, Stry S, Sacher JR, Schael F. Appl Opt 2003;42:2110–8.
[258] Butcher DJ, Zybin A, Bolshov MA, Niemax K. Rev Anal Chem 2001;XX (2):79–100.
[259] Koch J, Zybin A, Niemax K. Spectrochim Acta B 2002;57:1547–61.
[260] Wizemann HD, Niemax K. Anal Chem 1997;69:4291–3.
[261] Alnis J, Gustafsson U, Svanberg S, Somesfalean G, Svanberg S. Appl Phys Lett 2000;76:1234.
[262] Carruthers AE, Lake RK, Shah A, Allen JW, Sibbett W, Dholakia K. Opt Commun; 2005:255–66.
[263] Uhl R, Wolff O, Franzke J, Haas U, Fresenius J. Anal Chem 2000;366:156.
[264] Anderson TN, Magnuson JK, Lucht RP. Appl Phys B 2007;87:341–53.
[265] Magnuson JK, Anderson TN, Lucht RP, Vijayasarathy UA, Oh H, Annamalai K, et al. Energy Fuels 2008;22:3022–8.
[266] Laurila T, Oikari R, Hernberg R, Kuittinen M. Spectrochim Acta B 2005;60:701–83.
[267] Jackson JD. Classsical electrodynamics. NY: Wiley & Sons; 1975.
[268] Winstead CB, Mazzotti FJ, Mierzwa J, Miller GP. Anal Commun 1999;36:277–9.
[269] Paul JB, Lapson L, Anderson JG. Appl Opt 2001;40:4904–10.
[270] Friedrichs G, Zeitschr. Physikal Chem 2009;222:31–61.
[271] Tao S, Mazzotti F, Winstead CB, Miller GP. Analyst 2000;125:1021–3.
[272] Winstead CB, Miller GP. J Anal Atom Spectrosc 1997;12:907–12.
[273] Wang C, Mazzotti FJ, Miller GP, Winstead CB. Appl Spectrosc 2003;57 (9):1167–72.
[274] Jongma RT, Boogaarts, Holleman I, Meijer G. Rev Sci Instr 1995;66:2821–8.
[275] Spuler S, Linne M, Sappey A, Snyder S. Appl Opt 2000;39:2480–6.
[276] Mazurenka MI, Fawcett BL, Elks JMF, Shallcross DE, Orr-Ewing AJ. Chem Phys Lett 2003;367:1–9.
[277] Yalin AP, Surla V, Butweiller M, Williams JD. Appl Opt 2005;44:6496–505.
[278] Carter CC. A CRDS mercury continuous emission monitor, Final Technical Report DOE DE-FC26–01FT41221; 2004.

[279] Mellqvist J, Rosen A. J Quant Spectrosc Rad Transf 1996;56:187–208. 225–240.
[280] IACM: EP 12210036. International patent application PCT/SE 00/01866. 2000.
[281] Forsberg C, Broström M, Backman R, Edvardsson E, Badiei S, Berg M, et al. Rev Sci Instr 2009;80:023104.
[282] Broström M, Kassman H, Helgesson A, Berg M, Andersson A, Backman R, et al. Fuel Proc Technol 2007;88:1171–7.
[283] Kassman H, Andersson C, Högberg J, Amand LE, Davidsson K. 19th FBC Conference. Vienna, Austria; May 21–24 2006.
[284] Henderson P, Szakalos P, Pettersson R, Andersson C, Högberg J. Mater Corros 2006;57(2):128.
[285] Broström M, Andersson C, Axner O, Nordin A. 2nd World Conference for energy. Rome, Italy: Industry and Climate Protection; 2004.
[286] Karlsson M, Amand L-A, Leckner B. Finnish-Swedish flame days. Naantali, Finland: IFRF; Sept. 3–4, 1996.
[287] Cheng C-M, Lin H-T, Wang Q, Chen C-W, Wang C-W, Liu M-C, et al. Energy Fuels 2008;22:3040–9.
[288] Cheng C-M, Chen C-W, Zhu J, Chen C-W, Kuo Y-W, Lin T-H, et al. Energy Fuels 2009;23:4831–9.
[289] Myers J, Kelly T, Lawrie C, Riggs K. Environmental technology verification report. Report. Batelle Columbus: ETV advanced monitoring systems center; 2002. OH 43201.
[290] Johnsen B, Cooper J, Milliken, Cooper. Environmental servies report for US Army Corps of Engineers. Contract nr. DACA42-00-P-0245; 2000.
[291] van Eyk P, Ashman PJ, Alwahabi ZT, Nathan GJ. Combust Flame 2008;155:529–37.
[292] van Eyk P, Ashman PJ, Alwahabi ZT, Nathan GJ. Proc Symp Combust 2009;32:2099–106.
[293] Saw WL, Ashman PJ, Nathan GJ, Alwahabi ZT. Combust Flame 2009;156:1471–9.
[294] Saw WL, Nathan GJ, Ashman PJ, Alwahabi ZT, Hupa M. Combust Flame 2009;56(7):1471–9.
[295] Zhou JX, Hou X, Tsai S-JJ, Yang KX, Michael RG. Anal Chem 1997;69:490–9.
[296] Simeonsson JB, Ezer M, Pacquette HL, Preston SL, Swart DJ. Spectrochim Acta B 1997;52:1955–63.
[297] Niefer RJ, Darrach M, Atkinson JB, Krause L. J Phys B 1987;20:531–40.
[298] Bras N, Afgani AE, Butaux J, Jeannet JC, Perrin D. J Chem Phys 1990;92: 6674–80.
[299] Resto W, Badini RG, Smith BW, Stevenson, Winefordner JD. Spectrochim Acta B 1993;48:627–32.
[300] Bauer D, Campuzano-Jost P, Hynes AJ. J Environ Monit 2002;4:339–43.
[301] Zeri Y, Balint-Kurti GG. J Mol Spec 1983;99:1–24.
[302] Biswas P, Zachariah MR. Environ Sci Tech 1997;31:2455–63.
[303] Monkhouse PB, Davidsson KO, Lönn B, Engvall K, Pettersson JBC, Gottwald UA. Fuel 2003;82:365–71.
[304] Chadwick BL, Griffin PG, Morrison RJS. Appl Spectrosc 1997;51:990–3.
[305] Hidalgo Nuñez M, Omenetto N. Appl Spectrosc 2001;55:809.
[306] Choi JH, Stipe CB, Koshland CP, Sawyer RF, Lucas D. J App Phys 2005;97:124315.
[307] Whitehurst C, King TA. J Phys D Appl Phys 1987;20:1577–83.
[308] Barat RB, Poulos AT. Appl Spectrosc 1998;52:1360–3.
[309] Tong X, Barat RB, Poulos AT. Environ Sci Technol 1999;33:3260–3.
[310] Tong X, Barat RB, Poulos AT. Rev Sci Instrum 1999;70:4180–94.
[311] Hoops AA, Reichardt TA. Appl Opt 2009;48:B32–42.
[312] Hoops AA, Reichardt TA, Kliner DAV, Koplow JP, Moore SW. Appl Opt 2007;46:4008–14.
[313] Hoops AA, Reichardt TA. Appl Opt 2006;45:6180–6.
[314] Spence D, Wang R-G, Dillon MA. J Chem Phys 1985;82:1883–9.
[315] Wadt WR. J Chem Phys 1980;72:2469–78.
[316] Buckley SG, Sawyer RF, Koshland CP, Lucas D. Comb Flame 2002;128:435–46.
[317] Buckley SG, Sawyer RF, Koshland CP, Lucas D. Proc Combust Inst 1996;25:325.
[318] Buckley SG, McEnally CS, Sawyer RF, Koshland CP, Lucas D. Combust Sci Tech 1996;118:171.
[319] Terenin A. Z Phys 1927;44:713.
[320] Wieland K. Z Phys 1932;76:801.
[321] Wieland K. Z Elektrochem 1960;64:761.
[322] Alfano AJ, Benard DJ. Photolysis-LIF diagnostic for GaCl. Appl Opt 1993;32:5373–8.
[323] Donnelly VM, Karliceck RF. J Appl Phys 1982;53:6399–407.
[324] Cool TA, Koffend JB. J Chem Phys 1981;74:2282–7.
[325] Eckbreth AC. Laser diagnostics for combustion temperature and species. CRC Press; 1996.
[326] Schulz C, Jeffries JB, Davidson DF, Koch JD, Wolfrum J, R.K. Hanson RK. Proc Combust Inst 2002;29:2735–42.
[327] Science-softCon UV/Vis^{+} spectra database, stand, www.science-softcon.de/spectra; 2008.
[328] Spectral Atlas of Gaseous Molecules. MPI-Mainz-UV–Vis, stand, www.atomsphere.mpg.de/enid/2295; May 2009.
[329] Hartinger KT, Nord S, Monkhouse PB. Appl Phys B 2000;70:133–7.
[330] Davidson DF, Chang AY, Kohse-Höinghaus K, Hanson RK, Quant J. Spec Rad Transf 1989;42:267–78.
[331] Okabe H. Photochemistry of small molecules. New York: Wiley; 1978.
[332] Vattulainen J, Wallenius L, Stenberg J, Hernberg R, . Linna V. Appl Spectrosc 1997;51(2):1314.
[333] Joutsenoja T, D'Anna, D'Alessio A, Nazzaro MI. Appl Spectrosc 2002;55 (2):130–5.
[334] Dushin VK, Zabelinski IE, Shatalov OP. Zh Prikl Spektrosk 1983;39(3):440–4.
[335] Zabelinski IE, Ibragimova IB, Shatalov OP. Zh Prikl Spektrosk 2006;73 (1):13–7.
[336] Lee MP, Hanson RK. J Quant Rad Transfer 1986;36(5):425–40.
[337] Thompson BA, Harteck P, Reeves RR. J Geophys Res 1963;68:6431.
[338] Wu CYR, Chen FY. J Quant Spec Rad Transf 1998;60:17–23.
[339] Monkhouse P, Wolfrum J. Proc. Joint Meeting of the Soviet and Italian sections of the Combustion institute. Tacchi Editione, Pisa, Paper 2.3; Nov. 1990.
[340] Reichardt TA, Klassen MS, King GB, Laurendeau NM. Appl Opt 1995;36: 973–6.
[341] Barker JR, Weston Jr RE. J Chem Phys 1976;65:1427–42.
[342] Earl BL, Herm R. J Chem Phys 1974;60:4568–78.
[343] Breckenridge W, Renlund AM. J Phys Chem 1979;83:1145–50.
[344] Umemoto H, Matsumoto K-i. Chem Phys Lett 1995;236:408–12.
[345] Yamamoto S, Nishimura N. Bull Chem Soc Jpn 1982;55:1395–400.
[346] Breckenridge W, Renlund AM. J Phys Chem 1978;82:1474–91.
[347] Breckenridge W, Renlund AM. J Phys Chem 1979;83:303–9.
[348] Zhang FM, Oba D, Setser DW. J Phys Chem 1987;91:1099–114.
[349] Michael JV, Suess GN. J Phys Chem 1974;78:482–7.
[350] Husain D, Littler JGF. Int J Chem Kinet 1974;6:61–75.
[351] Husain D, Littler JGF. J Photochem 1972/73;1:327–32.
[352] Bell CF, Husain D. J Photochem 1985;29:267–83.
[353] Lee K, Son HS, Baue SC, Ku JK. Chem Phys Lett 1998;288:531–7.
[354] Haider N, Husain D, Kabir M. Photochem Photobiol A Chem 1993;72: 97–107.
[355] Haider N, Husain D, Kabir M. JCS Faraday Trans 1993;89:1653–8.
[356] Chowdury MA, Husain D. JCS Faraday Trans 1977;73:1805.
[357] Nizamov B, Dagdigian PJ. J Phys Chem A 2000;104:6345–50.
[358] Slater JC, Kirkwood JC. Phys Rev 1931;37:682.
[359] Takubo Y, Okamoto T, Yamamoto M. Appl Opt 1986;25:740–3.
[360] Ke CB, Chou S-H, Lin K-C, Luh W-T. J Phys Chem 1993;97:604–9.
[361] Zizak G, Bradshow JD, Winefordner JD. Appl Opt 1980;19:3631–9.
[362] Linton C, Broida HP. J Mol Spec 1976;62:396–415.
[363] Mandl A, Parks JH. Appl Phys Lett 1978;33:498–500.
[364] Chadwick BL, Morrison RJS. JCS Faraday 1995;91:1931.
[365] Anderson JB, Maya J, Grossman MW, Lagushenko R, Waymouth JF. Phys Rev A 1985;31:2968–75.
[366] Herd MT, Lawler JE, Menningen KL. J Phys D 2005;38:3304–11.
[367] Oldenburg RC, Baugham SL. Anal Chem 1986;58:1430.
[368] Poole DJ, Sharifi VN, Swithenbank J, Ardelt D. J Anal at Spectrom 2005;20:912–38.
[369] Clarkson PJ, Poole DJ, Ryu CK, Sharifi VN, Swithenbank J, Waarlo HJ, et al. Anal Bioanal Chem 2003;377:39–47.
[370] Poole DJ, Sharifi VN, Swithenbank J. Waste Managem 2007;27(4):519–32.
[371] Poole DJ, Sharifi VN, Swithenbank J, Kilgallon P, Simms N, Oakey J, et al. J Anal at Spectrom 2007;22:532–9.
[372] Ludwig C, Wochele J, Jorimann U. Anal Chem 2007;79:2992–6.
[373] Abanades S, Flamant G, Gauthier GD. Combust Flame 2003;134:315–26.
[374] Falcoz Q, Flamant G, Abanades S, Gauthier D, Patsson F. Environ Sci Technol 2009;43(6):2184–9.
[375] Baldwin DP, Bajic SJ, Eckels DP, Zamzow DS, Miller GP, Tao S. Report IS-5144. Waggoner, CA: Ames Laboratory-USDOE, www.cmst.org/cmst/reports.html; March 2001.
[376] Seltzer MD, Meyer GA. Environ Sci Tech 1997;31:2665–72.
[377] Timmermans H, de Groote FPJ, Jonkers J, Gamero A, Sola A, van der Mullen JJAM. Spectrochim Acta B 2003;58(5):823–36.
[378] Moisan M, Sauvé G, Zakrewski Z, Hubert J. Plasma Sources Sci Techn 1994;3:584.
[379] Broekaert JAC, Siemens V. Spectrochim Acta B 2004;59(12):1823–39.
[380] Woskov PP, Hadidi K, Thomas P, Green K, Flores G. Waste Manag 2000;20:395–402.
[381] Häyrinen V, Hernberg R, Aho M. Fuel 2004;83:791–7.
[382] Oikari R, Häyrinen V, Parviainen T, Hernberg R. Appl Spectrosc 2001;55 (10):1469–77.
[383] Oikari R, Aho M, Hernberg R. Energy Fuels 2003;17:87–94.
[384] Oikari R, Parviainen T, Eteläaho, R, Hernberg R. Proc. Int. Conference on Emission Monitoring. Arnhem, The Netherlands; 25-27 April, 2001.
[385] Oikari R, Häyrinen V, Kettunen L, Hernberg R. J Anal Atom Spectrom 2002;17:1421–4.
[386] Häyrinen V, Oikari R, Hernberg R. –. Appl Spectrosc 2004;58:111–21; (a) Häyrinen V, Oikari R, Hernberg R. J Phys D 2004;37(1):25–33.
[387] Runge ER, Minck RW, Bryan FR. Spectrochim Acta B 1964;20:733.
[388] Cremers DA, Radziemski LJ. Handbook of laser induced breakdown spectroscopy. New York: J. Wiley & Sons; 2006.
[389] Singh JP, Thakur SN. Laser-induced breakdown spectroscopy. Elsevier; 2007.
[390] Miziolek W, Palleschi V, Schechter I, editors. Laser-induced breakdown spectroscopy (LIBS): fundamentals and applications. UK: Cambridge University Press; 2007.
[391] Casavola AR, Colonna G, Capitelli M. Kinetic model of titanium laser induced plasma expansion in nitrogen environment. Plasma Sources Sci Technol 2009;18:025027.
[392] Vidal F, Laville S, Johnston TW, Barthélemy O, Chaker M, Le Drogoff B, et al. Spectrochim Acta B 2001;56:973–86.

[393] Babushok VI, DeLucia Jr FC, Dagdigian PJ, Nusca MJ, Miziolek AW. Appl Opt 2003;42:5947.
[394] Buckley SG. Environ Eng Sci 2005;22(2):195–204.
[395] Fisher BT, Johnsen HA, Buckley SG, Hahn DW. Appl Spectrosc 2001;55:1312–9.
[396] Carranza JE, Hahn DW. Spectrochim Acta B 2002;57:779–90.
[397] Carranza JE, Hahn DW. J Anal at Spectrom 2002;17:1534–9.
[398] Carranza JE, Hahn DW. Anal Chem 2002;74:5454–60.
[399] Gleason R, Hahn DW. Spectrochim Acta B 2001;56:419–30.
[400] Molina A, C.R., Sickafoose SM, Walsh PM, Blevins LG. Spectrochim Acta 2005;60:1103–14.
[401] Yalcin S, Crosley DR, Smith GP, Faris GW. Appl Phys 1999;B 68:121–30; (a) Hohreiter V, Hahn DW. Anal Chem 2005;77:1118–24.
[402] Lithgow G, Buckley SG. Spectrochim Acta B 2005;60(7–8):1060–9.
[403] Lazic R, Barbini R, Calao F, Fantoni R, Palucci A. Spectrochim B 2001;56:807–20.
[404] Bulajic D, Corsi M, Cristoforetti G, Legnaioli S, Palleschi V, Solvetti A, et al. Spectrochim Acta 2002;57:339–53.
[405] Hunter AJR, Davis SJ, Piper LG, Holtzclaw KW, Fraser ME. Appl Spec 2000;54 (44):575–82.
[406] Fraser ME, Panagiotou T, Hunter AJR, Anderson EB, Davis SJ, Braybrooke G, et al. Plating Surf Finishing 2000;87(1):80–7.
[407] Hunter AJR, Wainner RT, Piper LG, Davis SJ. Appl Opt 2003;42:2102–9.
[408] Suess DT, Prather KA. Chem Rev; 1999:3007–35.
[409] Davidsson KO, Engvall K, Hagström M, Lönn B, Pettersson JBC. Energy Fuels 2002;16:1369–77.
[410] Davidsson KO, Korsgren JG, Pettersson JBC, Jäglid U. Fuel 2002;81:137–42.
[411] Kowalski T, Ludwig C, Wokaun A. Energy Fuels 2007;21:3017–22.
[412] Tran K-Q, Iisa K, Steenari BM, Lindqvist O. Fuel 2005;84:169–75.
[413] Bläsing M, Müller M. Combustion and Flame 2010;157:1374–81.
[414] Wolf KJ, Müller M, Hilpert K, Singheiser L. Energy Fuels 2004;18:1841–50.
[415] Guilhaus M. Spectrochim Acta B 2000;55:1511–25.
[416] Nichigushi K, Utani K, Fujimori E. J Anal Spectrom 2008;23:1125–9.
[417] Svane M, Hagstrom M, Pettersson JBC. Aerosol Sci Technol 2004;38: 655–63.
[418] Svane M, Janhäll S, Hagström M, Hallquist M, Pettersson JBC. Atm Environ 2005;39:6919–30.
[419] Svane M, Gustafsson TL, Kovacevik B, Noda J, Andersson PU, Nilsson ED, et al. Aerosol Sci Technol 2009;43(7):653–61.
[420] Liu P, Ziemann PJ, Kittelson DB, McMurry PH. Aerosol Sci Technol 1996;22:292–313.
[421] Liu P, Ziemann PJ, Kittelson DB, McMurry PH. Aerosol Sci Technol 1996;22:314–24.
[422] Su Y, Sipin MF, Furutani H, Prather KA. Anal Chem 2004;76:712–9.
[423] Wood SH, Prather KA. Trends Anal Chem 1998;17:346–56.
[424] Mahadevan R, Lee D, Sakurai, Zachariah MR. J Phys Chem A 2002;106:11083–92.
[425] Bente M, Adam T, Ferge T, Gallavardin S, Sklorz M, Streibel, et al. Int J Mass Spectrom 2006;258:86–94.
[426] ChlorOut, Swedish patent SE 0100220-3, Pat. Appl. PCT/SE 00/01866; 2003.
[427] Schürmann H, Monkhouse PB, Unterberger S, Hein KRG. Proc Combust Inst 2007;31:1913.
[428] Schürmann H, Monkhouse PB, Unterberger S, Hein KRG. 8th International Conference on Energy for a Clean Environment (Clean Air 2005). Lissabon; 27–30 June 2005.
[429] Gottwald U, Monkhouse P, Wulgaris N, Bonn B. Fuel Proc Technol 2003;80:143–53.
[430] Gottwald U, Monkhouse P, Wulgaris N, Bonn B. Fuel Proc Technol 2002;75:215.
[431] Greger F, Monkhouse P, Hartinger KT, Wolfrum J, Bonn B, Baumann H. Proc Int Combust 1996;26:3301.
[432] Hartinger KT, Monkhouse PB, Wolfrum J, Bonn B, Baumann H. Proc Int Combust 1994;25:193.
[433] Jakob A, Stucki S, Kuhn P. Environ Sci Technol 1996;30:3275.
[434] Rice S, Allendorf MD. Glass Sci Technol 2005;78:45.
[435] Continuous metal emissions monitoring CRADA, http://www.navair.navy.mil/techTrans/index.cfm?map=local.ccms.view.aB&;doc=crada.4 [last accessed November 2009].
[436] Wochele J, Ludwig C, Schuler AJ. Proc EMC; 2001.
[437] Annual activity report, 2008. Competence center energy & mobility. CCEM; Jan. 2009. p. 71.
[438] Blevins LG, Shaddix CR, Sickafoose SM, Walsh PM. Appl Opt 2003;42:6107–18.
[439] Radziemski LJ, Cremers DA. In: Radziemski LJ, Cremers DA, editors. Laser-induced plasmas and applications. N. York: Marcel Dekker; 1989. p. 295–325.
[440] Noda M, Deguchi Y, Iwasaki S. Spectrochim Acta B 2002;57:701–9.
[441] Brysch A, Sturm V, Noll R. VDI Ber 2002;1667:149–54.
[442] Sturm V, Brysch A, Noll R. Berg- und Hüttenmännische Monatsh 2007;1:28–32.
[443] Deguchi Y, Noda M, Fukuda Y, Ichinose Y, Endo Y, Inada M, et al. Meas Sci Technol 2002;13:R103–15.
[444] Zhang H, Yueh F-Y, Singh JP. Appl Opt 1999;38:1459–66.
[445] Zhang H, Yueh F-Y, Singh Jp. J Air Waste Managem Assoc 2001;51:681–7.
[446] Buckley SG, Johnsen HA, Hencken KR, Hahn DW. Waste Managem; 2000:455–62.
[447] Monts DL, Singh JP, Abilasha YSu, Zhang H, Yueh F-Y, Jang PR, et al. Combust Sci Technol 1998;134:103–26.
[448] Neuhauser RE, Panne U, Niessner R. Anal Chim Acta 1999;392:47–54.
[449] Panne U, Neuhauser RE, Theisen M, Fink H, Niessner R. Spectrochim Acta B; 2001:839–50.
[450] Molina A, Walsh PM, Shaddix CR, Sickafoose SM, Blevins LG. Appl Opt 2006;45:4411–23.
[451] Molina A, Walsh PM, Shaddix CR, Neufled JW, Blevins LG. J Energy Inst 2006;79(2):84–91.
[452] Molina A, Shaddix CR, Blevins LG, Walsh PM, Neufeld JW. Europ J Glass Sci Techn 2006;47(6):177–87.
[453] Buckley SG, Walsh PM, Hahn DW, Gallagher RJ, Misra MK, Tong SSC, et al. Ceram Eng Sci Proc 2000;21:183–205.
[454] Walsh PM, Johnsen HA, Ottesen DK, England GC. 94th Ann. Conf. Air & Waste Management Assoc. Orlando, Florida; June 24–28, 2001.
[455] Hahn D, Hencken KR, Johnsen HA, Ross JR, Walsh PM, Christy RH, et al. In: Emission inventory: living in a global environment, Vol. 2. Sewickley, Pa: Air & Waste Mangement Assoc.; 1998. p. 1175–93.
[456] Hahn D, Hencken KR, Johnsen HA. Report SAND97-8270. Livermore, California: Sandia National Labororatories; 1997.
[457] Panne U, Neuhauser E, Haisch C, Fink H, Niessner R. Appl Spectrosc 2002;56:375–80.
[458] Neuhauser RE, Panne U, Niessner R, Wilbring P, Fresenius J. Anal Chem 1999;364:720–6.
[459] Stepputat M, Noll R, Miguel R. VDI-Berichte 2002;1694:15–20.
[460] Dayton DC, Frederick Jr WC. Energy Fuels 1996;10:284–92.
[461] Heger HJ, Zimmermann R, Dorfer R, Beckamnn M, Griebel H, Kettrup, et al. Anal Chem 1999;71:46–57.
[462] Svane M, Hagström M, Davidsson KO, Boman J, Pettersson JBC. Energy Fuels 2006;20(3):979–85.
[463] Toner SM, Sodeman DA, Kimberly A, Prather KA. Environ Sci Technol 2006;40(12):3912–21.
[464] Zhang Y, Wang X, Chen H, Yang X, Chen J, Allen JO. Chemosphere 2009;74:501–7.
[465] Lee DG, Miller A, Park KH, Zachariah MR. Int J Automotive Technol 2006;7 (6):667–73.
[466] Zimmermann R, Ferge T, Galli M, Karlsson R. Rapid Commun Mass Spectrom 2003;17(8):851–9.
[467] Docquier N, Candel S. Prog Energy Combust Sci 2002;28:107–50.
[468] Furlong ER, Baer DS, Hanson RK. Proc Comb Inst 1998;27:103–11.
[469] Klepper CC, Carlson EP, Hazelton RC, Yadlowsky EJ, Feng B, Taher MA, et al. IEEE 31st Int Conf Plasma Sci 2005;33(2):265.